INVESTIGATION OF THE STEREO STRUCTURES OF CHIRAL MOLECULES USING VIBRATIONAL CIRCULAR DICHROISM, OPTICAL ROTATION, AND DENSITY FUNCTIONAL THEORY

By

Jiangtao He

Dissertation

Submitted to the Faculty of the

Graduate School of Vanderbilt University

in partial fulfillment of the requirements

for the degree of

DOCTOR OF PHILOSOPHY

in

Chemistry

December, 2005

Nashville, Tennessee

Approved:

Professor Prasad L. Polavarapu

Professor Michael P. Stone

Professor Carmelo J. Rizzo

Professor Charles M. Lukehart

Professor David W. Wright

To my lovely wife, Hongjuan An

ACKNOWLEDGEMENTS

I would like to express my gratitude to my research advisor Professor Prasad Polavarapu. During my graduate study, he has provided invaluable guidance and warm encouragement. Also, I want to thank my Ph. D. committee members: Dr. Stone, Dr. Rizzo, Dr. Lukehart, and Dr. Wright for their professional advices to my research work.

I appreciate the dedication of my research collaborators. Without them, some of my research work would not have been possible. They are Dr. Gabriella Roda, Dr. Paola Conti, and Dr. Marco De Amici from University of Milano, Italy (Chapter V); Dr. Hong-Zhi Tang, and Dr. Bruce M. Novak from North Carolina State University, Raleigh, NC (Chapter VI); and Dr. Kenneth Ruud from University of Tromsø, Norway. I also want to thank Jeremy Wardman of A.H. Marks for providing the analytical grade samples of the acids studied in Chapter IV

I thank Dr. Feng Wang for the helping of instrument operation and our group members, Dr. Ganesh Shanmugam, Peng Zhang, and Ana Petrovic for helpful discussion about various research projects. I also want to thank all faculty and staff members in chemistry department for all kinds of support.

Finally, I want to thank National Science Foundation for financial support. I want to thank Warren Fellowship for travel grant. I want to thank Vanderbilt University for providing an excellent research environment for my research work.

TABLE OF CONTENTS

Page

LIST OF TABLES

LIST OF FIGURES

CHAPTER I

INTRODUCTION

Vibrational Circular Dichroism (VCD)

The vibrational circular dichroism (VCD) instrument measures the difference in absorbance of left and right circularly polarized infrared (IR) light components when they pass through a chiral sample. This is similar to normal circular dichroism which operates in the ultraviolet or visible region. The first VCD spectrum was measured on a dispersive instrument around 1975.[1, 2] The first Fourier Transform (FT) VCD instrument was built around 1979.[3] The FT-VCD instrument has throughout and multiplex advantages compared to dispersive instrument. The application of dual polarization modulation technique further improves the baseline in VCD measurement.[4]

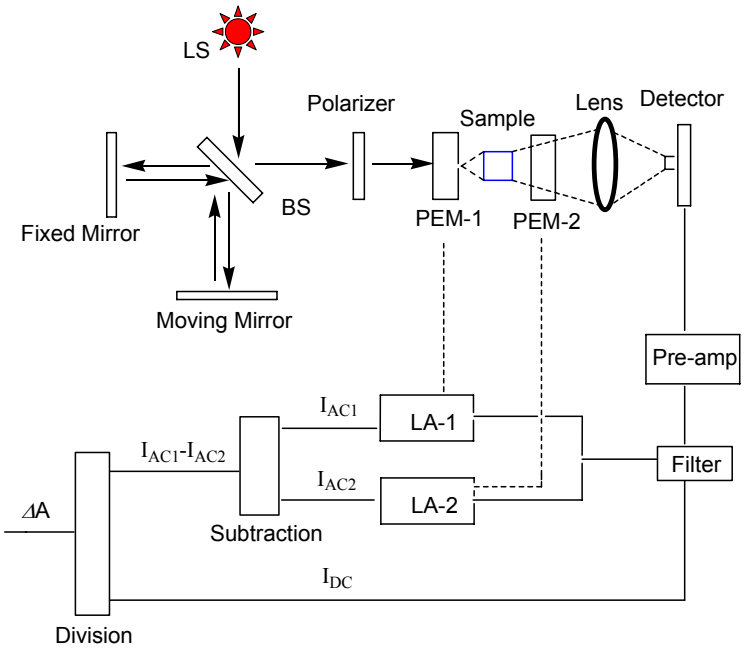

Figure 1-1. The block diagram of a FT-VCD instrument.

Figure 1-1 shows a general diagram of FT-VCD instrument. The infrared radiation passes through Michelson interferometer and is modulated by the interferometer. The light is then linearly polarized by a linear polarizer. The linearly polarized light is turned to alternating left and right circularly polarized light by a photo-elastic modulator (PEM). The circularly polarized light then passes through the sample and a second PEM, which cancels out the linear birefringence intensity. The light is finally focused on the HgCdTe detector by a zinc selenide lens. The signal is amplified by the pre-amplifier and separated by the electronic filter to a low frequency DC signal, which is normal absorption spectrum, and a high frequency AC signal, which is related to the VCD spectra. The Fourier transform is done by the computer and the raw signal is demodulated to get the absorption and VCD spectrum.

The interpretation of VCD spectra was greatly benefited from the development of theoretical chemistry, especially the development of density functional theory (DFT).[5, 6] The theoretical quantity which corresponds to the normal vibrational absorption is dipole strength (D_{01}) and the theoretical quantity which corresponds to the VCD is rotational strength (R_{01}). Their expressions are listed in Equations 1-1 and 1-2. Ψ_0 and Ψ_1 are the vibrational wave functions of 0 and 1 levels in the ground electronic state. μ and m are electric dipole moment and magnetic dipole moment operators.

$$D_i = |\langle \Psi_0 | \mu | \Psi_1 \rangle|^2 \tag{1-1}$$

$$R_i = \mathrm{Im}[\langle \Psi_0 | \mu | \Psi_1 \rangle \bullet \langle \Psi_1 | m | \Psi_0 \rangle] \tag{1-2}$$

The implementation of calculating these properties into both Gaussian[7, 8] and Dalton[9] program made it easy to theoretically predict these properties. The dipole strength and rotational strength can be obtained experimentally by the Equations 1-3 and 1-4,[10] where $\varepsilon(\nu)$ is the molar absorptivity (in L mol^{-1} cm^{-1}) at frequency ν (in cm^{-1}), $\Delta\varepsilon(\nu)$ is the differential molar absorptivity (in L mol^{-1} cm^{-1}) at frequency ν (in cm^{-1}), and ν_0 is the center frequency of a vibrational band. Therefore, quantitative comparison between theoretical and experimental values can be made.

$$D_i = \frac{0.92 \times 10^{-38}}{\nu_o} \int \varepsilon(\nu)\, d\nu \qquad (1\text{-}3)$$

$$R_i = \frac{0.23 \times 10^{-38}}{\nu_o} \int \Delta\varepsilon(\nu)\, d\nu \qquad (1\text{-}4)$$

By combining the experimental VCD spectra with theoretical prediction, VCD can be used as a powerful tool in studying the absolute configuration and conformation of chiral molecules. It can complement the X-ray crystallography to assign the absolute configuration of chiral molecules and NMR method to study the conformation of chiral molecules in solution. In my study, I try to establish the error ranges of VCD predictions by quantitatively comparing experimental and predicted values and also to determine the absolute configuration of some chiral molecules.

Optical Rotation

Optical rotation is a century old technique which measures the rotation of linearly polarized light after it passes through a chiral sample.[11] The sign of optical rotation is

related to the absolute configuration of chiral molecules. Optical rotation contributes to the development of modern stereochemistry and is widely used in the organic labs. Although the measurement of optical rotation is very simple, the theoretical prediction of optical rotation is rather complex. The first *ab intio* prediction of optical rotation was published at 1997.[12] The density functional theory also was applied in prediction of optical rotaiton.[13] The quantum chemistry quantity related to optical rotation is the electric dipole-magnetic dipole polarizability tensor as shown in Equation 1-5.[14] μ and m are electric dipole moment and magnetic dipole moment operators. ψ_s^0 and ψ_n^0 are the wave functions of ground and excited electronic state. ω_{ns} relates to the excitations energy between n and s. ω is the angular frequency of exciting radiation, which is usually the sodium D line.

$$G'_{\alpha\beta} = \frac{-4\pi}{h} \sum_{n \neq s} \frac{\omega}{\omega_{ns}^2 - \omega^2} \times \mathrm{Im}\left\{ \left\langle \psi_s^0 \mid \hat{\mu}_\alpha \mid \psi_n^0 \right\rangle \left\langle \psi_s^0 \mid \hat{m}_\beta \mid \psi_n^0 \right\rangle \right\} \tag{1-5}$$

The specific rotation in units of deg·cm^3·g^{-1}·dm^{-1} can be related to *G'* by Equations 1-6 and 1-7, where $\bar{\nu}$ is wavenumber where the optical rotation is measured. n is refractive index and M is concentration in g·mol^{-1}.

$$[\alpha] = 0.1343 \times 10^{-3} \beta \bar{\nu}^2 (n^2 + 2) / 3M \tag{1-6}$$

$$\beta = -\omega^{-1} (G'_{xx} + G'_{yy} + G'_{zz}) / 3 \tag{1-7}$$

In my study, I use optical rotation as a tool to research the conformation and absolute configuration of different chiral molecules. The combination of VCD and optical rotation will provide a powerful and convenient tool for stereochemistry research.

Instruments

The VCD was measured on a modified commercial Chiral*ir* (BioTools, Wauconda IL) VCD instrument which has dual PEMs. The instrument has a ZnSe beam splitter (BS) and BaF_2 polarizer. The detector is a 2X2mm mercury cadmium telluride (HgCdTe) detector which needs to be kept at liquid nitrogen temperature. The PEMs are PEM-80 and PEM-90 (Hinds Instrument, Hillsboro, OR) without antireflection coating on the ZnSe optical element. Samples were held in variable pathlength cell with BaF_2 windows or fixed pathlength cell with CaF_2 windows.

The optical rotation was recorded on either Autopol III or Autopol IV polarimeter (Rudolph, Hackettstown, NJ). Samples were held in a 0.5dm cell with quartz windows. More detailed experimental condition will be given out in the following chapters.

Calculation

The theoretical prediction was carried out using either Gaussian or Dalton software package. More detailed calculation details will be given out in the following chapters.

CHAPTER II

QUANTITATIVE DETERMINATION OF CONFORMER POPULATION: ASSESSMENT OF SPECIFIC ROTATION, VIBRATIONAL ABSORPTION, AND VIBRATIONAL CIRCULAR DICHROISM IN SUBSTITUTED BUTYNES

Introduction

Determination of stable conformers, and of their populations, for a given molecule in solution phase is a challenging task in many cases. While microwave spectra or electron diffraction methods yield such information for favorable gas phase molecules, unique methods for determining this information in solution phase are difficult to find. Nuclear magnetic resonance (NMR) has been the method of choice for obtaining this information, but slow time scale of NMR phenomenon permits the determination of only the average conformation in many cases (3-butyn-2-ol, for example).

Since vibrational spectroscopy is uniquely sensitive to molecular structure, and hence to molecular conformation, and vibrational transitions occur on a faster time scale, vibrational spectroscopy in principle should be capable of providing the individual conformer populations. During the earlier decades, when ab initio methods were not either practical or fully developed, the interpretation of vibrational spectral intensities was done in a semi-empirical and qualitative manner. As a result, much reliance was not placed on vibrational spectroscopic methods for determining the conformer populations quantitatively. The recent availability of density functional theoretical (DFT) methods[15] lead to improved predictions of vibrational spectra, in particular infrared vibrational absorption (VA) and vibrational circular dichroism (VCD). This capability enhances the utility of VA and VCD for determining the conformer populations. Although numerous

VA and VCD studies have been reported in the literature, most studies have focused[16-19] on qualitative "eyeballing" of experimental and predicted spectra, with emphasis on determining the absolute configuration. Although some efforts have been made to determine the conformer populations[20, 21] from VA and/or VCD, error limits or uncertainties involved in the resulting conformer populations have not been established or analyzed to date.

As reported recently the variations in specific rotation as a function of temperature[22] or solvent[23] can be used to determine the conformer populations. The specific rotations measured in gas phase[24, 25] are ideal for comparison with theoretical predictions on isolated molecules, but such measurements require special instrumentation and are not routine. As the condensed phase experimental specific rotations (often reported for neat liquids or in some convenient solvent at some convenient concentration) can be influenced by solute-solute interactions, a quantitative comparison of predicted and condensed phase experimental specific rotations may not be reliable. This drawback can be alleviated with the measurement of intrinsic rotation[23] (specific rotation in the limit of zero concentration) which is devoid of solute-solute interactions. Intrinsic rotation may still be influenced by the solvent (due to solute-solvent interactions), but such solvent influence can be established by measuring the intrinsic rotation in different solvents. The combined use of experimental intrinsic rotations and predicted specific rotations is one approach to determine the conformer populations.

The purpose of this research is to evaluate the limits of reliability of specific rotation, VA and VCD for determining the conformer populations. For this purpose, we have synthesized (+)-3-chloro-1-butyne [HCCC(Cl)(CH_3)H], one of the simplest single

conformer molecules, and investigated its experimental intrinsic rotation (in CCl_4 and CH_3OH solvents) and VA and VCD (in CCl_4 solvent). DFT predictions of specific rotation, VA and VCD of (+)-3-chloro-1-butyne were also obtained using large basis sets, namely, aug-cc-pVDZ, 6-311++G(2d,2p), aug-cc-pVTZ. A comparison of these observed and predicted quantities provided the limits of quantitative reliability in using these methods. Then we applied these methods for determining the conformer populations of (-)-3-butyn-2-ol [HCCC(OH)(CH_3)H] in dilute solutions.

Experimental Section

Racemic 3-chloro-1-butyne has been synthesized[26, 27] before, but individual enantiomers of 3-chloro-1-butyne have not been reported before to our knowledge. Following the literature procedure for racemic 3-choloro-1-butyne, (+)-3-chloro-1-butyne was synthesized from (*S*)-(-)-3-butyn-2-ol by reaction with 1-chloro-N,N,2-trimethyl-1-propenylamine. The product was purified by distillation. The amount of CH_2Cl_2 impurity was minimized by collecting the distilled product at 68-72^oC. The final product was characterized using NMR. [^{1}H NMR ($CDCl_3$): δ1.76 (d, 3H, CH_3, J= 7Hz), 2.59 (d, 1H, C≡CH, J = 2Hz), 4.62 (dq, 1H, CHCl, J = 7 Hz and 2 Hz)]. The electronic circular dichroism spectrum of (+)-3-chloro-1-butyne (0.5 mM in cyclohexane) exhibited one positive band at 192 nm. The enantiomeric purity of (+)-3-chloro-1-butyne was determined as 100% using a chiral GC column (Chiraldex G-TA, 20m x 0.25, Astec Inc), with column temperature at 33°C, helium as carrier gas (at 10 psi), and FID detection method. Only one GC peak was observed for (+)-3-chloro-1-butyne, while two peaks were observed for racemic 3-chloro-1-butyne.

Optical rotation as a function of concentration was measured on either Autopol III [for (-)-3-butyn-2-ol)] or Autopol IV [for (+)-3-chloro-1-butyne] polarimeter, using a 0.5 dm cell. Optical rotation in this chapter was measured at sodium D line (589nm). For (-)-3-butyn-2-ol, the following procedure was used. To minimize the errors in concentration/optical rotation, the concentrations were generally chosen to give an observed rotation of about 0.01^{o} or greater and the weights of the samples were chosen appropriate for 5 or 10 mL solutions. The weight of empty volumetric flask and the weight of flask with solute were measured each five different times (by removing the flask from, and reinserting the flask into, the balance compartment) to avoid accidental mistakes in the weights. The volumetric flasks were filled with appropriate solvent, as carefully as humanly possible, up to the mark. This solution was then transferred to a 0.5 dm cell and optical rotation was measured five different times (by removing the cell from, and reinserting the cell into, the sample compartment) to check for consistency. The averages of these measurements were used to calculate specific rotation. This procedure ensured that no unusual data scatter was present in the measurements. The concentration ranges studied were 0.06-0.33 M in CCl_4 and 0.06-0.29 M in CH_3OH. For (+)-3-chloro-1-butyne, due to the limited amount of sample, we did not follow the procedure used for (-)-3-butyn-2-ol. Instead, solutions were prepared by successive dilution. The concentration ranges studied were 0.01-0.18 M in CCl_4 and 0.02-0.13 M in CH_3OH.

When the observed rotation α varies linearly with concentration [as $\alpha = Ac$, where c is the concentration of optically active substance in solution and A is proportionality constant], the specific rotation will be a constant (independent of

concentration). Non-linear variation of the observed rotation α with concentration may indicate the influence of solute-solute interactions. If the observed rotation α follows the quadratic equation, as $\alpha = A_2c^2 + B_2c$, then the specific rotation follows the equation $[\alpha]= A_1c + B_1$. As c tends to zero, observed rotation α should always approach zero in achiral solvents, and hence the plot of α vs. c data should be forced to go through the origin. However, specific rotation $[\alpha]$ has a finite value when approaching infinite dilution; the constant B_1 in $[\alpha]= A_1c + B_1$, represents the specific rotation at infinite dilution, which is referred[28] to as *intrinsic rotation* and designated as $[\alpha]_{c=0}$ or $\{\alpha\}$. The linear relation, $[\alpha]= A_1c + B_1$, may not apply in all situations; in some cases $[\alpha]$ may follow quadratic, cubic or some other complicated relation, in which case the experimental specific rotations are fit to an appropriate model equation. These equations are given in the figure legends. Plots of both α vs. c and $[\alpha]$ vs. c were prepared. In the normal least squares fitting procedure, it is a common practice to assume that all of the errors are in the y-values. While this type of fitting is appropriate for α vs. c data, weighted least squares fitting is needed for fitting the $[\alpha]$ vs. c data. When these precautions are taken the intrinsic rotation determined from α vs. c plot will be the same as that obtained from $[\alpha]$ vs. c plot.

VA and VCD spectra usually contain numerous vibrational bands. In the past, VA and VCD predictions were evaluated[7] against the corresponding experimental observations, by preparing the plots of predicted vs experimental integrated band intensities. These plots however do not provide a quantitative estimate of agreement/differences. Here we present, what is believed to be, the first quantitative approach to evaluate VA and VCD intensities. For a single conformer molecule, the

agreement between experimental and predicted intensities can be quantified using percent difference (PD) and root-mean-square percent difference (RMSP):

$$PD = \frac{(P_i - E_i)}{E_i} x100 \tag{2-1}$$

$$RMSP = 100 \times \sqrt{\sum_{i=1}^{m} \frac{\left[(P_i - E_i)/E_i\right]^2}{m}} \tag{2-2}$$

where E_i is the observed intensity and P_i is the predicted intensity for band i. and the summation runs over m bands of the molecule investigated. For molecules existing in two or more conformations, the experimental intensities of these bands, in conjunction with predicted intensities for individual conformers, can be used to determine the conformer populations as follows. If the experimental band intensities are represented by a column vector, {E}, predicted band intensities for different conformers by rectangular matrix **P**, then the fractional populations of conformers, represented by column vector {X}, are related to {E} and **P** by Equation 2-3a.

$$\begin{bmatrix} E_1 \\ E_2 \\ E_3 \\ - \\ - \\ - \\ E_m \end{bmatrix} = \begin{bmatrix} P_{1,1} & P_{1,2} & - & P_{1,N} \\ P_{2,1} & P_{2,2} & - & P_{2,N} \\ P_{3,1} & P_{3,2} & - & P_{3,N} \\ - & - & - & - \\ - & - & - & - \\ - & - & - & - \\ P_{m,1} & P_{m,2} & - & P_{m,N} \end{bmatrix} \begin{bmatrix} X_1 \\ X_2 \\ - \\ X_N \\ \\ \\ \end{bmatrix} \tag{2-3a}$$

In other words, the experimental intensity E_i for band i is expressed as

$$E_i = \sum_{j=1}^{N} P_{ij} X_j \quad \text{for } i = 1,2,...m \tag{2-3b}$$

where P_{ij} is the predicted intensity for band i of jth conformer. Usually the number of vibrational bands (m), is far greater than the number of conformations (N), so the column

vector of fractional populations, {X} can be determined by regression methods, with the constraints that the sum of the fractional populations of conformers is 1 and fractional populations cannot be negative. That is,

$$\sum_{j=1}^{N} X_j = 1 \text{ and } X_j \geq 0 \qquad (2\text{-}4)$$

The experimental VA and VCD spectra were measured on a commercial instrument Chiral*ir*. The integrated areas of the bands in the experimental spectra were obtained by fitting (R^2=0.99) the experimental bands to Lorentzian band shapes using the PeakFit program[29]. The experimental band intensities in VA spectra were expressed[10] as dipole strengths (D_i) and in VCD spectra as rotational strengths (R_i) and can be calculated according to Equations 1-3 and 1-4.

Vibrational band positions (frequencies) are not needed to use Equations 2-1~2-3. However, the predicted counterparts of the experimental bands have to be identified and correlated one-by-one. A commercial program DataFit[30] was used for determining the fractional populations using Equations 2-3 and 2-4.

All specific rotation calculations were performed using a developmental version of the DALTON program.[9] For density functional predictions, a B3LYP density functional available in this DALTON program was used. The basis sets used with DALTON were either available in the program library or were obtained from EMSL library.[31] All specific rotation calculations reported here were based on gauge including atomic orbitals (GIAOs, also called London orbitals) and the dynamic method.[32] Geometry optimizations and VCD calculations were undertaken with Gaussian 98 program.[8] The solvent influence on optimized geometries, vibrational frequencies and intensities was investigated with PCM model incorporated in Gaussian 03 program.

(+)-3 -chloro-1-butyne:

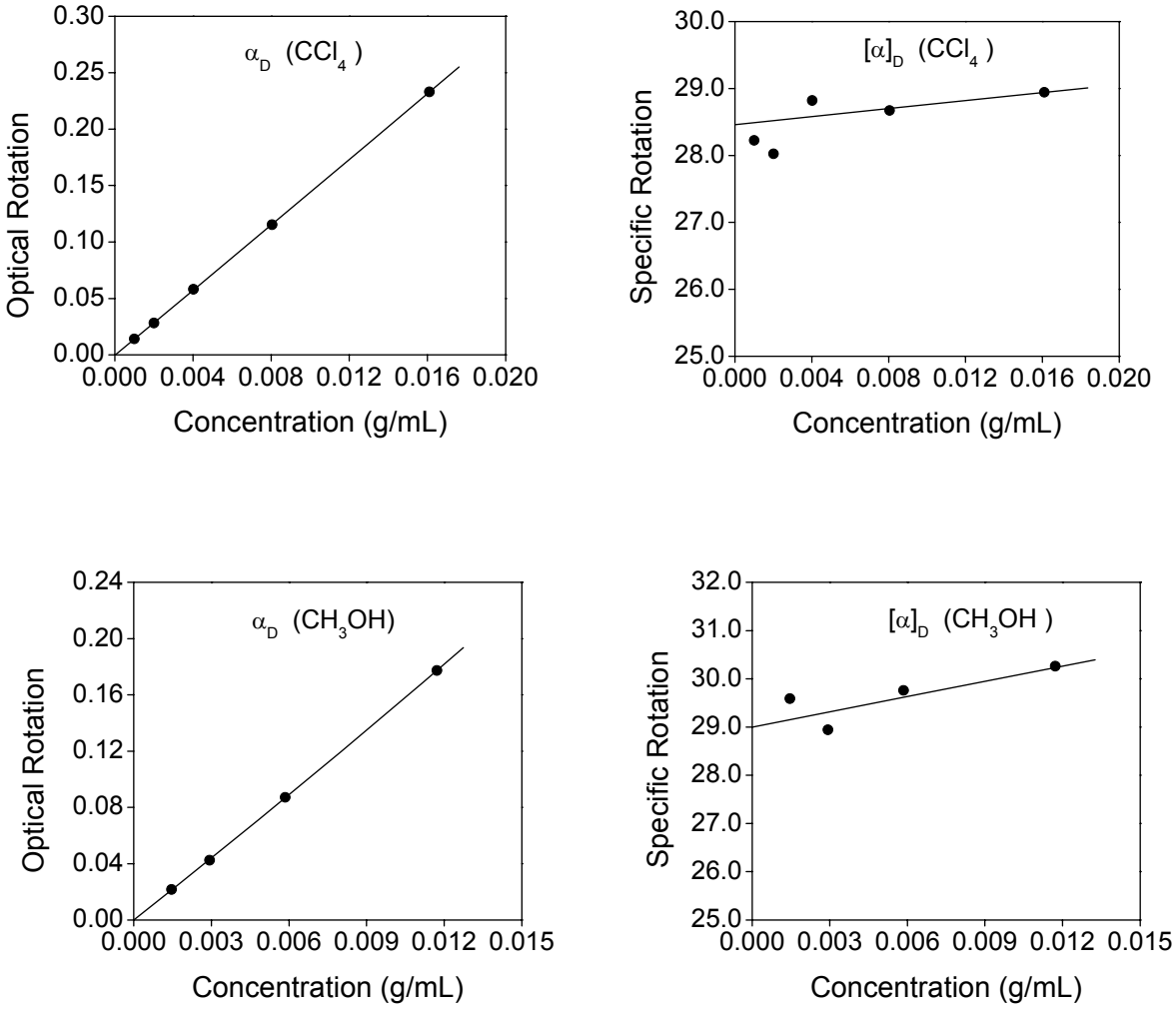

Figure 2-1. Optical rotation α_D, and specific rotation $[\alpha]_D$, of (+)-3-chloro-1-butyne as a function of concentration in CCl_4 and CH_3OH solutions. In CCl_4, α_D vs. concentration was fit to $\alpha_D=15.1c^2+14.2c$; $[\alpha]_D$ vs. concentration was fit to $[\alpha]_D=30.0c+28.4$. In CH_3OH, α_D vs. concentration was fit to $\alpha_D=52.6c^2+14.5c$. $[\alpha]_D$ vs. concentration was fit to $[\alpha]_D=105.2c+29.0$. Specific rotation vs. concentration fit used the weighted least squares method.

The concentration dependence of both optical rotation and specific rotation are displayed in Figure 2-1. The intrinsic rotations derived from these data are 28.4±0.2 in

CCl_4 and 29.0±0.3 in CH_3OH solvent. The polarization effect of solvent on the observed intrinsic rotation is quite small, as would be expected for a single conformer molecule without any H-bonding capability. The specific rotation predicted for (*R*)-3-chloro-1-butyne with B3LYP functional and a small 6-31G* basis set is 26.8 while those with large basis sets, aug-cc-pVDZ, 6-311++G(2d,2p) and aug-cc-pVTZ are 32.8, 28.3 and 28.6 respectively, as summarized in Table 2-1. The average value of three large basis set predictions is 30, which differs from the experimental value in CCl_4 by 7% and in CH_3OH by 3.5%. However, since the uncertainty in the predicted average from three large basis set calculations is ±2, it can be concluded that the experimental intrinsic rotation is within the uncertainty associated with the three large basis set predictions.

Table 2-1. B3LYP predicted specific rotation, $[\alpha]_D$, of (*R*)-3-chloro-1-butyne and experimental intrinsic rotation, $\{\alpha\}_D$, of (+)-3-chloro-1-butyne[a]

Predicted $[\alpha]_D$	6-31G*	26.8
	aug-cc-pVDZ	32.8
	6-311++G(2d,2p)	28.3
	aug-cc-pVTZ	28.6
	Average[b]	30±2
Experimental[c] $\{\alpha\}_D$	CCl_4	28.4±0.2
	CH_3OH	29.0±0.3

[a]The Gibbs energies (in Hartrees) of 3-chlorobutyne at 6-31G*, aug-cc-pVDZ, 6-311++G(2d,2p) and aug-cc-pVTZ levels of theory are, respectively, -615.512457, -615.556092, -615.598301, and -615.615345.
[b]The average value is the average results of three large basis set [aug-cc-pVDZ, 6-311++G(2d,2p) and aug-cc-pVTZ] calculations.
[c]Intrinsic rotation (specific rotation in the limit of zero concentration of solute) as derived from optical rotation vs concentration plot (see Figure 2-1).

The VA and VCD spectra predicted for (*R*)-3-chloro-1-butyne using B3LYP functional and a smaller 6-31G* basis set and three larger basis sets, aug-cc-pVDZ, 6-311++G(2d,2p) and aug-cc-pVTZ, are shown in Figure 2-2. The vibrational bands of 3-chloro-1-butyne are well separated from each other (except for bands 1 and 2), so there is minimal overlap between the bands, which makes it an ideal candidate to quantify the agreement between experimental and theoretical band intensities. In Figure 2-2, one can notice an excellent qualitative agreement between the predicted and experimental spectra.

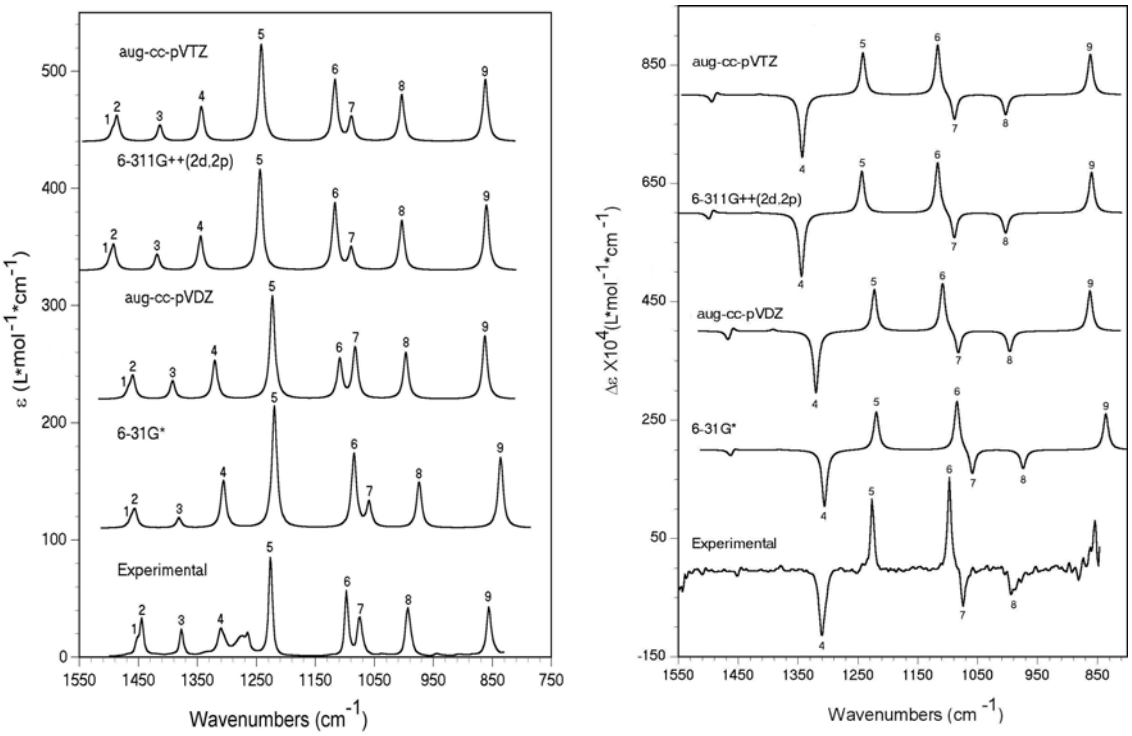

Figure 2-2. Comparison of experimental absorption (left panel) and VCD (right panel) spectra of 3-chloro-1-butyne (0.182M in carbon tetrachloride, path length 300 μm) with the predicted spectra with different basis sets. 6-31G* frequencies were scaled by 0.9613; 5 cm^{-1} band width was used in spectral simulation. Two small absorption bands seen in the experimental absorption spectrum at ~1270 cm^{-1} are due to CH_2Cl_2 impurity.

The qualitative "eyeballing" comparison between the simulated and observed VCD spectra clearly confirms the absolute configuration of (+)-3-chloro-1-butyne as (*R*). To evaluate the agreement between predicted and observed band intensities, the plots of experimental vs predicted dipole strengths and rotational strengths are shown in Figure 2-3. Here the predicted quantities in B3LYP/aug-cc-pVDZ calculation are used for illustrative purposes. As noted earlier, it is difficult to quantify the agreement between experimental observations and predicted results from these plots. Therefore we use percent differences (PDs) and root mean square percent (RMSP) differences, as defined in Equations 2-1 and 2-2. For this purpose, the frequencies, dipole strengths and rotational strengths obtained in all calculations are compared to the corresponding experimental quantities in Table 2-2. The PD and RMSP differences are summarized in Table 2-3.

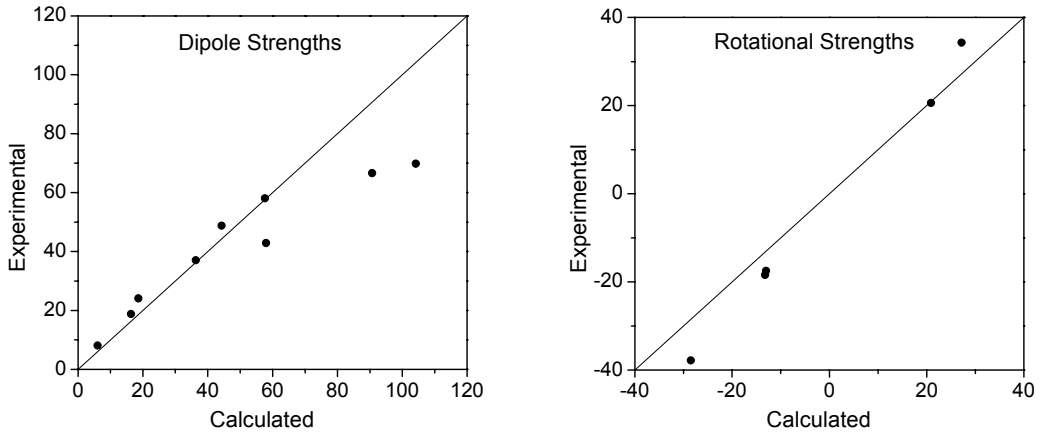

Figure 2-3. Plot of experimental vs predicted dipole strengths (left) and rotational strengths (right) for 3-chloro-1-butyne. The predicted quantities were obtained in B3LYP/aug-cc-pVDZ calculation for the (*R*)-configuration and experimental quantities were obtained for (+)-enantiomer from integrated areas using Equations 1-3 and 1-4. The solid line is of unit slope.

Table 2-2. Frequencies (ν_i), dipole strengths (D_i) and rotational strengths (R_i) for (*R*)-3-chloro-1-butyne[a]

Band No	B3LYP												Experiment		
	6-31G*			aug-cc-pVDZ			6-311++G(2d,2p)			aug-cc-pVTZ					
	ν_i	D_i	R_i	ν_i	D_i	R_i	ν_i	D_i	R_i	ν_i	D_i	R_i	ν_i	D_i	R_i
1	1522	5.0	-2.7	1467	6.0	-4.2	1499	5.4	-3.1	1494	5.5	-3.4	1452	8.1	--
2	1515	14.3	1.1	1459	18.6	2.4	1492	19.9	2.1	1496	20.1	1.9	1444	24.1	--
3	1437	8.7	0.3	1392	16.3	1.0	1418	13.9	0.4	1414	14.1	0.4	1377	18.8	--
4	1358	43.1	-26.4	1320	36.3	-28.5	1344	31.4	-29.1	1343	32.0	-28.5	1310	37.0	-37.8
5	1268	118.7	19.2	1223	104.2	20.9	1244	99.7	20.6	1242	96.4	20.9	1226	69.8	20.6
6	1128	81.3	28.1	1109	44.3	27.2	1117	74.4	28.2	1117	67.9	27.9	1097	48.8	34.3
7	1101	27.5	-14.6	1083	58.0	-13.2	1089	24.9	-14.9	1089	26.7	-14.7	1075	42.9	-18.4
8	1013	55.9	-11.7	997	57.6	-13.0	1003	61.2	-12.2	1004	57.7	-12.1	993	58.7	-17.5
9	870	100.3	26.4	863	90.7	28.7	860	93.9	29.1	862	89.8	28.9	856	66.6	--

[a]Frequencies are in cm^{-1}; dipole strengths are in 10^{-40} esu^2cm^2; rotational strengths are in 10^{-44} esu^2cm^2.

Table 2-3. Percent difference[a] between predicted and experimental frequencies, dipole strengths and rotational strengths for 3-chloro-1-butyne.

	B3LYP														
	6-31G*			aug-cc-pVDZ			6-311++G(2d,2p)			aug-cc-pVTZ			average[b]		
Band No	ν_i	D_i	R_i	ν_i	D_i	R_i	ν_i	D_i	R_i	ν_i	D_i	R_i	ν_i	D_i	R_i
1	5	-37	--	1	-26	--	3	-32	--	3	-32	--	2	-30	--
2	5	-40	--	1	-23	--	3	-17	--	4	-16	--	3	-19	--
3	4	-53	--	1	-13	--	3	-26	--	3	-25	--	2	-22	--
4	4	16	-30	1	-2	-24	3	-15	-23	3	-14	-25	2	-10	-24
5	3	70	-7	0	49	1	1	43	0	1	38	1	1	43	1
6	3	67	-18	1	-9	-21	2	52	-18	2	39	-19	2	27	-19
7	2	-36	-20	1	35	-28	1	-42	-19	1	-38	-20	1	-15	-22
8	2	-5	-33	0	-2	-26	1	4	-30	1	-2	-31	1	0	-29
9	2	50	--	1	36	--	0	41	--	1	35		1	37	--
RMSP[c]	4	46	24	1	27	22	2	34	21	2	29	22	2	26	21

[a]Percent difference is calculated according to Equation 2-1. For each of the three quantities, ν_i, D_i, and R_i. The values are rounded off to whole number.
[b]Average of aug-cc-pVDZ, 6-311++G(2d,2p) and aug-cc-pVTZ differences.
[c]Root-mean-square-percent difference (RMSP) is calculated according to Equation 2-2.

The RMSP differences for unscaled frequencies are 1%, 2%, and 2% respectively in aug-cc-pVDZ, 6-311++G(2d,2p) and aug-cc-pVTZ basis set calculations with B3LYP functional. The average frequencies from these three calculations also have a RMSP difference of 2%. For dipole strengths, RMSP differences are 27%, 34%, and 29% respectively in aug-cc-pVDZ, 6-311++G(2d,2p) and aug-cc-pVTZ basis set calculations, with the average dipole strengths from these calculations giving a RMSP difference of 26%. For rotational strengths, RMSP differences are 22%, 21%, and 22% respectively in aug-cc-pVDZ, 6-311++G(2d,2p) and aug-cc-pVTZ basis set calculations, with the average rotational strengths from these calculations giving a RMSP difference of 21%. These observations indicate that root mean square percent differences are rather large for dipole and rotational strengths. Thus, when VA and VCD spectra are used to deduce the

quantitative conformer populations in a multiple conformer molecule, one should expect large uncertainties in the populations determined there from.

In order to evaluate if large RMSP differences seen in the B3LYP calculations can be reduced by choosing another functional, calculations were repeated with B3PW91 functional and aug-cc-pVDZ basis set. For dipole and rotational strengths, the RMSP differences are found to be 36% and 34% respectively, which are larger than those obtained with B3LYP/aug-cc-pVDZ calculation. Thus we have not undertaken any further calculations with B3PW91 functional.

(-)-3-butyn-2-ol:

A comparison between experimental and B3LYP/6-31G* predicted vibrational absorption and circular dichroism spectra of (-)-3-butyn-2-ol has been reported before[33], with emphasis on determining the absolute configuration. A theoretical investigation on the influence of intermolecular H-bonding in (*S*)-(-)-3-butyn-2-ol was also reported.[34] However, quantitative determination of conformer populations in (-)-3-butyn-2-ol has not been addressed before. Three different conformations are possible for 3-butyn-2-ol, as depicted in Figure 2-4.

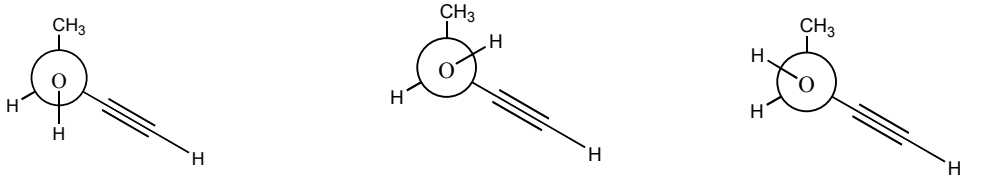

(a).Trans-methyl (b).Trans-H (c).Trans-ethynyl

Figure 2-4. Three conformations of 3-butyn-2-ol: (a). trans-methyl; (b). trans-H; (c). trans-ethynyl.

These conformations are labeled as trans-methyl, trans-H and trans-ethynyl, indicating the relative orientation of hydroxyl hydrogen atom with respect to the methyl, C*-H and ethynyl groups, respectively. The Gibbs energies, populations and specific rotations predicted for these three conformations of isolated molecule, using B3LYP functional and aug-cc-pVDZ, 6-311++G(2d,2p) and aug-cc-pVTZ basis sets are summarized in Table 2-4.

Table 2-4. B3LYP calculated Gibbs energies[a], populations, and specific rotations[b] of three conformers of isolated (*S*)-3-butyn-2-ol

		Trans-methyl	Trans-H	Trans-ethynyl
Gibbs Energy[a]	aug-cc-pVDZ	-231.15361	-231.15321	-231.15070
	6-311 ++G (2d,2p)	-231.20386	-231.20352	-231.20095
	aug-cc-pVTZ	-231.21788	-231.21752	-231.21508
Population (%)	aug-cc-pVDZ	58.7	38.6	2.7
	6-311 ++G (2d,2p)	57.2	40.2	2.6
	aug-cc-pVTZ	57.6	39.4	3.0
Specific Rotation[b]	aug-cc-pVDZ	-110.4	28.9	64.4
	6-311 ++G (2d,2p)	-88.7	29.2	84.6
	aug-cc-pVTZ	-108.4	25.2	61.4

[a]in units of Hartree
[b]$[\alpha]_D$

To evaluate the influence of solvent on these populations, Gibbs energies were also calculated (by optimizing the geometries and carrying out the vibrational frequency calculations) in CCl_4 and CH_3OH solvents using the PCM model implemented in Gaussian 03 program.[8] The population of trans-ethynyl conformer in CCl_4 solvent was predicted to be 4.4%, 4.3% and 4.7% respectively with aug-cc-pVDZ, 6-311++G(2d,2p) and aug-cc-pVTZ basis sets. This is not significantly different from ~3% predicted for isolated molecule (Table 2-4). Therefore, one can conclude that, for 3-butyn-2-ol as isolated molecule and in CCl_4 solvent, trans-ethynyl conformer population is negligibly

small (~3%), and the populations of trans-methyl and trans-H conformers are significant. In CH_3OH solvent, however, the population of trans-ethynyl conformer is predicted to be significant (12.2%, 12.9% and 13.2 % respectively with aug-cc-pVDZ, 6-311++G(2d,2p) and aug-cc-pVTZ basis sets respectively).

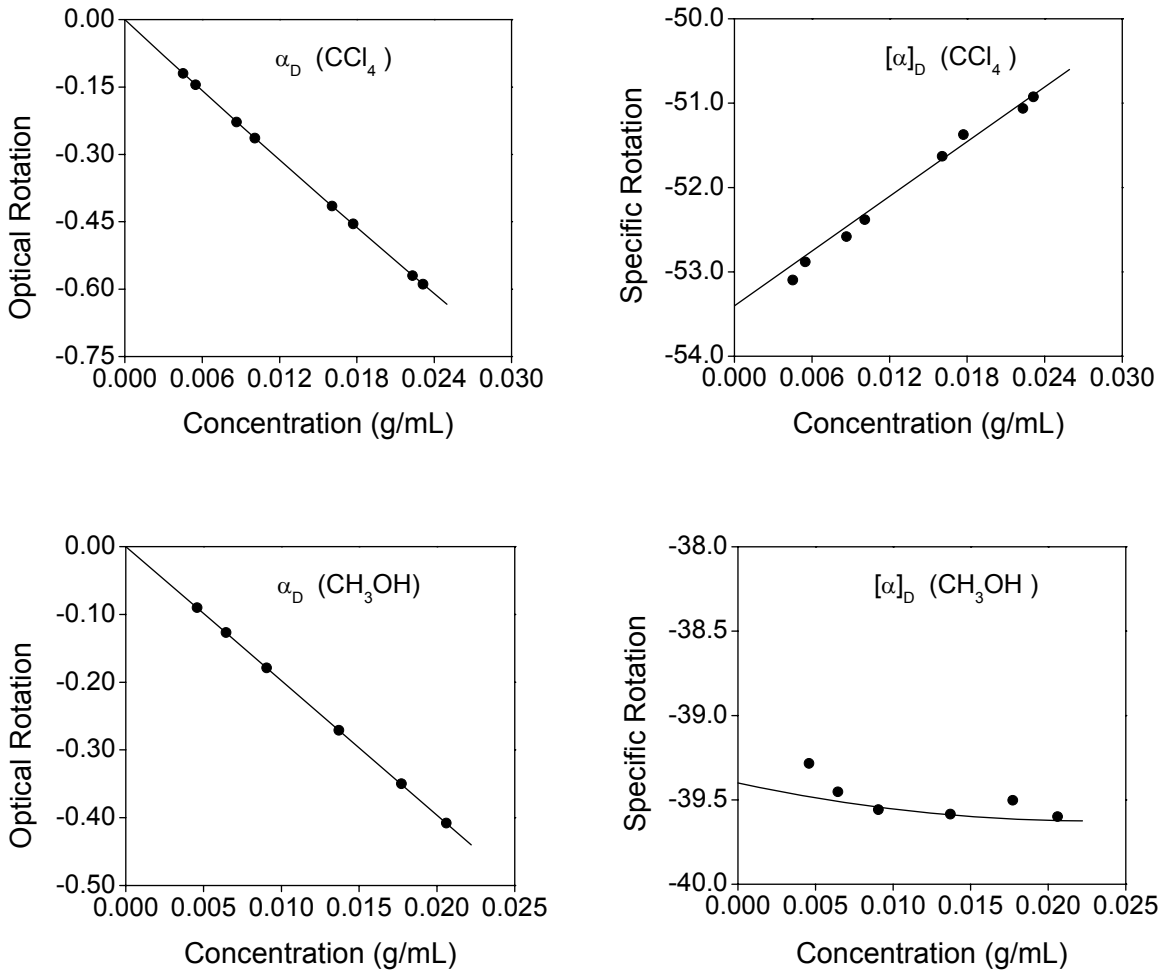

Figure 2-5. Optical rotation α_D, and specific rotation $[\alpha]_D$, of (-)-3-butyn-2-ol as a function of concentration in CCl_4 and CH_3OH solutions. In CCl_4, α_D vs. concentration was fit to $\alpha_D=54.0c^2-26.7c$; $[\alpha]_D$ vs. concentration was fit to $[\alpha]_D=108.0c-53.4$. In CH_3OH, α_D vs. concentration was fit to $\alpha_D=218.4c^3-9.9c^2-19.7c$. $[\alpha]_D$ vs. concentration was fit to $[\alpha]_D=436.8c^2-19.8c-39.3$. Specific rotation vs concentration fit used the weighted least squares method.

Table 2-5. Intrinsic rotation[a], $\{\alpha\}_D$, of (-)-3-butyn-2-ol in different environments

Environment	$\{\alpha\}_D$
Isolated[b]	-46±8
Carbon Tetrachloride[a]	-53.4±0.1
Methanol[a]	-39.3±0.3

[a]Intrinsic rotations in CCl_4 and methanol were determined from optical rotation vs concentration plot (see Figure 2-5).
[b]For isolated molecule, reported value is the specific rotation that was obtained from the average of three large basis set [aug-cc-pVDZ, 6-311++G(2d,2p), and aug-cc-pVTZ] calculations. At a given theoretical level, predicted specific rotation of each conformer was multiplied with its population obtained from the Gibbs energy at the same theoretical level and summed over all three conformations.

The concentration dependence for optical rotation and specific rotation are shown in Figure 2-5 for CCl_4 and CH_3OH solutions. The intrinsic rotation derived from these data (Table 2-5) is –53.4±0.1 in CCl_4 and –39.3±0.3 in CH_3OH. The large difference seen among the intrinsic rotations in CCl_4 and CH_3OH may be attributed to the difference in conformer populations. Although the influence (besides inducing a change in conformer populations) of hydrogen bonding between CH_3OH and 3-butyn-2-ol cannot be ruled out, it is usually very weak in dilute alcohol solution. Thus we assume that the difference in intrinsic rotation of (-)-3-butyn-2-ol in CCl_4 and CH_3OH solvents arises from conformer population difference, and determine the conformer populations in these solvents as follows. The predicted Gibbs energies for 3-butyn-2-ol in CCl_4 and CH_3OH suggest that the population of trans-ethynyl conformer is ~3% in CCl_4 and ~13% in CH_3OH. Thus, fixing the population of trans-ethynyl conformer in CCl_4 at 3% and in CH_3OH at 13%, the observed intrinsic rotation $\{\alpha\}_D$ in CCl_4 and CH_3OH were fit to the populations of the remaining conformers using the equation, $\{\alpha\}_D = X_A[\alpha]_{D,A} + (1-X_c-X_A)[\alpha]_{D,B} + X_c[\alpha]_{D,C}$, where $[\alpha]_{D,C}$ is the predicted specific rotation of conformer C (trans-ethynyl)

with fractional population X_c. The populations determined in this manner, using the specific rotations predicted in aug-cc-pVDZ, 6-311++G(2d,2p) and aug-cc-pVTZ basis set calculations, are summarized in Table 2-6. The average populations obtained in the three large basis set calculations are: 64±7 for trans-methyl and 33±7 for trans-H in CCl_4; 56±7 for trans-methyl and 31±7 for trans-H in CH_3OH. These populations represent those at infinite dilution, because intrinsic rotations are obtained at infinite dilution.

Table 2-6. Percent population of (*S*)-(-)-3-butyn-2-ol conformers[a] in different environments, deduced from intrinsic rotation.

Basis set	CCl_4		CH_3OH	
	Conformer[b]		Conformer[b]	
	A	B	A	B
aug-cc-pVDZ	60	37	52	35
6311++G(2d,2p)	72	25	65	22
aug-cc-pVTZ	60	37	52	35
Average[c]	64±7	33±7	56±7	31±7

[a]conformation labels are as follows: trans-methyl (A); trans-H (B); trans-ethynyl (C) .
[b]Population of trans-ethynyl conformer (C) was assumed to be constant at 3% in CCl_4 and at 13% in CH_3OH and the populations of trans-methyl (A) and trans-H (B) conformers were adjusted to reproduce the experimental intrinsic rotation, using predicted specific rotation for each conformer. The sum of populations of three conformers is constrained to equal 100%. The equation used is: $\{\alpha\}_D = X_A[\alpha]_{D,A} + (1-X_C-X_A)[\alpha]_{D,B} + X_C[\alpha]_{D,c}$
[c]average from three calculations.The errors reported are standard deviations.

To determine the conformer populations using VA and VCD spectra, the vibrational spectral intensities are predicted for each of the three conformers of isolated molecule using B3LYP functional and three large basis sets, aug-cc-pVDZ, 6-311++G(2d,2p) and aug-cc-pVTZ (see Table 2-7). For illustration, the simulated spectra

Table 2-7. Calculated frequencies in cm^{-1}, dipole strengths in 10^{-40} esu^2cm^2, and rotational strengths are in 10^{-44} esu^2cm^2 for three conformers of isolated (*S*)-3-butyn-2-ol at B3LYP level using three large basis sets

aug-cc-pVDZ									
	Trans-ethynyl			Trans-H			Trans-methyl		
No	ν_i	D_i	R_i	ν_i	D_i	R_i	ν_i	D_i	R_i
1	1471	7.8	-7.7	1465	24.5	-1.1	1470	5.5	4.3
2	1462	14.2	4.1	1464	2.7	2.8	1460	13.2	-4.4
3	1395	106.8	-35.0	1396	159.7	-31.9	1398	63.4	24.9
4	1385	23.4	-1.2	1385	24.1	-3.5	1372	97.3	65.5
5	1326	17.8	-17.3	1324	33.1	17.6	1331	43.5	0.3
6	1240	177.7	53.3	1253	30.9	13.1	1271	142.2	-64.3
7	1115	310.7	-13.9	1118	223.5	-54.8	1123	141.3	-18.5
8	1089	107.0	19.6	1089	90.1	-6.0	1075	32.4	34.4
9	1033	22.2	-1.0	1030	248.7	-5.8	1041	233.0	-14.6
10	928	148.1	3.0	923	54.3	6.5	929	110.9	3.1
6-311++G(2d,2p)									
	Trans-ethynyl			Trans-H			Trans-methyl		
No	ν_i	D_i	R_i	ν_i	D_i	R_i	ν_i	D_i	R_i
1	1502	7.1	-7.0	1496	1.3	0.4	1502	6.2	4.0
2	1493	15.2	3.5	1495	24.0	0.7	1491	13.4	-4.2
3	1416	72.5	-18.4	1413	130.0	-37.2	1416	35.3	5.9
4	1409	37.1	-15.9	1409	45.0	7.6	1395	110.0	83.3
5	1348	16.7	-16.9	1345	29.2	14.0	1355	32.0	-2.4
6	1252	170.4	37.5	1275	33.1	9.5	1283	160.9	-61.0
7	1122	266.5	-7.2	1126	211.1	-49.0	1132	122.4	-17.9
8	1095	137.4	19.9	1089	56.3	-11.8	1088	27.0	32.6
9	1034	41.1	1.2	1035	313.9	-4.8	1033	274.2	-11.1
10	929	163.4	5.8	925	65.6	5.2	931	117.0	4.5
aug-cc-pVTZ									
	Trans-ethynyl			Trans-H			Trans-methyl		
No	ν_i	D_i	R_i	ν_i	D_i	R_i	ν_i	D_i	R_i
1	1497	6.0	-4.9	1491	2.3	2.0	1497	6.1	4.2
2	1488	15.0	2.9	1490	22.4	-0.8	1486	13.5	-4.4
3	1410	75.2	-13.4	1407	83.9	-35.2	1411	33.0	4.2
4	1405	42.7	-18.2	1404	90.2	6.3	1390	108.0	81.4
5	1346	16.2	-15.4	1343	29.4	13.2	1352	30.5	-3.5
6	1245	165.7	40.1	1267	32.4	10.6	1277	161.5	-59.5
7	1121	272.2	-11.1	1125	203.6	-52.3	1131	119.2	-18.4
8	1094	142.0	19.0	1088	58.7	-11.5	1086	25.7	31.7
9	1034	36.3	3.3	1033	312.0	-3.2	1032	274.2	-9.4
10	929	169.6	3.3	926	63.0	3.6	931	116.8	2.8

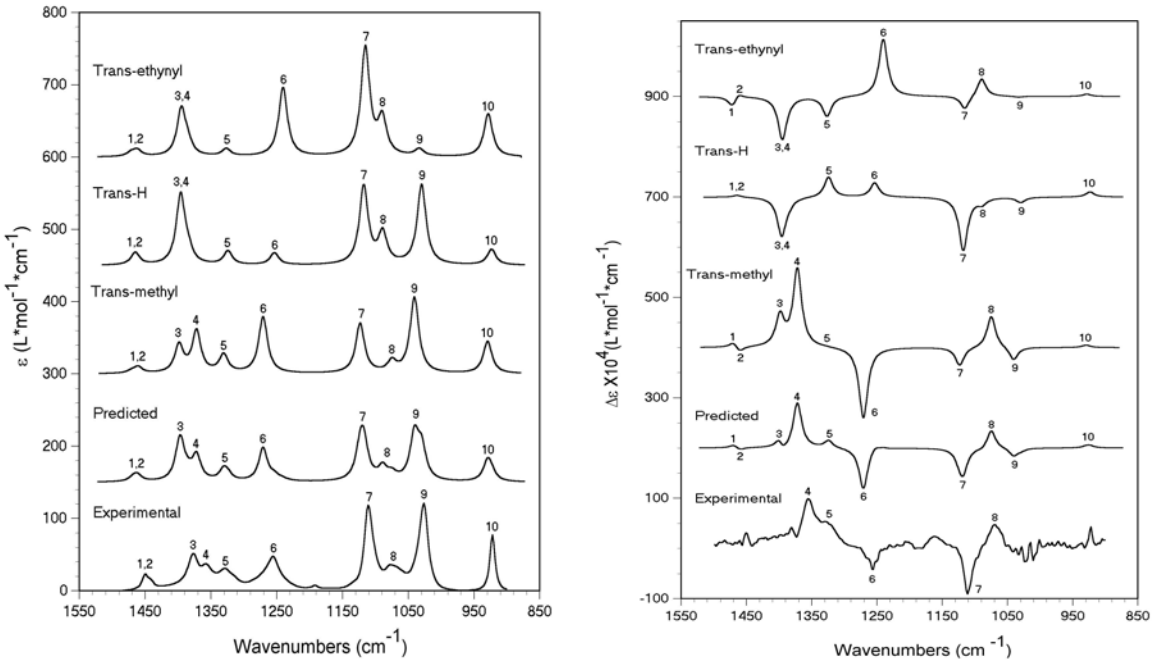

Figure 2-6. Comparison of experimental absorption (left) and VCD (right) spectra of 3-butyn-2-ol (0.103M in carbon tetrachloride, path length 500 μm) with the simulated absorption spectra (B3LYP/aug-cc-pVDZ, 8 cm^{-1} band width was used in spectral simulation) for individual conformers and with the predicted absorption spectrum (population weighted sum of conformer spectra). Populations determined from the Gibbs energies (Table 2-4) are used in obtaining the predicted spectrum.

for individual conformers obtained for (*S*)-3-butyn-2-ol in B3LYP/aug-cc-pVDZ calculation are compared to the corresponding experimental spectra of (-)-3-butyn-2-ol in Figure 2-6. The predicted spectrum (which is obtained as the population weighted sum of individual conformer spectra, using populations obtained from Gibbs energies of isolated molecule) is also displayed in these figures. The band numbers listed in these spectra provide correlation between the experimental bands and the corresponding theoretical bands. The qualitative "eyeballing" comparison between the simulated and observed VCD spectra clearly confirms the absolute configuration[33] of (-)-3-butyn-2-ol as (*S*). For quantitative comparison, the experimental frequencies, dipole strengths and

Table 2-8. Experimental[a] frequencies, dipole strengths, and rotational strengths of (-)-3-butyn-2-ol and their correlation to B3LYP predicted quantities for (*S*)-3-butyn-2-ol in aug-cc-pVDZ calculation.

	Experimental			aug-cc-pVDZ								
				trans-ethynyl			trans-H			trans-methyl		
No	ν_i	D_i	R_i	ν_i	D_i	R_i	ν_i	D_i	R_i	ν_i	D_i	R_i
1,2	1448	32.1	--	1471, 1462	22.0	--	1465, 1464	27.2	--	1470, 1460	18.7	--
3	1377	95.7	--	1395, 1385	130.2	--	1396, 1385	180.8	--	1398	63.4	--
4	1356	45.8	44.8	--	--	--	--	--	--	1372	97.3	65.5
5	1327	82.5	39.2	1326	17.8	-17.3	1324	33.1	17.6	1331	43.5	0.3
6	1257	144.2	-20.0	1240	177.7	53.3	1253	30.9	13.1	1271	142.2	-64.3
7	1110	220.5	-44.2	1115	310.7	-13.9	1118	223.5	-54.8	1123	141.3	-18.5
8	1072	128.0	38.1	1089	107	19.6	1089	90.1	-6.0	1075	32.4	34.4
9	1027	258.6	--	1033	22.2	--	1030	248.7	--	1041	233	--
10	922	101.7	--	928	148.1	--	923	54.3	--	929	110.9	--

[a]frequencies are in cm^{-1}, dipole strengths are in $10^{-40}esu^2cm^2$, rotational strengths are in $10^{-44}esu^2cm^2$

Table 2-9. Percent population of trans-methyl conformer[a] of (*S*)-(-)-3-butyn-2-ol, deduced from vibrational absorption and circular dichroism intensities.

B3LYP/ Basis set	Percent Population of trans-methyl conformer			
	I[b]		II[c]	
	absorption	VCD[d]	absorption	VCD[d]
aug-cc-pVDZ	60±30	55±34	61±27	62±41
6311++G(2d,2p)	52±42	51±37	54±40	60±42
aug-cc-pVTZ	51±41	52±37	52±40	61±41
average	54±37	53±36	56±36	61±41

[a]trans-ethynyl conformer population was assumed to be 3% and sum of the populations of three conformations is constrained to equal 100%. The equation used for fitting is: $E_i = k[X_A P_{A,i} + (1-X_A-0.03)P_{B,i} + 0.03 P_{C,i}]$ where E_i and P_i are experimental and predicted band intensities, k is a multiplicative variable, X_A, X_B and X_C are fractional populations of trans-methyl, trans-H and trans-ethynyl conformations.
[b]Using predicted intensities for isolated molecule; The average value of k obtained from the absorption intensity data in three basis set calculations is 1.12 (0.27).
[c]Using predcited intensities in CCl_4 solvent with PCM model; The average value of k obtained from the absorption intensity data in three basis set calculations is 0.88 (0.20).
[d]Band number 5 was not used in the regression; k value obtained in the absorption fit was fixed as constant in the VCD intensity fit.

rotational strengths are summarized in Table 2-8 along with their correlation to aug-cc-pVDZ predictions. It is to be noted that experimental band number 4 originates from trans-methyl conformer, so one can estimate the population of trans-methyl conformer from this band alone by comparing its experimental band intensity with the corresponding predicted band intensity. Thus, using the intensities predicted in aug-cc-pVDZ calculation for band number 4, one would get the population of trans-methyl conformer as 47% from dipole strengths and as 68% from rotational strengths. However, since a predicted population should reproduce the entire experimental spectrum quantitatively, the population predicted from one band intensity would not be a true measure. For this reason, we used a regression method, utilizing Equation 2-3 and fixing the population of trans-ethynyl conformer at 3%. Since path lengths used for VA and VCD measurements are usually very small (of the order of few hundred microns), and low concentrations are used to avoid aggregation effects, any error in these quantities may influence the populations. Thus a multiplicative variable, k, is introduced into the regression analysis. The equation used for regression analysis is $E_i = k[X_A\ P_{A,i}+(1-X_A-0.03)P_{B,i}+0.03\ P_{C,i}\ ]$, where conformer C is trans-ethynyl. The populations derived from regression analysis and associated uncertainties, at 95% confidence level, are summarized in Table 2-9. Large uncertainties, as expected earlier from the quantitative comparison for 3-chloro-1-butyne, are obtained here for the populations. The uncertainties in populations are slightly higher if the multiplicative variable k was not included in the regression analysis. These large uncertainties are a direct result of the discrepancies (see Figure 2-6) among predicted and observed vibrational band intensities. While for some bands, the experimental and predicted band intensities are close to each other, for other

bands significant differences remain. Thus, overall quantitative agreement between experimental and predicted VA and VCD intensities is not as good as one would like.

In order to evaluate the role of solvent on predicted vibrational absorption and VCD intensities, we have repeated the B3LYP calculations (using aug-cc-pVDZ, 6-311++G(2d,2p), and aug-cc-pVTZ basis sets) of frequencies, absorption intensities and VCD intensities using CCl_4 solvent in PCM model. The populations obtained from these data are also included in Table 2-9. It is evident that the use of intensities predicted with PCM model does not improve the errors estimated for populations. We have not pursued calculations with B3PW91 functional for 3-butyn-2-ol, as this functional did not lead to any improved results for 3-chloro-1-butyne.

In summary, for substituted butynes studied here, the absolute configuration could be established in a straightforward manner using either intrinsic rotation or VCD intensities in conjunction with quantum mechanical prediction of the corresponding properties. The predicted specific rotation for (+)-3-chloro-1-butyne is in excellent quantitative agreement with observed intrinsic rotation. The predicted VA and VCD intensities for 3-chloro-1-butyne differed from the corresponding experimental quantities with an RMSP difference of ~20-30%. Similar observations are noted for (-)-3-butyn-2-ol, where the errors in populations determined from intrinsic rotation of (-)-3-butyn-2-ol are not large. But when the populations were derived from VA and VCD intensities, the error associated with the determined conformer populations is found to be much larger. Some caution must be exercised in generalizing the success noted here for substituted butynes with specific rotation, because for an apparently similar molecule, (-)-3-chloro-1-butene, the predicted specific rotations were reported[22] to be different from observed

specific rotations by a factor of 2.6. Thus more investigations are needed to establish the generality of small errors noted for conformer populations determined from the combined use of intrinsic rotation and specific rotation.

Conclusion

One of the smallest chiral molecules with a single conformer, (+)-3-chloro-1-butyne, has been synthesized for the first time and its absolute configuration is determined from specific rotation and vibrational circular dichroism as (*R*). A quantitative comparison between experimental and predicted vibrational band intensities in VA and VCD spectra reveal that root mean square percent differences are rather large (~30). On the other hand, the experimental intrinsic rotation of (+)-3-chloro-1-butyne is within the uncertainties associated with specific rotation predicted by large basis sets using B3LYP functional. Similar studies, using specific rotation, VA and VCD on a related molecule (-)-3-butyn-2-ol, with three different conformers, indicate that the absolute configuration of this molecule is (*S*). The population for trans-methyl conformer, determined from observed intrinsic rotation in CCl_4 and predicted specific rotations using large basis sets with B3LYP functional, is 64±7%. The analogous population determined from VA and VCD intensities is close to that determined from intrinsic rotation, but uncertainty in the deduced population is substantially larger.

CHAPTER III

DETERMINING THE CONFORMER POPULATION OF (R)-(+)-3-METHYLCYCLOPENTANONE USING VIBRATIONAL ABSORPTION, VIBRATIONAL CIRCULAR DICHROISM, AND SPECIFIC ROTATION

Introduction

Five-member ring compounds attracted a lot of attention because they can be found in a wide variety of natural products, such as steroids[35, 36] and alkaloids[37]. Several studies on their structure have been reported before. Conformational analysis of five member ring molecules is an interesting and challenging subject. Different methods, including electron diffraction[38], infrared absorption spectroscopy[39], and nuclear magnetic resonance (NMR)[40] have been used to analyze the conformations of these compounds.

In particular, cyclopentanone and substituted cyclopentanones have attracted much attention because of the interesting conformation of cyclopentanone ring. Furthermore 3-methylcyclopentanone has exhibited[41] anticonvulsant activity, suggesting an important medicinal role for this molecule. It is not known if the conformation or absolute configuration of 3-methylcyclopentanone has any role in its anticonvulsant activity. Nevertheless, the conformations of this molecule have been a subject of research interest since very early days. Djerassi and coworkers[42] found that the magnitude of electronic circular dichroism (ECD) of (+)-3-methylcyclopentanone increased upon lowering the temperature, indicating a conformational equilibrium at room temperature. Richardson and coworkers[43] considered the twisted conformation with equatorial-methyl and axial-methyl group and planar conformation of (+)-3-methylcyclopentanone to explain the observed ECD using INDO molecular orbital model. Their calculations

indicated that axial-methyl conformation is favored over other conformations. Li suggested[44] that the microwave spectrum of 3-methylcyclopentanone can be satisfactorily explained by the twisted conformation with equatorial-methyl group and estimated that this conformation would have an energy at least 250 cm^{-1} (~3 kJ/mol) lower than other conformers. More recently Fourier transform microwave spectrum has been reported[45] for 3-methylcyclopentanone, but conformational issue was not addressed. Using experimental and ab initio predicted vibrational Raman optical activity spectra, Polavarapu et al concluded[46] that the major features in the observed spectrum can be explained by the twisted conformation with equatorial-methyl group. In resonance enhanced multiphoton ionization spectrum of 3-methylcyclopentanone, Potts et al identified[47] both equatorial-methyl and axial-methyl conformers, with equatorial-methyl form being dominant. Their ab initio calculations also suggested that equatorial-methyl form is energetically favored. The equatorial-methyl conformer was also used[12, 48-50] to compare the predicted specific rotations for (3R)-methylcyclopentanone with experimental specific rotation of (+)-methylcyclopentanone. The first experimental study[51] to determine the energy difference between axial-methyl and equatorial-methyl conformers of 3-methylcyclopentanone appears to be that of Kim and Baer, where they have used resonance enhanced multiphoton ionization (REMPI) spectroscopy and determined the ΔH^o to be 4.98 ± 0.59 kJ/mol at 323 K. The twisted conformation with equatorial-methyl group was suggested to be more populated than that with axial-methyl group at room temperature. These observations were supported by their ab initio calculations. 3-methylcyclopentanone has also been used[52] as one of the systems to monitor the charge transfer reactions between chiral Rydberg atoms and chiral molecules,

although the focus was not on the conformational issues. The near infrared (1300nm-800nm) circular dichroism spectra of (R)-3-methylcyclopentanone were reported and analyzed.[53, 54] Molecular mechanics calculations on 3-methylcyclopentanone were also reported before.[55]

Vibrational spectroscopy has been widely used for conformational analysis[56] of organic molecules. If vibrational bands characteristic of conformers can be identified, then the intensities of those bands as a function of temperature can be used to determine the energy difference between conformers. The identification of characteristic conformer bands in the experimental spectra is facilitated by the availability of accurate quantum mechanical methods for predicting the vibrational properties. Despite these developments, vibrational absorption spectra have not been employed for determining the energy differences between conformers or to obtain the conformer populations of 3-methylcyclopentanone. In recent years, vibrational circular dichroism (VCD)[57, 58] has emerged as a valuable tool for conformational analysis. Here the experimental VCD spectra are analyzed using the corresponding DFT predicted VCD spectra. Some examples of conformation analyses using VCD have appeared in the literature[16-20], but quantitative estimates of conformer populations are lacking.

In addition to vibrational absorption and VCD, the experimental measurement and quantum theoretical prediction of specific rotation may also be used to analyze the conformer populations. The first ab initio prediction of specific rotation and subsequent developments employing density functional methods has lead to a renewed interest in the use of specific rotation for structural analyses.[22, 59-62] In this chapter, we use the vibrational absorption, vibrational circular dichroism, and specific rotation methods to

analyze the conformers of (R)-(+)-3-methylcyclopentanone. Both experimental measurements and quantum theoretical predictions are presented and analyzed.

Experimental Section

The vibrational absorption and VCD spectra were recorded on Chiral*ir*. The sample was held in a variable path length cell with BaF_2 windows. The sample concentration and path length are 1.4 M in CCl_4 and 100 μm respectively. The spectra were recorded with 3-hour data collection time at 4 cm^{-1} resolution. In the absorption spectrum presented here the solvent absorption was subtracted. In the presented VCD spectrum, the baseline was obtained from VCD measurement for solvent under identical conditions. Optical rotations were measured on Autopol III (in CCl_4 and CH_3OH solvents) or Autopol IV (in CH_3CN solvent) polarimeters at sodium D line (589nm), using a 0.5 dm cell. The intrinsic rotation (specific rotation at infinite dilution) was extracted from the optical rotations at different concentrations as described in detail in Chapter II. The concentration range studied for optical rotation measurements was 0.05-0.19 M in CCl_4, 0.06-0.25 M in CH_3OH, and 0.06-0.44 M in CH_3CN.

Geometry optimizations and VCD calculations are similar to the calculation mentioned in Chapter II. The regression method used for conformer population analysis is also described in detail in Chapter II.

Results and Discussion

Conformers: The two major conformers of (R)-3-methylcyclopentanone, namely equatorial-methyl and axial-methyl, were optimized with B3LYP functional and 6-31G*,

aug-cc-pVDZ, 6-311++G(2d,2p) and aug-cc-pVTZ basis sets. The structures for the two conformers and atomic numbering are shown in Figure 3-1.

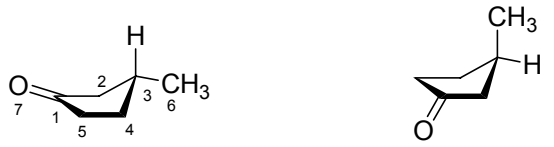

Equatorial-methyl Axial-methyl

Figure 3-1. Conformers of (R)-3-methylcyclopentanone.

Table 3-1. The Gibbs energies and populations of conformers of (R)-3-methylcyclopentanone obtained with B3LYP functional and different basis sets.

	Conformer[b]	6-31G*	aug-cc-pVDZ	6-311++G(2d,2p)	aug-cc-pVTZ
Enthalpy, H[a]	1	-309.730654	-309.769788	-309.833518	-309.850720
	2	-309.728656	-309.767850	-309.831579	-309.848693
ΔH^o		5.25[c]	5.09[c]	5.09[c]	5.32[c]
Gibbs Energy, G[a]	1	-309.769505	-309.808733	-309.872402	-309.889599
	2	-309.767473	-309.806761	-309.870418	-309.887524
ΔG^o		5.34[c]	5.18[c]	5.21[c]	5.45[c]
Percent Population	1	89.6	89.0	89.1	90.0
	2	10.4	11.0	10.9	10.0

[a]at 298 K, 1 atm (in atomic units); [b]1: equatorial-methyl; 2: axial-methyl; [c] in kJ/mol (axial-equatorial)

Vibrational frequencies, absorption intensities and rotational strengths were calculated at each of the two optimized geometries using the same functional and basis set. The Gibbs energies and population of these two conformations are listed in Table 3-1. The populations obtained with the three large basis sets are close to each other. Conformer 1 has about 90% population and conformer 2 has about 10% population.

Vibrational absorption and VCD spectra: The experimental vibrational absorption and VCD spectra of (+)-3-methylcyclopentanone were measured in CCl_4 solution. The calculated absorption and VCD spectra, obtained with all four basis sets, for (R)-3-methylcyclopentanone, are shown in Figure 3-2, along with the corresponding experimental spectra for (+)-enantiomer. The agreement between the experimental and calculated spectra is very good except for the strongest peak (around 1150 cm^{-1}) obtained in B3LYP/aug-cc-pVDZ calculation. The B3LYP/aug-cc-pVDZ spectra show two peaks in both absorption and VCD spectra at ~1150 cm^{-1}, but the experimental spectrum shows only one corresponding peak.

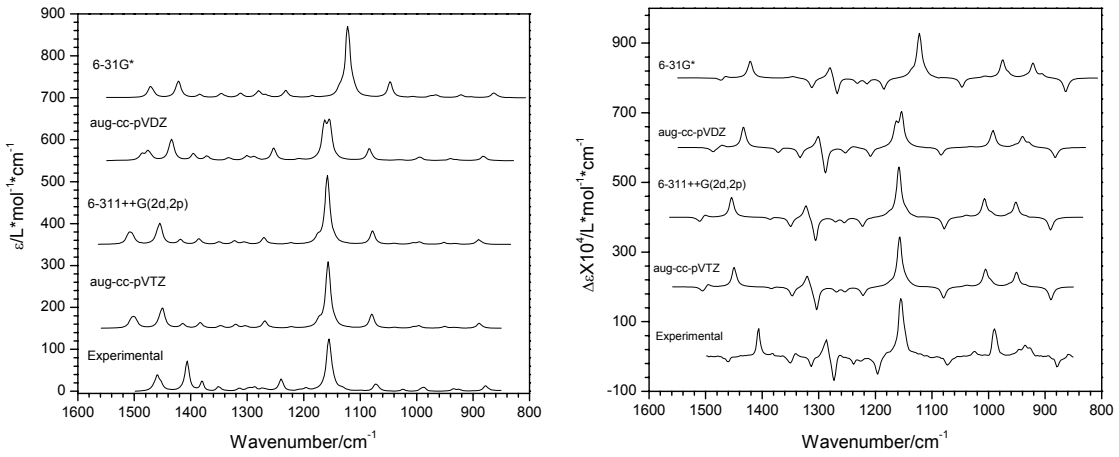

Figure 3-2. The experimental (bottom trace) and predicted (top four traces) spectra of (R)-(+)-3-methylcylcopentanone. 6-31G* frequencies were scaled with 0.9613; aug-cc-pVDZ, 6-311++G(2d,2p) and aug-cc-pVTZ frequencies were not scaled. *Left panel*: Absorption spectra; *Right panel*: VCD spectra

To derive the populations from VA and VCD spectra, the correspondence between experimental and calculated bands needs to be identified. If the difference between predicted vibrational band positions of two conformers is less than 5 cm^{-1} then they are treated as corresponding together to one experimental band. If the difference is

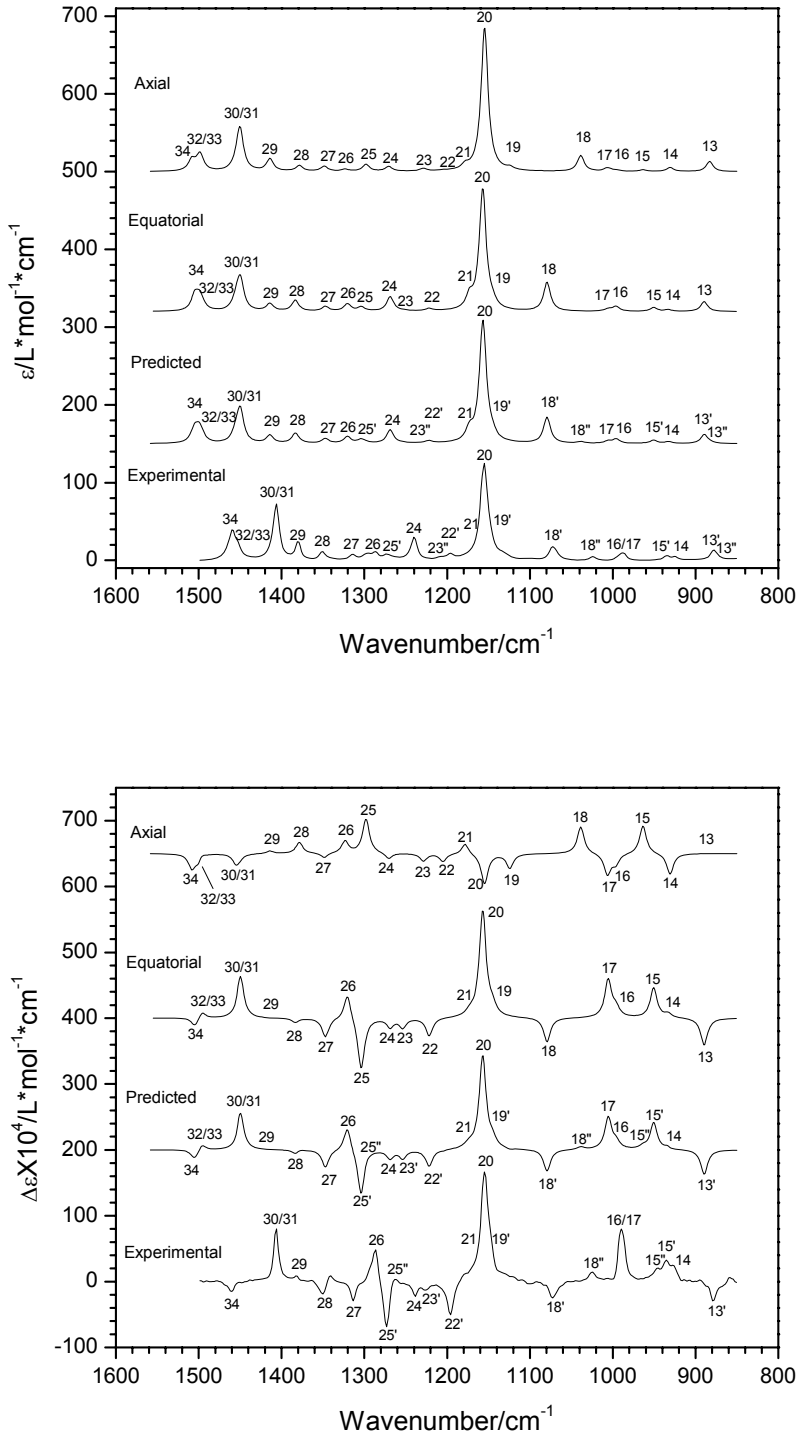

Figure 3-3. Correlation between the predicted spectra obtained at B3LYP/aug-cc-pVTZ level and the experimental spectra. Top panel: Absorption spectra; Bottom Panel: VCD spectra.

Table 3-2. The frequencies[a], dipole strengths[b], and rotational strengths[c] of (R)-(+)-3-methylcyclopentanone.

No.	Experimental			B3LYP/aug-cc-pVTZ					
				equatorial-methyl			axial-methyl		
	ν_i	D_i	R_i	ν_i	D_i	R_i	ν_i	D_i	R_i
13”	873	3.3	---	---	---	---	883	21.2	0.1
13’	878	18.4	-10.1	890	20.6	-16.8	---	---	---
14	925	5.9	6.6	933	3.3	2.4	931	7.7	-12.4
15’	935	7.8	8.8	951	7.3	17.3	---	---	---
15”	946	---	5.5	---	---	---	963	3.1	16.1
16	988	14.6	24.9	996	8.8	4.7	996	2.2	-5.4
17				1005	4.2	20.7	1006	6.2	-11.5
18”	1024	5.4	4.0	---	---	---	1039	28.3	14.4
18’	1072	23.2	-7.8	1079	49.8	-12.3	---	---	---
19”	---	---	---	---	---	---	1124	4.4	-7.0
19’	1148	17.7	9.2	1145	8.4	4.1	---	---	---
20	1155	138.5	41.6	1157	195.5	50.7	1155	232.1	-14.4
21	1161	10.5	5.2	1173	20.1	2.0	1178	7.4	5.1
22”	---	---	---	---	---	---	1205	0.9	-3.5
22’	1196	6.0	-13.2	1222	3.6	-8.1	---	---	---
23”	1205	0.9	---	---	---	---	1229	3.8	-3.3
23’	1226	---	-2.8	1254	0.8	-4.1	---	---	---
24	1240	28.5	-4.7	1269	21.1	-3.8	1271	6.9	-2.5
25”	1264	---	2.6	---	---	---	1298	9.8	14.5
25’	1272	5.0	-16.6	1304	5.8	-21.7	---	---	---
26	1287	7.4	12.3	1320	10.2	11.0	1323	2.8	5.0
27	1314	4.1	-6.4	1347	6.4	-7.7	1348	6.8	-1.9
28	1350	7.2	-4.8	1383	14.7	-1.7	1378	7.5	4.4
29	1380	17.6	1.0	1414	9.8	-0.2	1414	16.0	1.0
30	1407	65.8	14.5	1450	40.3	16.1	1450	53.6	-1.2
31				1455	13.3	-0.6	1455	6.9	-3.7
32	1453	14.3	---	1496	5.2	2.4	1498	16.1	2.7
33				1499	14.7	-0.2	1500	6.0	-4.3
34	1460	33.7	-3.6	1505	18.1	-3.0	1508	13.3	-5.2

[a]frequencies, ν_i, in cm^{-1}; [b]dipole strengths, D_i, in 10^{-40} esu^2cm^2;[c]rotational strengths, R_i, in 10^{-44} esu^2cm^2.

larger than 5 cm^{-1}, then they are treated as corresponding to two separate experimental bands. We use prime ‘ to indicate the bands coming from equatorial-methyl conformer, and double prime “ to indicate the bands coming from axial-methyl conformer. The correspondence between experimental bands and B3LYP/aug-cc-pVTZ predicted peaks,

following the above criterion, is summarized in Figure 3-3 and Table 3-2. The numbering of bands is based on the predicted vibrational frequencies with lowest predicted vibrational frequency being band number 1.

The bands 18' and 18" are of special significance because they originate from equatorial-methyl and axial-methyl conformers respectively and are well separated from each other (unlike other bands of these conformers). The vibrational origins of these two bands involve the 3-methyl group, which has different orientations in the two conformers. The 18' band originates from C-C bond stretch between 3-methyl group and ring deformation. The 18" band originates from $-CH_3$ wag and ring deformation. These two bands serve as conformer markers.

Experimental determination of Conformer Populations: In the following discussion, results obtained from three different approaches to determine the conformer populations will be presented. These are based on (1). Temperature dependent vibrational absorption band intensities, (2). Regression analysis of experimental and DFT predicted vibrational band intensities and (3). Analysis of experimental intrinsic rotation and DFT predicted specific rotations.

(1). *Temperature dependent vibrational absorption band intensities*: If the vibrational absorption bands due to individual conformers can be identified then the temperature dependence of their experimental intensities can be used to obtain ΔH^o. The bands 18' and 18", assigned to the equatorial-methyl and axial-methyl conformers, are appropriate for this purpose because they are isolated and separated from each other. To avoid the problems associated with solvent interference in the infrared absorption spectra,

we have investigated the temperature dependent spectra for neat liquid sample (Figure 3-4). The areas of bands 18' and 18", as a function of temperature were used for preparing

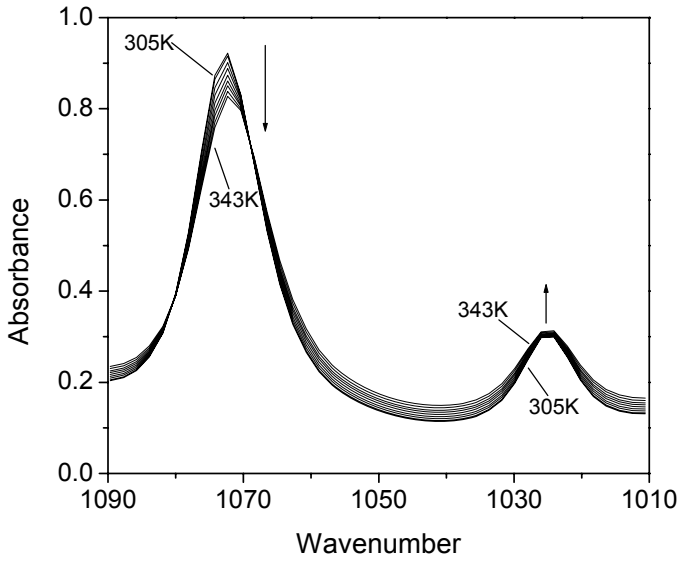

Figure 3-4. Temperature dependent absorption spectra between 305 and 343 K at ~5 degree intervals of liquid (+)-3-methylcyclopentanone. The absorption bands at 1072 cm^{-1} and 1024 cm^{-1} are assigned to equatorial and axial conformations, respectively, of 3-methylcyclopentanone and are labeled as 18' and 18" in text and Table 3-2. Arrows indicate the direction of intensity change.

the van't Hoff plot (see Figure 3-5). From this plot, $\Delta H°$ is found to be 4.84±0.08 kJ/mol. This value is very close to the value of 4.98 ± 0.59 kJ/mol obtained[51] from REMPI spectra of gas phase sample. Since the ΔH^o values obtained in the gas phase[15] and the present liquid phase measurements for methylcyclopentanone are the same (within experimental uncertainties), it is reasonable to assume that this ΔH^o value will apply for liquid solution in CCl_4 as well. The predicted ΔH^o values (Table 3-1) at 298 K in the current B3LYP calculations with aug-cc-pVDZ, 6-311++G(2d,2p) and aug-cc-pVTZ basis sets for isolated molecule are very close to the experimental value. The entropy

term, $T\Delta S^o$ at room temperature is negligible compared to ΔH^o as can be inferred from $\Delta G^o \sim \Delta H^o$ in Table 3-1. Then the experimental $\Delta H°$ value gives the populations as 87% for equatorial-methyl and 13% for axial-methyl conformers, with error estimated at less than 1%.

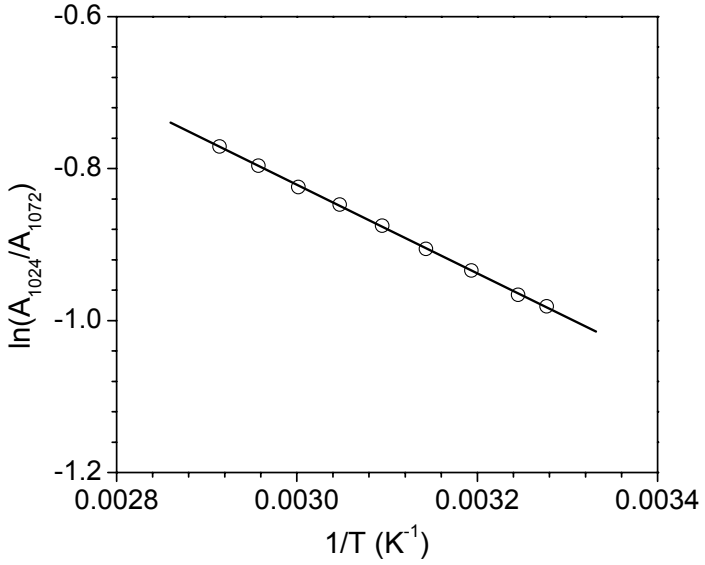

Figure 3-5. The van't Hoff plot obtained from the integrated areas of 1072 cm^{-1} and 1024 cm^{-1} bands assigned to equatorial-methyl and axial-methyl conformations, respectively at different temperatures. The circles represent the experimental data points and the solid line represents the equation, $\ln(A_{1024}/A_{1072}) = -582.7/T+0.927$. $\Delta H°$ derived from the slope is 4.84±0.08 kJ/mol.

(2). *Regression analysis of experimental and DFT predicted vibrational band intensities*: The calculated vibrational dipole strengths and rotational strengths from the largest basis set used in this study, B3LYP/aug-cc-pVTZ, are considered to be most accurate. Using the ratio of intensities for 18' and 18" bands obtained in this B3LYP/aug-cc-pVTZ calculation, the observed ratio for the corresponding experimental bands yields the population ratio of equatorial-methyl to axial-methyl conformer as 71:29, from absorption and 70:30 from VCD. However, this is based on only one each of the many

vibrational bands of the two conformers. If the predicted intensities happen to be in error for one or both of these two bands, then the conclusion on populations will be in error as well. To avoid such possibility, one has to consider as many vibrational bands as possible in the analysis. For using all vibrational bands possible in the analysis, we used Equations 2-3 and 2-4 with the correspondence between experimental bands and calculated peaks as shown in Figure 3-3 and Table 3-2 . Although several options have been attempted in the least square fitting between observed and calculated intensities, only two different options will be presented and discussed here. (a). Treating the bands 19', 20 and 21 together as one band or (b). Treating the bands 19', 20 and 21 as separate bands. The results are shown in Table 3-3.

Table 3-3. The population (X_e) of equatorial-methyl conformer of (R)-(+)-3-methylcyclopentanone determined from absorption and VCD spectra.

quantity[a]	Absorption		VCD	
	Normal[b]	Modified[c]	Normal[b]	Modified[c]
k	0.74±0.10	0.77±0.08	0.93±0.30	1.00±0.30
X_e	0.89±0.36	0.79±0.37	0.91±0.21	0.94±0.22
R^2	0.903	0.943	0.928	0.950

[a]k is the correction factor used to account for errors in concentration and path length; X_e is the fractional population of equatorial-methyl conformer; R^2 is the goodness of fit (1 for perfect fit). [b]with correspondence between experimental and predicted bands as in Table 3-2. [c]correspondence in Table 3-2 modified with peaks 19', 20, 21 combined together as one peak.

Judging from the correlation coefficient, R^2 the fit which combined the bands 19', 20, and 21 together is preferred. Irrespective of the option used, the error in the population determined from absorption band intensities is larger than that in the population determined from VCD intensities. This observation is consistent with that

noted earlier for a single conformer molecule 3-chloro-1-butyne in Chapter II. The deviations between calculated and experimental intensities is larger for absorption than that for VCD. In addition, the larger error in the population determined from absorption band intensities (than that determined from VCD band intensities) of 3-methylcyclopentanone may also arise from the similarity of the absorption spectra predicted for equatorial-methyl and axial-methyl conformers. When the spectra of the two conformers are similar, it will be difficult to distinguish between the populations of individual conformers and the precision in regression method will be lower. The differences between the VCD spectra of the equatorial-methyl and axial-methyl conformers are substantial, thereby making the population determination from VCD spectra more accurate. Note that the population predicted from intensities of 18' and 18" alone (vide supra), is within the error range in the populations predicted from full spectra.

Nevertheless the errors estimated in the populations, obtained from full spectra, are fairly large, as already pointed out for 3-chloro-1-butyne. This observation can be attributed to the deviation of the predicted dipole and rotational strengths from the corresponding experimental values, even at the very high levels of calculations employed.

(3). *Analysis of experimental intrinsic rotation and DFT predicted specific rotations*: The optical rotation of (+)-3-methylcyclopentanone was measured at 589 nm in CCl_4, CH_3OH and CH_3CN solvents as a function of concentration. The specific rotation at infinite dilution, known as intrinsic rotation, was deduced from these data. The intrinsic rotation, $\{\alpha\}_D$ was obtained as 150.3±0.2 in CCl_4, 138.9±0.3 in CH_3OH and 144.9±0.4 in CH_3CN.

Table 3-4. The specific rotations predicted with B3LYP functional and populations determined there from using experimental intrinsic rotation for (R)-(+)-3-methylcylcopentanone.

Basis Set	Equatorial-methyl				Axial-methyl			
	Predicted $[\alpha]_D$	Percent population			Predicted $[\alpha]_D$	Percent population		
		CCl_4	CH_3OH	CH_3CN		CCl_4	CH_3OH	CH_3CN
6-31G*	247.7	81.3	79.2	80.3	-274.3	18.7	20.8	19.7
aug-cc-pVDZ	291.2 (311.7[a], 300.3[b], 302.2[c])	77.6	75.8	76.8	-339.1 (-361.0[a], -343.4[b], -344.0[c])	22.4	24.2	23.2
6-311++G(2d,2p)	291.5	77.6	75.8	76.7	-338.2	22.4	24.2	23.3
aug-cc-pVTZ	280.9	78.5	76.6	77.6	-325.2	21.5	23.4	22.4
Average[d]	288±6	77.9 ±0.5	76.1 ±0.5	77.0 ±0.5	-334±8	22.1 ±0.5	23.9 ±0.5	23.0± 0.5

[a]specific rotations calculated with CCl_4 solvent influence using PCM model. [b]specific rotations calculated with CH_3OH solvent influence using PCM model. [c]specific rotations calculated with CH_3CN solvent influence using PCM model. [d]average values were obtained from the aug-cc-pVDZ, 6-311++G(2d,2p) and aug-cc-pVTZ calculations

The specific rotations for equatorial-methyl and axial-methyl conformers were calculated at 589 nm using B3LYP functional and different basis sets (Table 3-4). With these calculated specific rotations the populations can be estimated using $\{\alpha\}_D = [\alpha]_{D,e}\, p_e + [\alpha]_{D,a}\, p_a$, where $\{\alpha\}_D$ is the experimental intrinsic rotation and $[\alpha]_{D,e}$, $[\alpha]_{D,a}$ are the predicted specific rotations for equatorial-methyl and axial-methyl conformers, and p_e, p_a are the percent populations of equatorial-methyl and axial-methyl conformers (with the constraint that $p_e + p_a$ is 100%). The populations determined in this manner, using four different basis sets, are shown in Table 3-4. Among the three large basis set calculations, the values obtained in B3LYP/aug-cc-PVDZ and B3LYP/6-311++G(2d,2p) calculations are almost the same, while those obtained in B3LYP/aug-cc-pVTZ calculation are only slightly different. The average populations obtained from three large basis set

calculations (namely 77.9% for equatorial-methyl and 22.1 for axial-methyl) are within the error ranges of those predicted (Table 3-3) from absorption and VCD spectra.

Approaching this analysis from a different view point, if the conformer populations are known, then it would be useful to determine the errors in the predicted specific rotations by comparing the population weighted specific rotation with the experimental intrinsic rotation. If we take the populations of conformers determined from temperature dependent absorption intensities of liquid sample (87:13 for equatorial:axial, vide supra), which are same as those obtained from REMPI spectrum of gas phase sample[15], as accurate populations, then the population weighted values are 209, 209 and 202 respectively in B3LYP/aug-cc-pVDZ, B3LYP/6-311++G(2d,2p) and B3LYP/aug-cc-pVTZ calculations, with an average value of 207. The experimental intrinsic rotation in CCl_4 is 150. The difference in these two values suggests that the specific rotations predicted with large basis sets for (R)-3-methylcyclopentanone are overestimated by ~38%. The population weighted specific rotation obtained in a smaller B3LYP/-631G* calculation is 180, which is much closer to the experimental rotation.

To investigate if the larger difference obtained in three large basis set calculations is due to the absence of solvent influence in the predicted specific rotation, we have repeated the specific rotation calculations in the presence of CCl_4, CH_3OH and CH_3CN solvents using the PCM model incorporated in Gaussian 03 program. Since the specific rotations obtained in the absence of solvent influence with different large basis sets are very close to each other, we investigated the solvent influence with only one of the three large basis sets used in this investigation. The geometries were re-optimized and specific rotation calculated using B3LYP functional and aug-cc-pVDZ basis set by incorporating

the solvent influence. The specific rotations predicted in the presence of CCl_4 solvent influence (see Table 3-4) are 311.7 and –361.0, respectively for equatorial-methyl and axial-methyl conformers, whose magnitudes are larger than those (291.2 and –339.1) predicted for isolated molecule. The predicted population weighted specific rotation in B3LYP/aug-cc-pVDZ calculation with CCl_4 solvent influence is 224 (as opposed to 209 for isolated molecule), which is ~50% larger than the experimental value. Thus the deviation of the calculated value from experimental value is even larger when CCl_4 solvent influence is included.

Similar observations are obtained with CH_3OH and CH_3CN solvents. The specific rotations predicted in the presence of CH_3OH (or CH_3CN) solvent influence (see Table 3-4) are 300.3 (or 302.2) and –343.4 (or -344.0), respectively for equatorial-methyl and axial-methyl conformers, whose magnitudes are larger than 291.2 and –339.1 predicted for isolated molecule. The predicted population weighted specific rotation in B3LYP/aug-cc-pVDZ calculation with CH_3OH (or CH_3CN) solvent influence is 217 (or 218), as opposed to 209 for isolated molecule. The experimental intrinsic rotations obtained in CH_3OH and CH_3CN are 138.9 and 144.9, respectively.

These observations are consistent with those found for a single conformer molecule (R)-(+)-3-chloro-1-butyne. In the case of (R)-(+)-3-chloro-1-butyne (see Table 3-5), the predicted specific rotation for isolated molecule is in good quantitative agreement with experimental intrinsic rotation obtained in CCl_4 and CH_3OH solvents, but when solvent influence (CCl_4 or CH_3OH) is included with PCM model, the predicted value is overestimated by ~50%. Thus the current observations for 3-methylcyclopentanone and 3-chloro-1-butyne, contradict previously reported[63, 64]

conclusions that the PCM model improves the agreement between predicted and experimental specific rotations in CH_3OH and CH_3CN solvents. More theoretical developments appear needed to correctly model the solvent influence on specific rotation.

Table 3-5. Comparison of B3LYP predicted specific rotations for (R)-(+)-3-chloro-1-butyne with and without solvent influence

	without solvent[b]	with solvent	
		CCl_4	CH_3OH
6-31G*	26.8	37.0	36.6
aug-cc-pVDZ	32.8	41.2	41.8
6-311++G(2d,2p)	28.3	44.3	40.7
aug-cc-pVTZ	28.6	42.9	39.2
average[a]	30 ± 2	43 ± 2	41 ± 1
Observed[b] intrinsic rotation in CCl_4	28.4 ± 0.2		
Observed[b] intrinsic rotation in CH_3OH	29.0 ± 0.3		

[a]The average of three large basis set (aug-cc-pVDZ, 6-311++G(2d,2p), aug-cc-pVTZ) predictions. [b]from Chapter II.

Conclusion

The conformer populations of (R)-(+)-3-methylcyclopentanone are determined using experimental and predicted vibrational absorption spectra, VCD spectra and specific rotation. The temperature dependent absorption spectra of liquid 3-methylcyclopentanone provided ΔH^o for equatorial-axial equilibrium, which is in good agreement with that determined for gas phase molecules. The populations are 87% equatorial-methyl and 13% axial-methyl. On the other hand, the populations determined from experimental and predicted vibrational intensities are associated with large errors because the predicted vibrational intensities even with large basis sets are not sufficiently close to the experimental intensities. The predicted specific rotations for individual conformers and the observed intrinsic rotation yield conformer populations which are

within the error ranges associated with the populations obtained from predicted and experimental vibrational intensities. Using the populations determined from temperature dependent absorption spectra, the predicted population weighted specific rotation for isolated molecules is found to be larger than the experimental value in CCl_4, CH_3OH and CH_3CN solvents. This deviation is further increased when solvent influence is included in the calculations, indicating the need for better theoretical models for incorporating solvent influence on specific rotation.

CHAPTER IV

ABSOLUTE CONFIGURATION AND CONFORMATION OF CHIRAL α-ARYLOXYPROPANOIC ACIDS STUDIED BY VIBRATIONAL ABSORPTION AND VIBRATIONAL CIRCULAR DICHROISM

Introduction

Most herbicides, pesticides, and fungicides are made of chiral chemicals because most biological reactions are enzymatically mediated and involve chiral centers. Among the chiral herbicides, α-aryloxypropanoic acids are of particular importance. 2-(4-chloro-2-methylphenoxy) propanoic acid (Mecoprop) and 2-(2,4-dichlorophenoxy) propanoic acid (Dichloroprop) are two chiral herbicides belonging to the family of α-aryloxypropanoic acids. Each of these two compounds can exist in two enantiomeric forms. It is known that only their (+)-enantiomers are herbicidally active while the (-)-enantiomers are devoid of herbicidal activity but are powerful anti-auxins.[65-67] These compounds may undergo racemization by inversion of the absolute configuration at the asymmetrically substituted C-atom.[68] It is also of interest to note that Mecoprop was detected in Swiss lakes indicating that herbicides, when used in excess quantities, can become an environmental hazard.[69] For these reasons it is necessary to develop the methods that can detect not only the chemical identity of pollutant, but also the particular enantiomer of that pollutant. Furthermore, enantioselective microbial degradation was found to preferentially degrade one enantiomer over the other, both for Mecoprop and Dichloroprop.[70, 71] To understand biological reactivity at the molecular level, it is important to know the absolute configurations and predominant conformations of the active herbicides. The absolute configuration of Mecoprop has been stated[72] to be (+)-(*R*),

but this assignment has not been confirmed with spectroscopic methods. Moreover, the predominant conformations of Mecoprop and Dichloroprop are not known. Another two α-aryloxypropanoic acids that are closely related to Mecoprop and Dichloroprop are 2-(2-chlorophenoxy) propanoic acid and 2-(3-chlorophenoxy) propanoic acid. The chiral separation of these two compounds has been reported.[73-75] The absolute configurations of these two compounds were determined via chemical synthesis as (+)-(*R*).[76] But the predominant conformations of these two compounds in solution have not been determined.

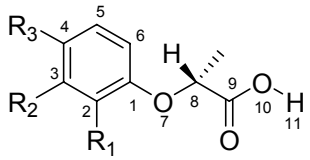

2-(2-chlorophenoxy) propanoic acid **1**, R_1=Cl, R_2=H, R_3=H;
2-(3-chlorophenoxy) propanoic acid **2**, R_1=H, R_2=Cl, R_3=H;
2-(4-chloro-2-methylphenoxy) propanoic acid **3**, R_1=CH_3, R_2=H, R_3= Cl;
2-(2,4-dichlorophenoxy) propanoic acid **4**, R_1=Cl, R_2=H, R_3= Cl;
Figure 4-1. Structure and atomic numbering of four α-aryloxypropanoic acids.

Chiroptical spectroscopic methods are appropriate for identifying and determining the molecular structures (both absolute configuration and predominant conformations) of chiral substances. Three chiroptical methods have been recently developed for identifying and determining the structures of chiral molecules. They are vibrational circular dichroism (VCD), vibrational Raman optical activity (VROA)[77, 78] and optical rotation. Among the three methods, VCD has been the most widely used. A combination of improved VCD instrumental performance and accurate density functional theory (DFT) predictions made VCD a reliable tool for confident determination of the absolute

configurations and predominant conformations of chiral molecules in solution phase. More examples for successful applications of VCD can be found in a review article.[58] In this chapter, we use experimental and theoretical VCD spectra for independently determining the absolute configuration and predominant conformation of compounds **1**, **2**, **3**, **and 4**.

Hydrogen bonding plays a very important role in the structures of molecules ranging from water[79] to biological molecules such as DNA[80] and proteins[81]. This is also the case for small carboxylic acids such as formic acid, acetic acid, and propanoic acid. The experimental and theoretical studies show that these carboxylic acids tend to form dimers through intermolecular hydrogen bonding.[82] There are also several efforts in understanding hydrogen bonding using different theoretical methods, including *ab initio* and density functional theory (DFT).[83]

The preliminary study showed that hydrogen bond affects the VCD spectra of these four acids. To address the hydrogen bond issue, two approaches were used in this study. First, hydrogen bond was eliminated by converting the acids to their methyl esters. Second, dimer model was built to include the hydrogen bond in the calculation. Right now, most theoretical VCD spectral calculations have dealt with monomer molecules. The calculations for dimer molecules with flexible structure are less common. A few attempts have been made to investigate dimers, where monomers have only a limited number of possible starting conformation.[34, 84] For monomers with several possible starting conformations, we are not aware of any attempts trying to address intermolecular hydrogen bonded dimers. In the present study, we address this problem and suggest an approach to deal with monomers possessing several possible starting conformations.

Experimental Section

Racemic **1** and **2** were obtained from TCI America and Aldrich Chemical Co, respectively. The enantiomers of **1** and **2** were separated in-house at 25 °C on a 4.6 x 250 mm chiral column (Chiralpak AD-H column from Daicel Chemical Industries, Ltd.) using a mobile phase of 3% isopropanol in hexane, with 0.03% trifluoroacetic acid, run at 1 mL/min with UV detection at 254 nm. (+)-Enantiomer of **3** and **4** were obtained as a gift from A. H. Marks Co (UK). The α-aryloxypropanoic acids were converted to the corresponding methyl esters by reacting with diazomethane.[85] Diazald and diazomethane generation apparatus were purchased from Aldrich Chemical Co. The structure of the methyl esters are shown in Figure 4-2.

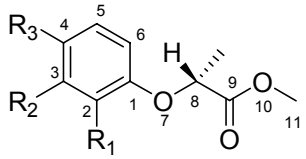

methyl 2-(2-chlorophenoxy) propanoate **5**, R_1=Cl, R_2=H, R_3=H;
methyl 2-(3-chlorophenoxy) propanoate **6**, R_1=H, R_2=Cl, R_3=H;
methyl 2-(4-chloro-2-methylphenoxy) propanoate **7**, R_1=CH_3, R_2=H, R_3= Cl;
methyl 2-(2,4-dichlorophenoxy) propanoate **8**, R_1=Cl, R_2=H, R_3= Cl;
Figure 4-2. Structure and atomic numbering of four methyl α-aryloxypropanoates.

The experimental optical rotations for acids and their methyl esters were measured on an Autopol IV polarimeter at sodium D line (589nm). The experimental specific rotations of the first elutants of **1** and **2**, respectively are $[\alpha]^{20}_D$= -26.6 (c=1.23, CH_3COCH_3) and $[\alpha]^{20}_D$= -49.7 (c=0.58, CH_3COCH_3). The experimental specific rotations of the second elutants of **1** and **2**, respectively are $[\alpha]^{20}_D$= +28.5 (c=0.97,

CH_3COCH_3) and $[\alpha]^{20}_D$= +53.5 (c=0.79, CH_3COCH_3). For second elutants, specific rotations measured in $CDCl_3$ solvent are; $[\alpha]^{20}_D$= +23.5 (c=0.77, $CDCl_3$) for **1** and $[\alpha]^{20}_D$= +63.4 (c=0.76, $CDCl_3$) for **2**. The experimental specific rotations for **3** and **4** are $[\alpha]^{20}_D$ = +16.3 (c 2.31, $CHCl_3$) and $[\alpha]^{20}_D$ = +19.0 (c 2.29, $CHCl_3$) respectively.

The experimental specific rotations for the methyl esters of the first elutants of compounds **1** and **2** are $[\alpha]^{20}_D$= -21.9 (c=2.11, $CHCl_3$) for methyl ester **5** and $[\alpha]^{20}_D$= -39.7 (c=1.48, $CHCl_3$) for methyl ester **6**. The experimental specific rotations for the methyl esters of the second elutants of compounds **1** and **2** are $[\alpha]^{20}_D$= +26.8 (c=1.72, $CHCl_3$) for methyl ester **5** and $[\alpha]^{20}_D$= +40.3. (c=0.62, $CHCl_3$) for methyl ester **6**. The specific rotation for **7** and **8** are $[\alpha]^{20}_D$ = +22.6 (c 2.29, $CHCl_3$) and $[\alpha]^{20}_D$ = +27.2 (c 2.46, $CHCl_3$).

The infrared and VCD spectra were recorded on a commercial FT-VCD spectrometer, Chiralir. The VCD spectra were recorded with 3-hour data collection time at 4 cm^{-1} resolution. Spectra of acids **1** and **2** were measured in $CDCl_3$ solvent at three different concentrations, 30.0 mg/mL (path length 180 μ m), 15.0 mg/mL (path length 400 μ m), and 6.0 mg/mL (path length 600 μ m). Spectra were measured in $CDCl_3$ solvent at 33.9mg/mL, 120 μm path length for **3**; and at 36.4mg/mL, 70 μm path length for **4**. Spectra were also measured for **3** and **4** at a lower concentration (around 3mg/mL).

Spectra of methyl esters **5** were measured in CCl_4 solution at 41.9 mg/mL (path length 150 μ m). Spectra of methyl esters **6** were measured in CCl_4 solution at 53.8 mg/mL (path length 100 μ m). The spectra for methyl esters **7** (45.7mg/mL, 60 μm pathlength) and **8** (49.1mg/mL, 100 μm pathelength) were also measured in CCl_4. The

sample was held in a variable path length cell with BaF_2 windows. In the absorption spectra presented, the solvent absorption was subtracted out. In the VCD spectra presented, the raw VCD spectrum of the solvent was subtracted.

The vibrational frequencies and absorption and VCD intensities were calculated using the Gaussian 98 and Gaussian 03 programs. The calculations used the density functional theory (DFT) with B3LYP functional and 6-31G* basis set. The theoretical absorption and VCD spectra were simulated with Lorentzian band shapes and 5 cm^{-1} band width. Since the predicted band positions are higher than the experimental values, the B3LYP/6-31G* frequencies were scaled with 0.96, as recommended by Wong.[86]

Results and Discussion

Monomer α-aryloxypropanoic acids model:

The absorption and VCD spectra were measured for both enantiomers of acids **1** and **2** (See Figures 4-4 to 4-7). The experimental VCD spectra for (+) and (-)-enantiomers (Figures 4-5 and 4-7) are mirror images to each other. A large difference in the absorption spectra of these two compounds (Figures 4-4 and 4-6) is seen for the 1590 cm^{-1} band, which is stronger for **2** than that for **1**. In the VCD spectrum of (+)-**1** (Figure 4-5), a positive-negative couplet around 1240 cm^{-1} and a positive peak around 1060 cm^{-1} are present. But these VCD bands are not present in the spectra of (+)-**2** (Figure 4-7). These differences between the VCD spectra of (+)-**1** and (+)-**2** must be due to the changes in compositions of benzene ring vibrations, arising from the difference in the position of chlorine atom on the benzene ring. The experimental absorption and VCD

spectra of (+)-**3** and (+)-**4** are shown in Figure 4-8 to 4-11. Their absorption spectra are different in the region from 1000 to 1400 cm^{-1}, but most of the VCD features are similar. The similar VCD sign pattern indicates that the two compounds may have the same absolute configuration. The differences in absorption and VCD spectra of (+)-**3** and (+)-**4** must be attributed to the difference in substitution at the 2-position of benzene ring. This difference in substitution leads to different predominant conformations and changes in vibrational compositions for different bands.

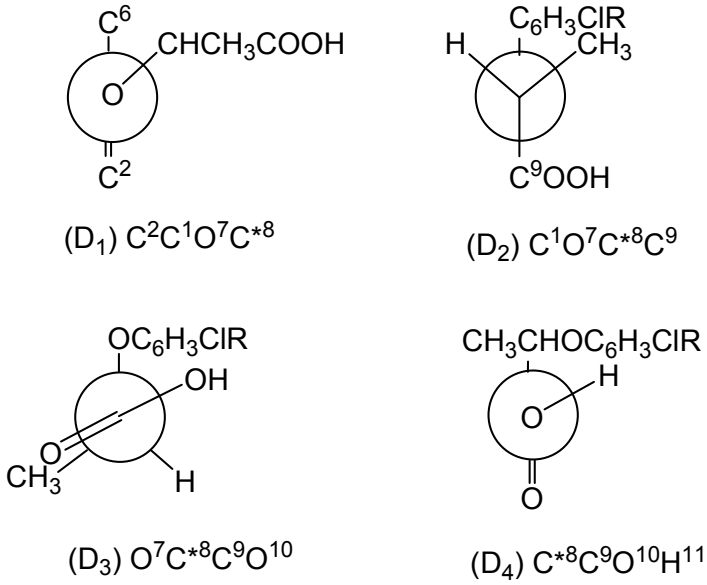

Figure 4-3. The Newman projection of the four dihedral angles.

To calculate the absorption and VCD spectra, we arbitrarily chose the (*R*)-configurations for **1**, **2, 3,** and **4**. The conformational flexibility of these four molecules arises from the rotation around four single bonds: C^1O^7, O^7C^8, C^8C^9, and C^9O^{10} (see Figure 4-1 and Figure 4-3). The initial dihedral angles for each of the $C^2C^1O^7C^8$, $C^1O^7C^8C^9$, $O^7C^8C^9O^{10}$, and $C^8C^9O^{10}H^{11}$ segments (see Figure 4-3) are chosen to be 60°,

180° and -60°. This resulted in 3^4=81 possible conformations, each for each molecule. But in some initial conformations, the distances between some atoms without bonds between them are too close to each other (less than the sum of their atomic radii). These initial conformations are discarded without geometry optimization. All the remaining conformations were optimized using B3LYP/6-31G* basis set. After the geometry optimization, we identified the low energy stable conformers for these four molecules. The most stable conformations are summarized in in Table 4-1 to Table 4-4 with converged dihedral angles, optimized Gibbs energies, and relative populations.

Table 4-1. The converged dihedral angles, Gibbs energy, and population of (*R*)-2-(2-chlorophenoxy) propanoic acid **1** conformers

Conformer	Converged dihedral angles[a]				ΔE	Pop.[b]
	D_1	D_2	D_3	D_4	(kJ/mol)	(%)
1	176.5	70.8	34.8	178.4	0	28.42
2	-164.1	145.5	-3.9	1.2	0.1680	26.55
3	177.2	72.7	-158.8	-176.4	0.3833	24.35
4	81.0	79.9	-169.4	-178.2	0.7877	20.68

[a]dihedral angles: D1:$C^2C^1O^7C^8$;D2:$C^1O^7C^8C^9$; D3:$O^7C^8C^9O^{10}$;D4:$C^8C^9O^{10}H^{11}$.
[b]population based on Gibbs energies

Table 4-2. The converged dihedral angles, Gibbs energy, and population of (*R*)-2-(3-chlorophenoxy) propanoic acid **2** conformers

Conformer	Converged dihedral angles[a]				ΔE	Pop.[b]
	D_1	D_2	D_3	D_4	(kJ/mol)	(%)
1	177.4	70.5	35.6	178.5	0	24.95
2	0.4	71.8	-157.6	-176.9	0.0158	24.79
3	178.2	72.5	-158.1	-176.5	0.2415	22.64
4	-1.9	70.4	32.7	178.6	0.5724	19.81
5	69.2	76.9	-168.3	-178.3	2.8802	7.81

[a]dihedral angles: D1:$C^2C^1O^7C^8$;D2:$C^1O^7C^8C^9$; D3:$O^7C^8C^9O^{10}$;D4:$C^8C^9O^{10}H^{11}$.
[b]population based on Gibbs energies

Table 4-3. The converged dihedral angles, Gibbs energy, and population of (*R*)-2-(4-chloro-2-methylphenoxy) propanoic acid **3** conformers

Conformer	Converged dihedral angles[a]				ΔE	Pop.[b]
	D_1	D_2	D_3	D_4	(kJ/mol)	(%)
1	178.3	70.2	34.8	178.6	0	45.74
2	180.0	71.9	-156.4	-176.5	0.137	43.29
3	-168.1	145.5	-30.8	-177.4	5.708	4.57
4	-173.7	151.2	-173.7	-179.3	5.805	4.40
5	89.3	80.9	-166.6	-177.7	7.761	2.00

[a]dihedral angles: D1:$C^2C^1O^7C^8$;D2:$C^1O^7C^8C^9$; D3:$O^7C^8C^9O^{10}$;D4:$C^8C^9O^{10}H^{11}$.
[b]population based on Gibbs energies

Table 4-4. The converged dihedral angles, Gibbs energy, and population of (*R*)-2-(2,4-dichlorophenoxy) propanoic acid **4** conformers.

Conformer	Converged dihedral angles[a]				ΔE	Pop.[b]
	D_1	D_2	D_3	D_4	(kJ/mol)	(%)
1	176.7	70.4	35.9	178.4	0	31.12
2	177.6	72.3	-160.4	-176.5	0.252	28.12
3	81.9	80.1	-170.9	-178.5	0.483	25.61
4	-165.9	146.9	-3.4	1.0	3.014	9.23
5	79.6	78.6	25.1	177.3	4.114	5.92

[a]dihedral angles: D1:$C^2C^1O^7C^8$;D2:$C^1O^7C^8C^9$; D3:$O^7C^8C^9O^{10}$;D4:$C^8C^9O^{10}H^{11}$.
[b]population based on Gibbs energies

In the crystal structures of (±)-**1** and (±)-**2**, the (*R*) and (*S*) molecules form a dimer through intermolecular hydrogen bonds. The dihedral angles D_1, D_2, D_3, and D_4 in the crystal structures are -179°, 66°, -161° and 180° for 2-(2-chlorophenoxy) propanoic acid[87] and 174°, 75°, -154 °, and -179° 2-(3-chlorophenoxy) propanoic acid[88], respectively. These angles are close to the calculated dihedral angles of conformer 3 of (*R*)-**1** and (*R*)-**2**. . The first most stable conformations for these four molecules have similar structure (The differences in the four torsion angles (D1 to D4) are in 2-degree

range). In addition to this, the conformers No 3 of **1** and **2** also have similar structure with the conformers No 2 of **3** and **4**.

The absorption and VCD intensities were calculated for the most stable conformers of these four molecules at the B3LYP/6-31G* level, and all these conformations were found to have potential energy minima at the B3LYP/6-31G* level. The predicted spectra for individual conformers and the population weighted spectra are shown in Figures 4-4 to 4-11 and compared to the corresponding experimental spectra.

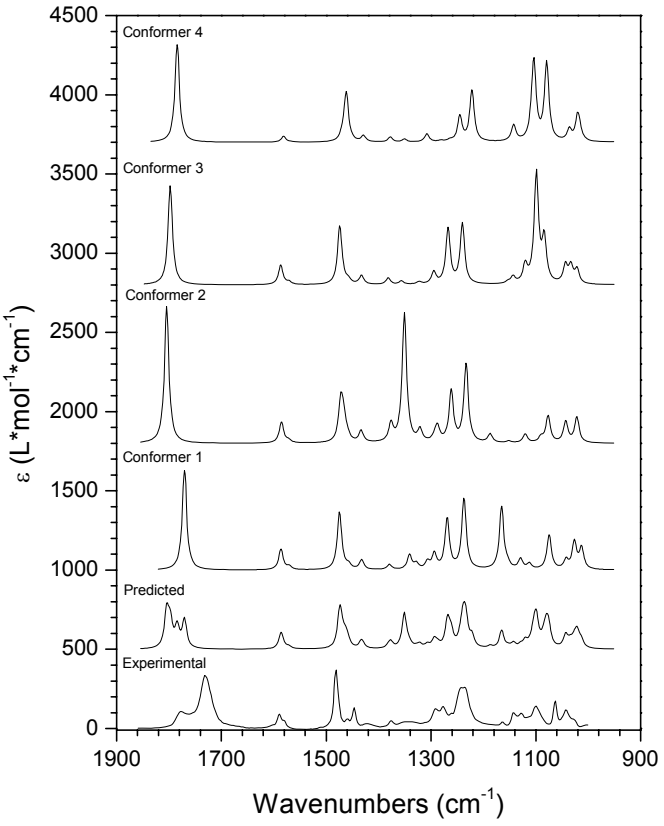

Figure 4-4.Comparison of the experimental absorption spectrum (bottom trace) with individual conformer spectra (top 4 traces) and predicted (population weighted) absorption spectrum of 2-(2-chlorophenoxy) propanoic acid. Spectra are displayed with offset for clarity.

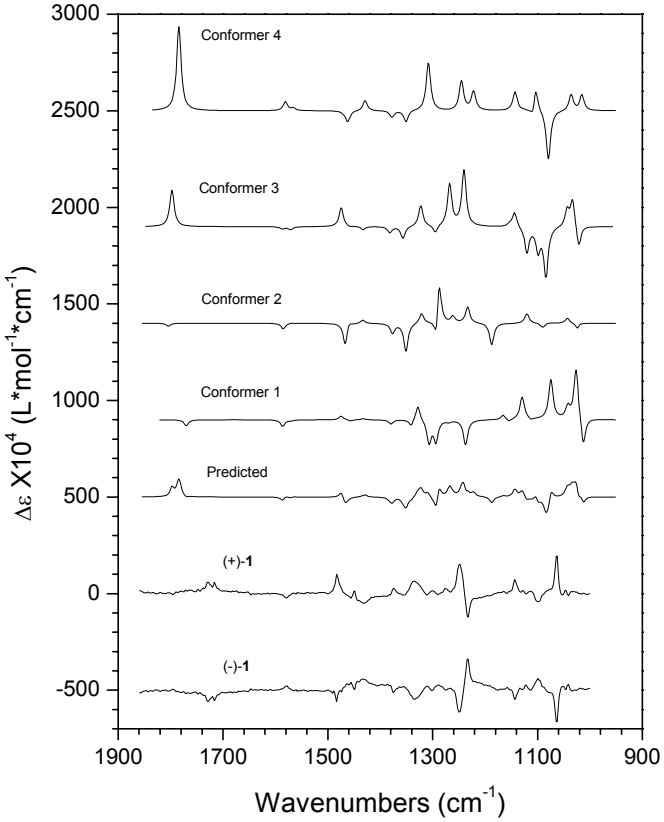

Figure 4-5. Comparison of the experimental VCD spectra of (+)- and (-)-2-(2-chlorophenoxy) propanoic acids with individual conformer spectra (top 4 traces) and predicted (population weighted) VCD spectrum of (*R*)-2-(2-chlorophenoxy) propanoic acid. Spectra are displayed with offset for clarity.

2-(2-chlorophenoxy) propanoic acid: In Figure 4-4, the most notable difference between experimental and predicted absorption spectra is seen for the peaks in the region from 1860 cm^{-1} to 1700 cm^{-1}. The predicted spectrum also contains a strong band at ~1350 cm^{-1}, which is not seen in the experimental spectrum. The calculated VCD spectra for individual conformers and the final population weighted VCD spectrum for (*R*)-**1** are compared to the corresponding experimental VCD spectra of both enantiomers in Figure 4-5. The predicted VCD spectrum for (*R*)-enantiomer does not match very well with the experimental VCD spectrum for either one of the two enantiomers. In the 1250 cm^{-1} region, where a positive-negative couplet is present in the experimental VCD spectrum of

(+)-enantiomer, there is no matching feature in the predicted VCD spectrum. The positive peak around 1060 cm^{-1} in experimental VCD spectrum of (+)-enantiomer does not have a counterpart in the predicted spectrum.

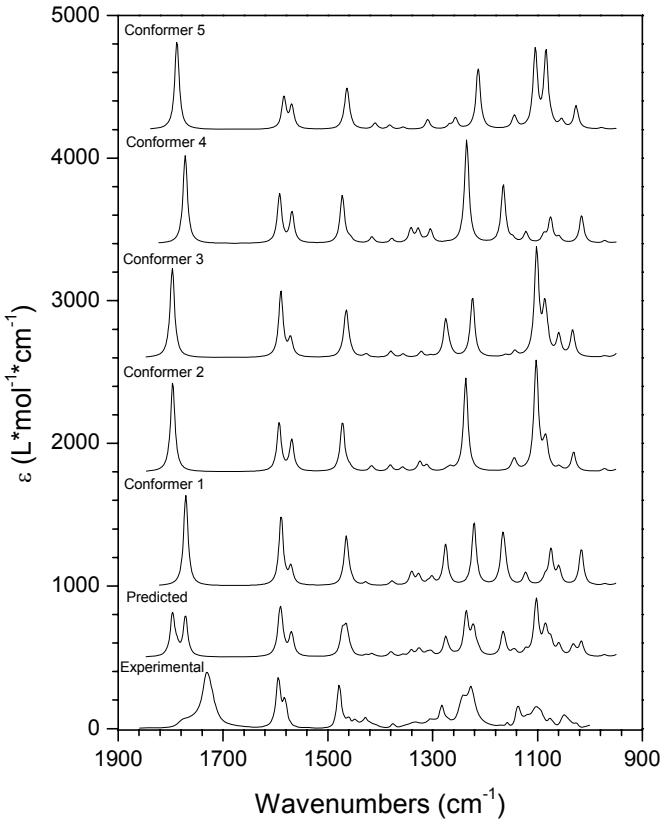

Figure 4-6. Comparison of the experimental absorption spectrum (bottom line) with individual conformer spectra (top 5 traces) and predicted (population weighted) absorption spectrum of 2-(3-chlorophenoxy) propanoic acid. Spectra are displayed with offset for clarity.

2-(3-chlorophenoxy) propanoic acid: For acid **2**, the comparison between experimental and predicted absorption spectra is shown in Figure 4-6. Again, the bands in the 1860 cm^{-1} to 1700 cm^{-1} region do not agree well. The predicted spectrum shows two peaks in this region. The predicted spectrum also has a strong peak around 1100 cm^{-1}

which does not show up in the experimental spectrum. The comparison between experimental and predicted VCD spectra is shown in Figure 4-7. The experimental VCD spectrum of (+)-**2** shows a small positive-negative-positive feature at ~ 1250 cm^{-1}, but in the predicted VCD spectrum of (*R*)-enantiomer, there are two positive bands at ~ 1250 cm^{-1}. The overall agreement between the predicted VCD spectrum of (*R*)-enantiomer and the experimental VCD spectrum, of either one of two enantiomers, is poor.

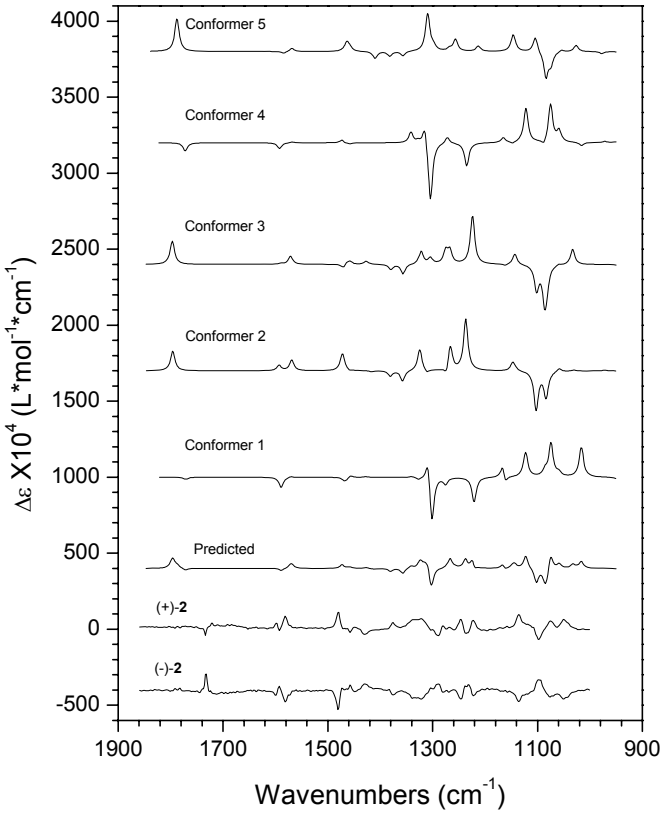

Figure 4-7. Comparison of the experimental VCD spectra of (+)- and (-)-2-(3-chlorophenoxy) propanoic acid with individual conformer spectra (top 5 traces) and predicted (population weighted) VCD spectrum of (*R*)-2-(3-chlorophenoxy) propanoic acid. Spectra are displayed with offset for clarity.

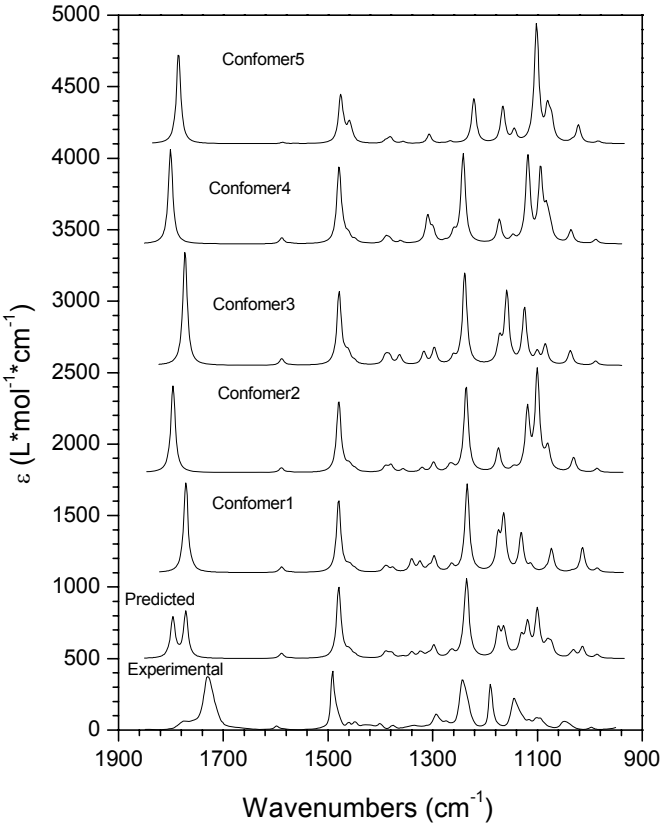

Figure 4-8. Comparison of the experimental absorption spectrum (bottom trace) with individual conformer spectra (top 5 traces) and predicted (population weighted) absorption spectrum of 2-(4-chloro-2-methylphenoxy) propanoic acid. Spectra are displayed with offset for clarity.

2-(4-chloro-2-methylphenoxy) propanoic acid: The experimental absorption spectrum of **3** obtained is shown in Figure 4-8. The absorption bands in the predicted spectrum do not show one-to-one correspondence with the absorption bands in the experimental spectrum of **3**. It should be noted that the influence of intermolecular hydrogen bonding causes the experimental bands specified for C=O stretching vibrations to appear at lower frequencies, while the bands specified for C-O stretching and COH bending vibrations to appear at higher frequencies. For isolated molecule the predicted band positions for C=O stretching vibrations are 1796 and 1771 cm^{-1} and those for

prominent COH bending are 1235, 1173, 1165 and 1119 cm^{-1}. As a result, the relative intensities of corresponding bands in experimental and predicted absorption spectra are not in good agreement.

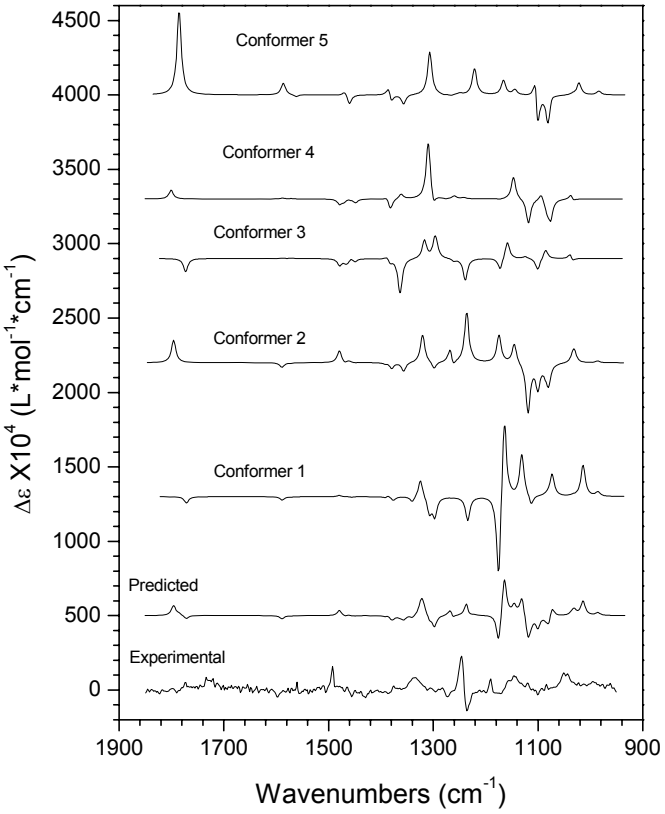

Figure 4-9. Comparison of the experimental VCD spectrum (bottom trace) of (+)-2-(4-chloro-2-methylphenoxy) propanoic acid with individual conformer spectra (top 5 traces) and predicted (population weighted) VCD spectrum of (*R*)-2-(4-chloro-2-methylphenoxy) propanoic acid. Spectra are displayed with offset for clarity.

The experimental VCD spectrum of (+)-**3** is shown in Figure 4-9. Large differences are observed between the experimental and predicted VCD spectra for **3**. The characteristic positive-negative couplet seen around 1250 cm^{-1} in the experimental

spectrum is not reproduced in the predicted spectrum. The negative-positive couplet seen around 1170 cm^{-1} in the predicted spectrum does not show up in experimental one. The spectra were also recorded at a lower concentration (around 3mg/mL) hoping to avoid the intermolecular hydrogen bonding effect. But no significant improvement was observed.

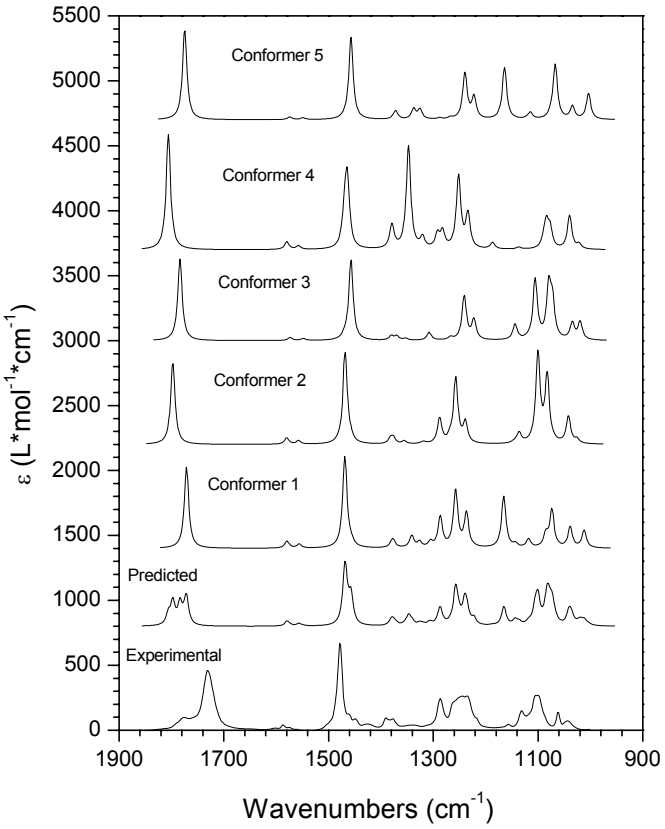

Figure 4-10. Comparison of the experimental absorption spectrum (bottom trace) with individual conformer spectra (top 5 traces) and predicted (population weighted) absorption spectrum of 2-(2,4-dichlorophenoxy) propanoic acid. Spectra are displayed with offset for clarity

2-(2,4-dichlorophenoxy) propanoic acid: In the same way, the experimental absorption and VCD spectra of (+)-**4** are compared with the predicted ones for (*R*)-**4** in Figures 4-10 and 4-11. A much larger difference between the experimental and predicted

VCD spectra is observed for **3** than that observed for **4**. Bands originated from C=O stretching, C-O stretching, and COH bending vibrations are anticipated to have influence from hydrogen bonding. Once again, the positive-negative couplet seen at ~1250 cm^{-1} in the experimental VCD spectrum of (+)-**4** is not reproduced in the predicted VCD spectrum of (*R*)-**4**.

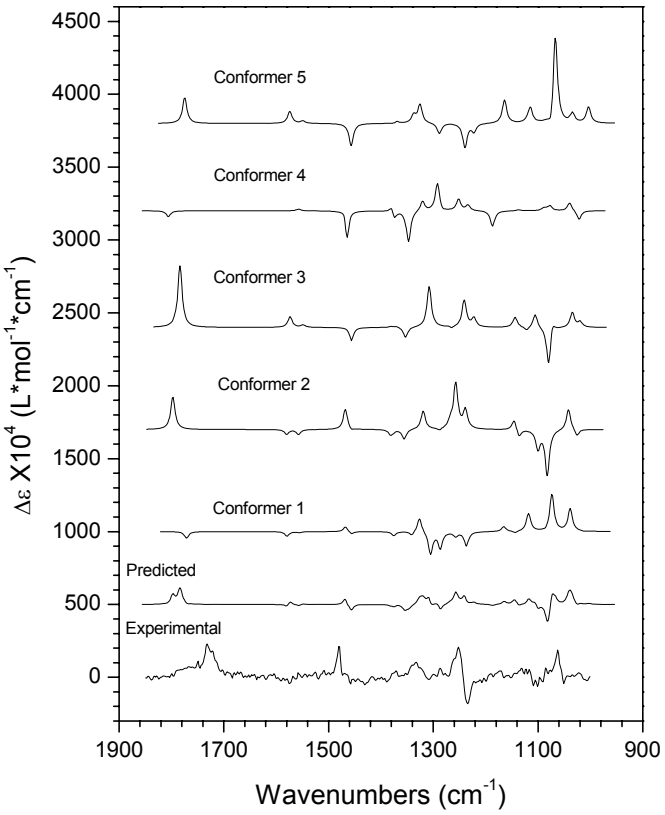

Figure 4-11. Comparison of the experimental VCD spectrum (bottom trace) of (+)-2-(2,4-dichlorophenoxy) propanoic acid with individual conformer spectra (top 5 traces) and predicted (population weighted) VCD spectrum of (*R*)-2-(2,4-dichlorophenoxy) propanoic acid. Spectra are displayed with offset for clarity.

Higher level calculation (B3LYP/6-311G(2d,2p) and B3PW91/6-311G(2d,2p)) were also done to compare the functional and basis set effect. These two higher-level calculations gave similar results to B3LYP/6-31G* calculation. Considering the energy of a general hydrogen bond (around 8.0-20.0 kJ/mol)[56], which is much larger than the energy difference among the conformers used in this calculation (see Table 4-1 to 4-4), one may conclude that stabilization resulting from intermolecular hydrogen bonding will lead to the formation of dimers. Because the above calculation only used single isolated molecules, the poor agreement between experimental and predicted spectra might originate from the discrepancy between monomer model used in calculation and dimer in the solution used in experiment. The hydrogen bond effect can be clearly observed in the absorption of carbonyl bands. In the absorption spectra of acid **1** with different concentration, the absorbance ratio of the two peaks at 1730 cm^{-1} and 1775 cm^{-1} changes with the concentration (see Figure 4-12). At higher concentrations, intermolecular hydrogen bonded dimers can form, whose carbonyl bands will appear at lower wavenumber than the carbonyl bands from acids that do not participate in intermolecular hydrogen bonds. Based on this explanation, the lower frequency band at 1730 cm^{-1} is assigned to intermolecularly hydrogen bonded dimers and the higher frequency band at 1775 cm^{-1} is assigned to acid molecules that do not participate in intermolecular hydrogen bonding. Then one would expect the intensity of 1775 cm^{-1} band to increase, and that of 1730 cm^{-1} band to decrease, as the concentration is lowered. This expected pattern is observed in the experimental absorption spectra as a function of concentration (Figure 4-12). We also measured the VCD spectra in the concentration range, however, VCD spectra do not change significantly in this range. In a highly dilute solution, the

intermolecular hydrogen bonding may become negligible, but at such dilute concentrations, the measurement of VCD spectra will not be possible due to the interference from solvent absorption.

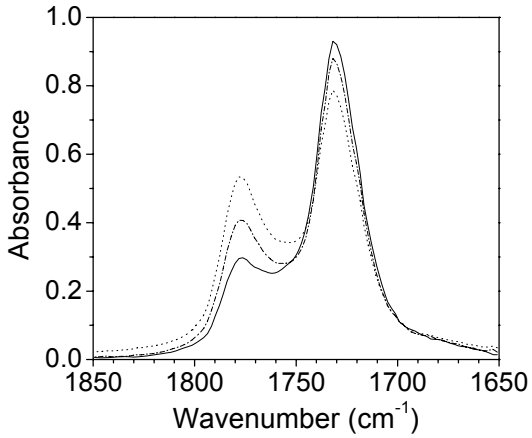

Figure 4-12. The infrared absorption spectra of (+)-**1** at different concentrations in $CDCl_3$. (Solid line: 30.0 mg/mL, dashed line: 15.0 mg/mL, dotted line: 6.0 mg/mL)

Since the comparison of experimental spectra in solution with predicted spectra for isolated molecule does not provide unambiguous conclusion about absolute configuration of these four acids, they were converted to the corresponding methyl esters via reaction of the acids with diazomethane to avoid hydrogen bond effect.

Monomer methyl α-aryloxypropanoates model:

We eliminated the intermolecular hydrogen bonding effects by converting the four acids **1**, **2**, **3**, and **4** to the corresponding methyl esters **5**, **6**, **7**, and **8** (see methods section Figure 4-2). Then we measured the absorption and VCD spectra for the methyl esters and compared these spectra to the predicted spectra for methyl ester molecules (Figure 4-13 to 4-20). We used the (*R*) configuration for the calculations on methyl

esters. Same atom numbering as that used for acids was used for methyl esters (see Figure 4-2), except that atom 11 in methyl esters becomes carbon. The geometries of 81 initial conformations, for each of the esters, were optimized using B3LYP/6-31G* basis set. The optimized dihedral angles, Gibbs energy, and poputaiton of the lowest energy conformers are listed in Table 4-5 for (*R*)-**5,** Table 4-6 for (*R*)-**6,** Table 4-7 for (*R*)-**7** and Table 4-8 for (*R*)-**8**

A comparison of the dihedral angles of lowest energy conformers of (*R*)-**1** to those of (*R*)-**5**, indicates that the conformers 1, 3, and 4 of (*R*)-**1** (Table 4-1) have similar structures with conformers 1, 2, and 3 of (*R*)-**5** (Table 4-5). Similar comparison between the dihedral angles of lowest energy conformers of (*R*)-**2** and (*R*)-**6**, indicate that the conformers 1, 2, 3, 4, and 5 of (*R*)-**2** (Table 4-2) correspond to conformers 1, 2, 4, 3, and 5 of (*R*)-**6** (Table 4-6). The conformers 1, 2, 3, and 4 of (*R*)-**3** (Table 4-3) and (*R*)-**7** (Table 4-7) have similar structures. The conformers 1, 2, 3, and 5 of (*R*)-**4** (Table 4-4) have similar structure with conformers 1, 2, 3, and 4 of (*R*)-**8** (Table 4-8). The absorption and VCD spectra for the lowest energy conformers of these four methyl esters are calculated at their optimized geometries.

Table 4-5. The converged dihedral angles, Gibbs energy, and population of (*R*)-methyl 2-(2-chlorophenoxy)propanoate **5** conformers

Conformer	Converged dihedral angles[a]				ΔE	Pop.[b]
	D_1	D_2	D_3	D_4	(kJ/mol)	(%)
1	177.1	69.8	35.2	178.8	0	41.27
2	177.2	72.0	-154.0	-176.1	0.5487	33.07
3	81.7	79.3	-167.2	-178.0	1.7591	20.30
4	79.8	77.5	28.8	176.8	5.0567	5.36

[a]dihedral angles: D1:$C^2C^1O^7C^8$;D2:$C^1O^7C^8C^9$; D3:$O^7C^8C^9O^{10}$;D4:$C^8C^9O^{10}H^{11}$.
[b]population based on Gibbs energies

Table 4-6. The converged dihedral angles, Gibbs energy, and population of (*R*)-methyl 2-(3-chlorophenoxy)propanoate **6** conformers

Conformer	Converged dihedral angles[a]				ΔE	Pop.[b]
	D_1	D_2	D_3	D_4	(kJ/mol)	(%)
1	178.1	69.5	35.5	178.9	0	24.96
2	0.5	70.8	-150.5	-176.8	0.1575	23.42
3	-1.4	69.7	33.4	178.9	0.5881	19.69
4	178.7	71.5	-152.1	-176.2	0.8402	17.78
5	64.8	74.2	-165.8	-178.2	1.4073	14.15

[a]dihedral angles: D1:$C^2C^1O^7C^8$;D2:$C^1O^7C^8C^9$; D3:$O^7C^8C^9O^{10}$;D4:$C^8C^9O^{10}H^{11}$.
[b]population based on Gibbs energies

Table 4-7. The converged dihedral angles, Gibbs energy, and population of (*R*)-methyl 2-(4-chloro-2-methylphenoxy)propanoate **7** conformers

Conformer	Converged dihedral angles[a]				ΔE	Pop.[b]
	D_1	D_2	D_3	D_4	(kJ/mol)	(%)
1	179.2	69.0	36.0	179.0	0	45.92
2	-179.8	71.0	-150.8	-176.2	0.097	44.16
3	-168.7	145.8	-36.0	-177.7	5.020	6.06
4	-175.1	152.4	-171.4	-178.9	6.138	3.86

[a]dihedral angles: D1:$C^2C^1O^7C^8$;D2:$C^1O^7C^8C^9$; D3:$O^7C^8C^9O^{10}$;D4:$C^8C^9O^{10}H^{11}$.
[b]population based on Gibbs energies

Table 4-8. The converged dihedral angles, Gibbs energy, and population of (*R*)-methyl 2-(2,4-dichlorophenoxy)propanoate **8** conformers

Conformer	Converged dihedral angles[a]				ΔE	Pop.[b]
	D_1	D_2	D_3	D_4	(kJ/mol)	(%)
1	178.0	69.0	36.6	178.8	0	43.52
2	178.2	71.7	-156.4	-175.9	1.210	26.70
3	81.9	79.5	-169.6	-178.3	1.318	25.57
4	80.0	78.1	27.1	176.6	5.792	4.21

[a]dihedral angles: D1:$C^2C^1O^7C^8$;D2:$C^1O^7C^8C^9$; D3:$O^7C^8C^9O^{10}$;D4:$C^8C^9O^{10}H^{11}$.
[b]population based on Gibbs energies

methyl 2-(2-chlorophenoxy) propanoate: For methyl ester **5**, the comparison between experimental spectra and predicted spectra of (*R*)-**5** are shown in Figure 4-13 for absorption and in Figure 4-14 for VCD. In these figures, the numbers listed with bands identify the correlation between experimental and predicted spectra.

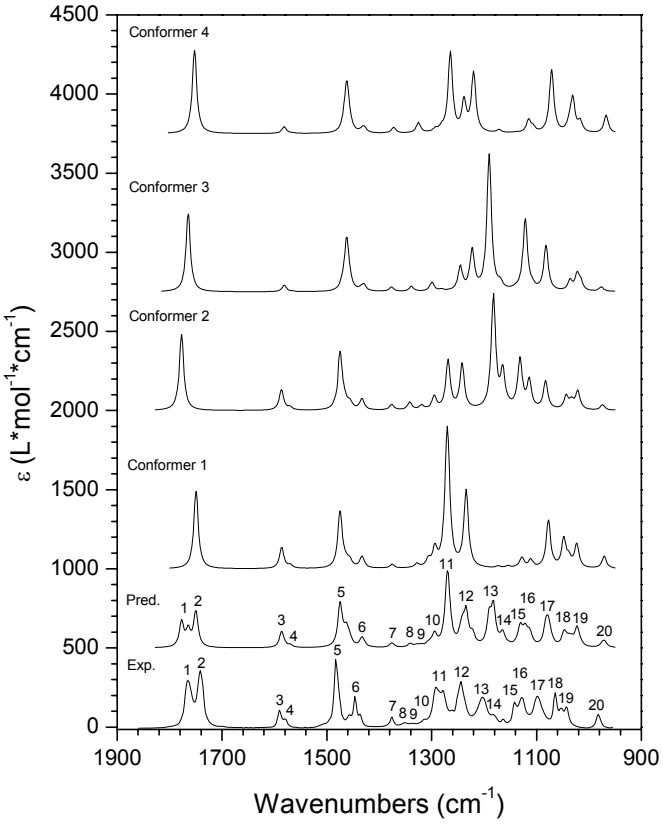

Figure 4-13. Comparison of the experimental absorption spectrum (bottom line) with individual conformer spectra and predicted (population weighted) absorption spectrum of (*R*)-methyl 2-(2-chlorophenoxy)propanoate. The numbers listed with bands identify the correlation between experimental and predicted spectra. Spectra are displayed with offset for clarity.

From Figure 4-13, it can be seen that the experimental and predicted absorption spectra match very well. The frequency calculation for carbonyl region has significant

improvement in esters than that in the case of acids. Band labeled 1 in the experimental absorption spectrum corresponds to two peaks in the predicted spectrum. Similarly two separated peaks in the experimental absorption spectrum for band 11, correspond to one peak in the predicted spectrum. These discrepancies may be attributed to the smaller 6-31G* basis set used for calculation. It is known from the literature that the error in the calculated frequencies with smaller basis set calculation cannot be eliminated only by a single scale factor. Higher-level calculation may be able to eliminate these discrepancies. The remaining peaks have good agreement in both frequency and intensity.

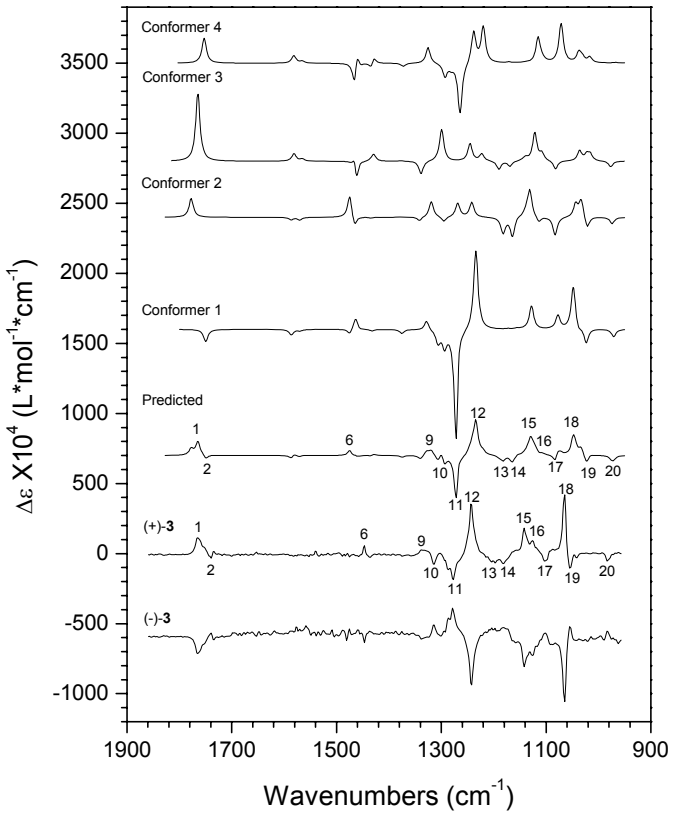

Figure 4-14. Comparison of the experimental VCD spectrum of (+)- and (-)-methyl 2-(2-chlorophenoxy)propanoates with individual conformer spectra and predicted (population weighted) VCD spectrum of (*R*)-methyl 2-(2-chlorophenoxy)propanoate. The numbers listed with bands identify the correlation between experimental and predicted spectra. Spectra are displayed with offset for clarity.

It can be seen in Figure 4-14 that the VCD spectra of (+)-**5** and (-)-**5** are mirror images to each other and that the VCD spectrum of (+)-**5** matches that predicted for (*R*)-**5**. The positive and negative VCD signs of the major peaks are same among experimental and predicted spectra. One major difference is in the intensity of band labeled 18. The experimental VCD spectrum of (+)-**3** shows a narrow intense positive band whereas the predicted spectrum shows a broader band of lower intensity. However, from the comparison of VCD spectral features in the entire region shown, it is certain that (+)-methyl 2-(2-chlorophenoxy)propanoate has the (*R*)-configuration.

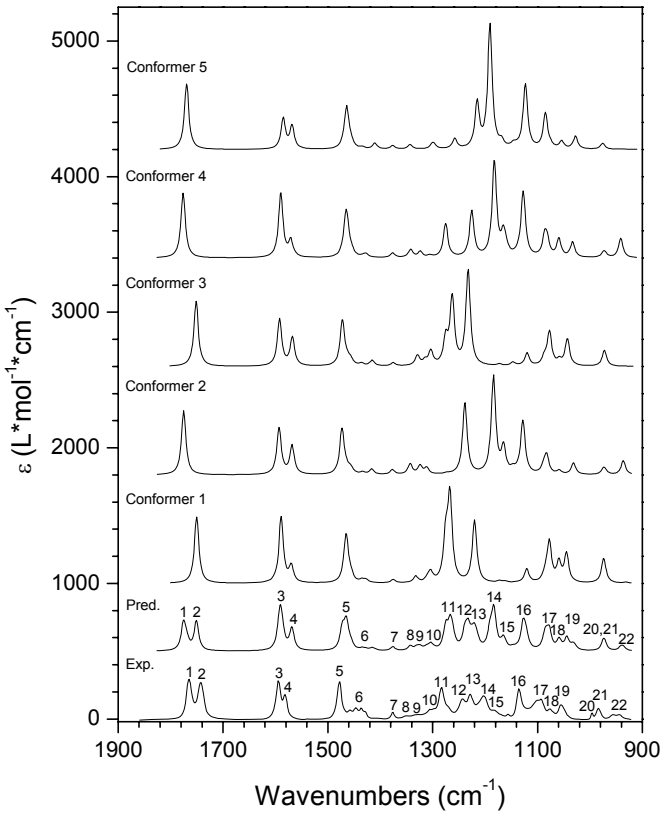

Figure 4-15. Comparison of the experimental absorption spectrum (bottom line) with individual conformer spectra and predicted (population weighted) absorption spectrum of (*R*)-methyl 2-(3-chlorophenoxy)propanoate. The numbers listed with bands identify the correlation between experimental and predicted spectra. Spectra are displayed with offset for clarity.

methyl 2-(3-chlorophenoxy) propanoate: The comparison between experimental spectrum and predicted spectrum for (*R*)-**6** are shown in Figure 4-15 for absorption and in Figure 4-16 for VCD. In these figures, the numbers listed with bands identify the correlation between experimental and predicted spectra. In the absorption spectrum, the observed bands labeled 1 and 2 in carbonyl region are perfectly reproduced in predicted spectrum. The bands labeled 6 in the experimental spectrum do not agree well with those in the predicted spectrum. However, the general agreement between experimental and predicted absorption spectra is good.

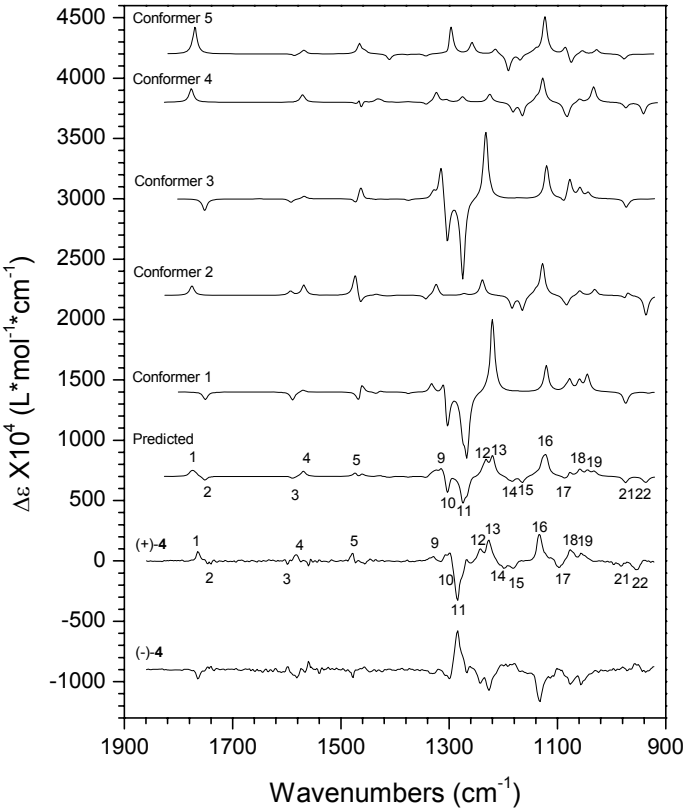

Figure 4-16. Comparison of the experimental VCD spectra of (+)- and (-)-methyl 2-(3-chlorophenoxy)propanoate with individual conformer spectra and predicted (population weighted) VCD spectrum of (*R*)-methyl 2-(3-chlorophenoxy)propanoate. The numbers listed with bands identify the correlation between experimental and predicted spectra. Spectra are displayed with offset for clarity.

In Figure 4-16, it can be seen that the VCD spectra of (+)-**6** and (-)-**6** are mirror images to each other and that the VCD spectrum of (+)-**6** matches that for (*R*)-**6**. The experimental and predicted bands agree well both in signs and intensity with one exception: bands labeled 10 and 11 merge into one in the experimental spectrum while the predicted spectrum shows distinguishable bands labeled 10 and 11. From the comparison of VCD spectral features in the entire region shown in Figure 4-16, the absolute configuration of (+)-methyl 2-(3-chlorophenoxy)propanoate can also be assigned as (*R*).

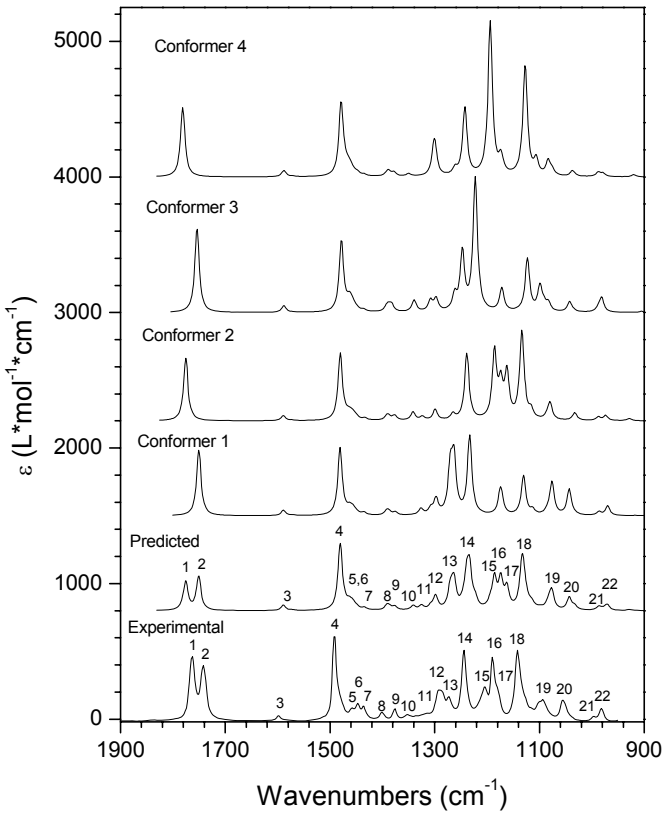

Figure 4-17. Comparison of the experimental absorption spectrum (bottom line) with individual conformer spectra and predicted (population weighted) absorption spectrum of methyl 2-(4-chloro-2-methylphenoxy)propanoate. The numbers listed with bands identify the correlation between experimental and predicted spectra. Spectra are displayed with offset for clarity.

methyl 2-(4-chloro-2-methylphenoxy) propanoate: The experimental and predicted absorption spectra for **7** are shown in Figure 4-17. Here we can see much better agreement compare to the case of **3**. The carbonyl region shows two peaks in both spectra. In the region from 1300 cm^{-1} to 1000 cm^{-1}, the experimental and predicted spectra match each other. One-to-one peak correspondence among experimental and predicted spectra is identified. All experimental peaks were assigned to the predicted peaks. The major differences are for the peaks 12, 13 and peaks 15-17, where the relative peak intensities do not match between experimental and predicted spectra.

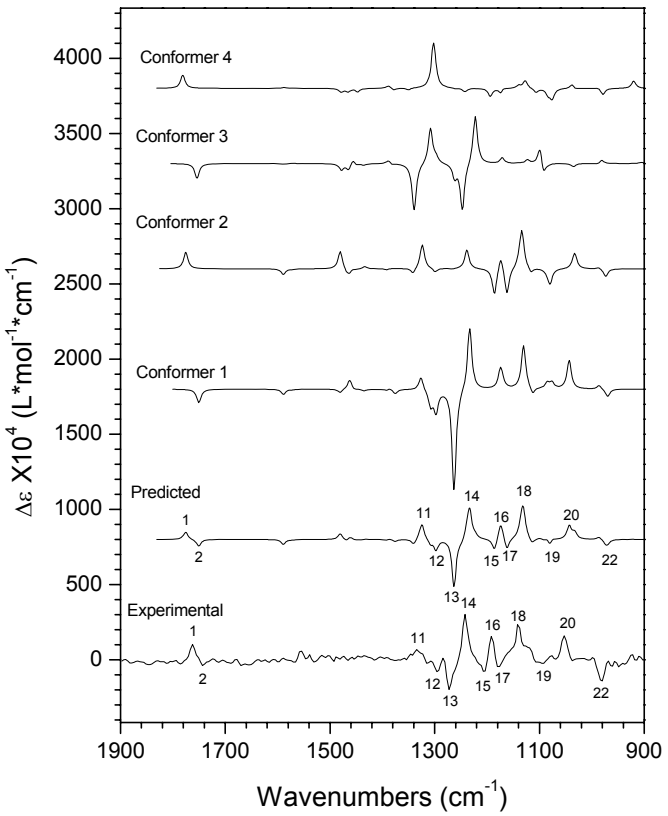

Figure 4-18. Comparison of the experimental VCD spectra of (+)-methyl 2-(4-chloro-2-methylphenoxy)propanoate with individual conformer spectra and predicted (population weighted) VCD spectrum of (*R*)-methyl 2-(4-chloro-2-methylphenoxy)propanoate. The numbers listed with bands identify the correlation between experimental and predicted spectra. Spectra are displayed with offset for clarity.

The experimental VCD spectrum of (+)-**7** and predicted spectrum for (*R*)-**7** are shown in Figure 4-18. The major positive negative peaks in the experimental spectrum are well reproduced in the population weighted predicted spectrum. The one-to-one band correspondence among experimental and predicted spectra is also shown in Figure 4-18. The relative peak intensities also match very well. From this comparison of VCD spectra, we can confidently state the configuration of the ester, (+)-**7**, to be (*R*).

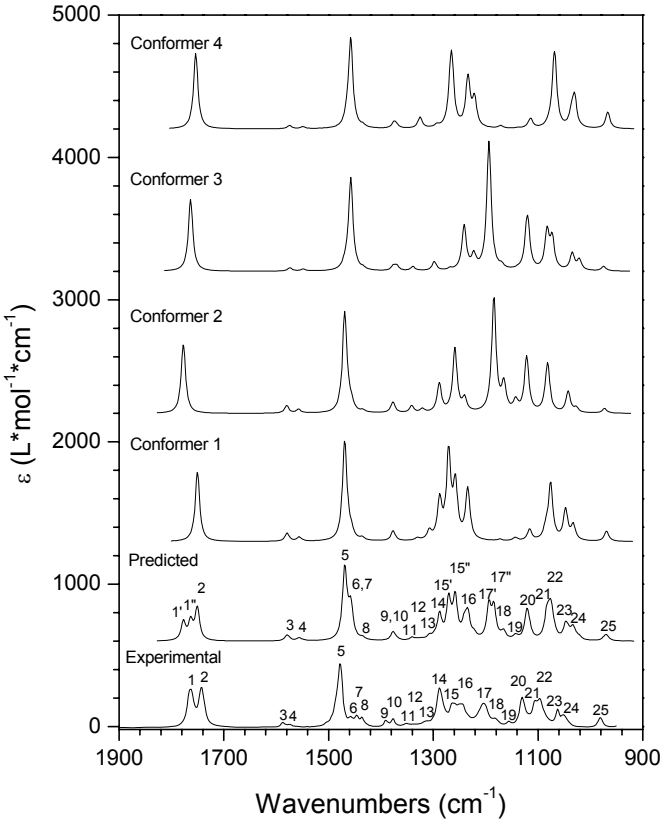

Figure 4-19. Comparison of the experimental absorption spectrum (bottom line) with individual conformer spectra and predicted (population weighted) absorption spectrum of methyl 2-(2,4-dichlorophenoxy)propanoate. The numbers listed with bands identify the correlation between experimental and predicted spectra. Spectra are displayed with offset for clarity.

methyl 2-(2,4-dichlorophenoxy) propanoate: The experimental and predicted absorption spectra of **8** are shown in Figure 4-19. The overall agreement is satisfactory, although not as good as that for compound **7**. There are three peaks in the carbonyl region in the predicted spectrum, whereas there are only two peaks in the experimental spectrum. The peaks 6 and 7 have different relative intensities between experimental and predicted spectra. In the experimental spectrum each of the bands 15 and 17 appear as single peaks. But in the predicted spectrum, each of the corresponding bands is split into two. Other than these differences, the overall agreement is good.

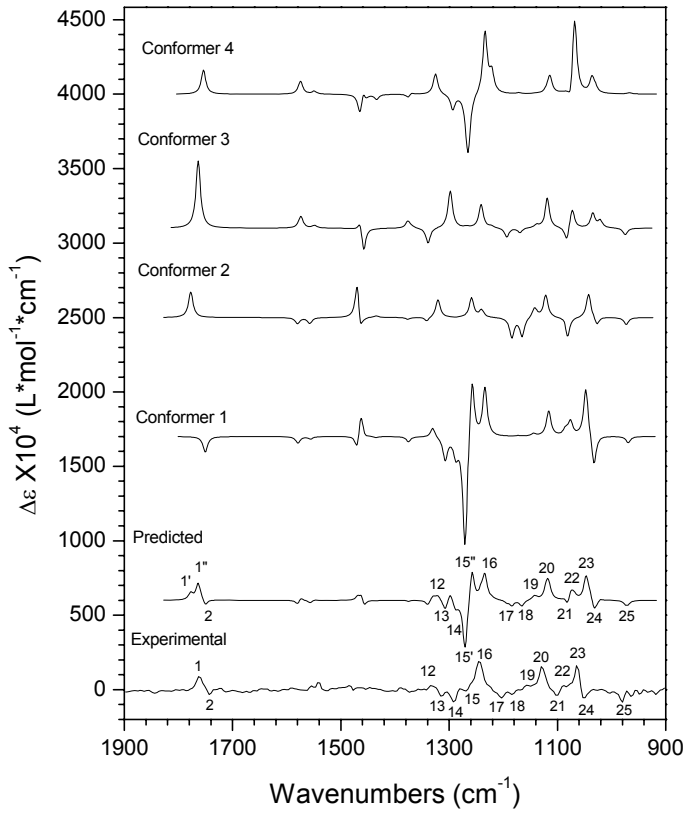

Figure 4-20. Comparison of the experimental VCD spectra of (+)-methyl 2-(2,4-dichlorophenoxy)propanoate with individual conformer spectra and predicted (population weighted) VCD spectrum of (*R*)-methyl 2-(2,4-dichlorophenoxy)propanoate. The numbers listed with bands identify the correlation between experimental and predicted spectra. Spectra are displayed with offset for clarity.

The VCD spectra of **8** are shown in Figure 4-20.We can see that VCD band patterns in the experimental and predicted spectra agree well. One major difference appearing for peak 15 is that the predicted spectrum shows a negative-positive couplet corresponding to a very small peak in the experimental spectrum. This discrepancy could be due to error in the frequencies obtained at B3LYP/6-31G* level. If calculated peaks 15' and 15" have almost the same frequencies then their negative and positive intensities will cancel each other and can produce a small peak. But the frequency error makes them separated and appears as two peaks. Except for this difference, the overall agreement between experimental VCD spectrum of (+)-**8** and predicted spectrum for (*R*)-**8** is excellent. Therefore, we can confidently assign the configuration of ester **8** as (+)-(*R*).

Because methyl esterification of acids with diazomethane does not change the absolute configuration of the chiral center in parent acids, and both parent acid and its ester have the same sign for optical rotation at sodium D line, the same conclusion can be extended to the parent acids. That is, (+)-2-(2-chlorophenoxy) propanoic acid and (+)-2-(3-chlorophenoxy) propanoic acid, which are the second elutants in HPLC with Chiralpak AD-H column, have the (*R*)-configuration. The herbicides, (+)-2-(4-chloro-2-methyl phenoxy) propanoic acid and (+)-2-(2,4-dichlorophenoxy) propanoic acid, also have (+)-(*R*) configuration.

Dimer α-aryloxypropanoic acids model:

Although methyl eserification removes the hydrogen bond effect and provides a way to determine the absolute configuration of these four α-aryloxypropanoic acids, this method can not provide the information about predominate conformation of these four α-

aryloxypropanoic acids in solution. It is known that carboxylic acids tend to form dimers via intermolecular hydrogen bond between two monomer units, as shown in Figure 4-21.

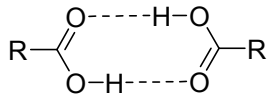

Figure 4-21. Carboxylic acid dimer.

The problem in constructing dimer conformations for the four acids under consideration is that these acids have too many possible starting conformations for monomers, making the calculations for dimers a tedious task. To construct a dimer conformation, the dihedral angle, D4, of $C^8C^9O^{10}H^{11}$ (see Figure 4-1) can be fixed at ~180 degree, but there are three other dihedral angles, D1, D2, and D3, which can be varied. If we take 60, 180, and –60 as possible starting angles for each of these three dihedral angles, then one has to consider 27 starting structures for each monomer unit in the dimer. Combining the two monomer units, the dimer formed will then have a total of (27+1)*27/2=378 possible starting conformations for each of the four acids considered.

However, upon looking at the predicted lowest energy conformers of monomeric acids and their methyl esters, we found that the dihedral angles D1, D2 and D3 of lowest energy conformers of monomeric acids and their esters are similar. Based on this observation, we developed the following working hypothesis for constructing dimer conformations. Since the dihedral angles D1, D2, and D3 are not influenced significantly by esterification, they probably would not be influenced by hydrogen bonding as well. Then the lowest energy conformers of monomeric acids can be used to represent the monomer units in a dimer. This hypothesis, along with the requirement that the

$C^8C^9O^{10}H^{11}$ dihedral angle, D4, should be ~180° for intermolecular hydrogen bonding, will greatly reduce the number of possible starting dimer conformations. With these guidelines, we have investigated the possible dimer conformations using the lowest energy monomeric acid (or their ester) conformations as the starting point. The notation used for dimers is as follows: if a dimer is formed from combining conformer 1 (labeled Con1) of one monomer unit and conformer 3 (Con3) of a second monomer unit, then the dimer is labeled as Con1-Con3. The reliability of final dimer conformations is then evaluated by comparing the predicted absorption and VCD spectra for these conformers with the corresponding experimental spectra in solution.

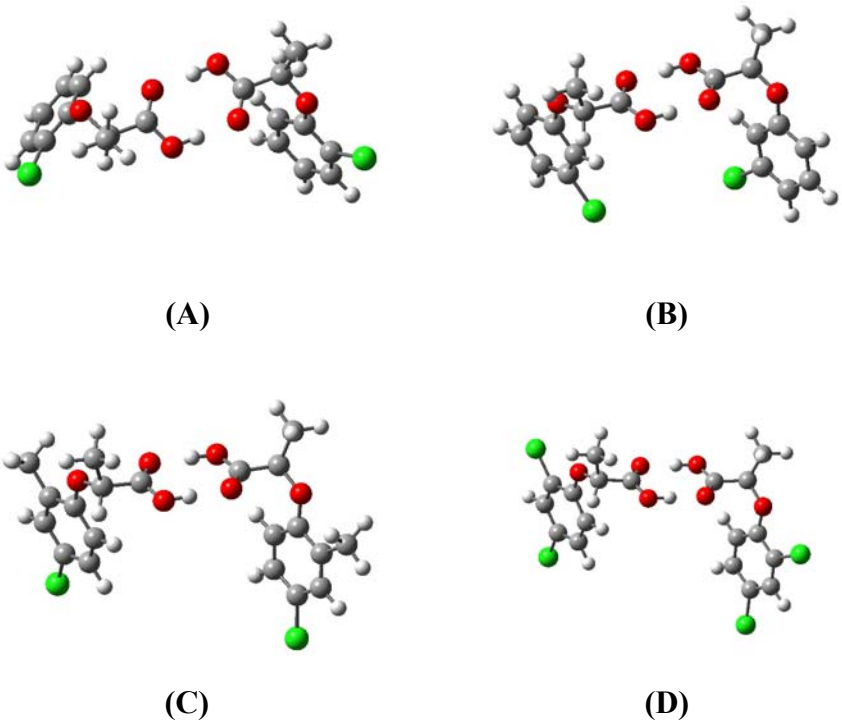

Figure 4-22. The structures of lowest energy conformers of dimeric acids. (A). Con3-Con4 of (*R*)-2-(2-chlorophenoxy) propanoic acid; (B). Con2-Con2 of (*R*)-2-(3-chlorophenoxy) propanoic acid; (C). Con2-Con2 of (*R*)-2-(4-chloro-2-methylphenoxy) propanoic acid; (D). Con2-Con2 of (*R*)-2-(2,4-dichlorophenoxy) propanoic acid.

2-(2-chlorophenoxy) propanoic acid: For (*R*)-**1**, we constructed the dimer conformations using the optimized structures of conformers 1, 3, and 4 of the monomeric acid (labeled as Con1, Con3 and Con4, see Table 4-1). The structures of these three conformations are similar to those of conformers 1, 2, and 3 of methyl ester. The conformer 2 of monomeric acid was not used because the dihedral angle D4 for this conformer (1.2^{o}) does not permit dimer formation. The length of hydrogen bond O—H-----O is taken from the literature[89] to be 2.70 Å. The three starting monomer conformations generated six starting dimer conformations and all of these conformers were submitted to geometry optimization. The final optimized structures are summarized in Table 4-9. In the optimized structures, the geometries of individual monomer units of dimer are very close to those of starting monomeric acids. The optimized hydrogen bond length, O—H-----O, is around 2.69 Å. The optimized structure of lowest energy dimer conformer, Con3-Con4 is shown in Figure 4-22 A.

Table 4-9. The optimized geometries, Gibbs energies, and populations of conformers of (*R*)-2-(2-chlorophenoxy) propanoic acid dimer[a].

Conformer	Monomer 1				Monomer 2				ΔE (kJ/mol)	Pop.[b] (%)
	D_1	D_2	D_3	D_4	D_1	D_2	D_3	D_4		
Con3-Con4	178	72	-159	-176	79	81	-169	-177	0	33.66
Con3-Con3	177	72	-154	-176	177	72	-154	-176	1.696	16.98
Con1-Con3	176	71	35	178	178	72	-155	-176	1.859	15.90
Con1-Con4	177	71	31	178	79	81	-169	-178	2.308	13.26
Con1-Con1	177	72	32	178	177	72	32	178	2.977	10.13
Con4-Con4	79	80	-167	-177	79	80	-167	-177	2.990	10.07

[a]The labels Con1, Con2, Con3, and Con4 are for the optimized conformations of monomeric acid. The dihedral angle definitions for D1, D2, D3, and D4 are, respectively, $C^2C^1O^7C^8$, $C^1O^7C^8C^9$, $O^7C^8C^9O^{10}$, $C^8C^9O^{10}H^{11}$.
[b]population based on Gibbs energies

To evaluate if these dimer conformers are in fact the ones that represent the spectra in solution, we calculated the vibrational frequencies and intensities for the six stable dimer conformers listed in Table 4-9. From the vibrational frequency calculation, we noted that all six structures represent energy minima, as there were no imaginary frequencies. The relative Gibbs free energies and populations generated there from are also listed in Table 4-9. The population weighted absorption and VCD spectra for (*R*)-**1** are compared to the corresponding experimental spectra in Figure 4-23.

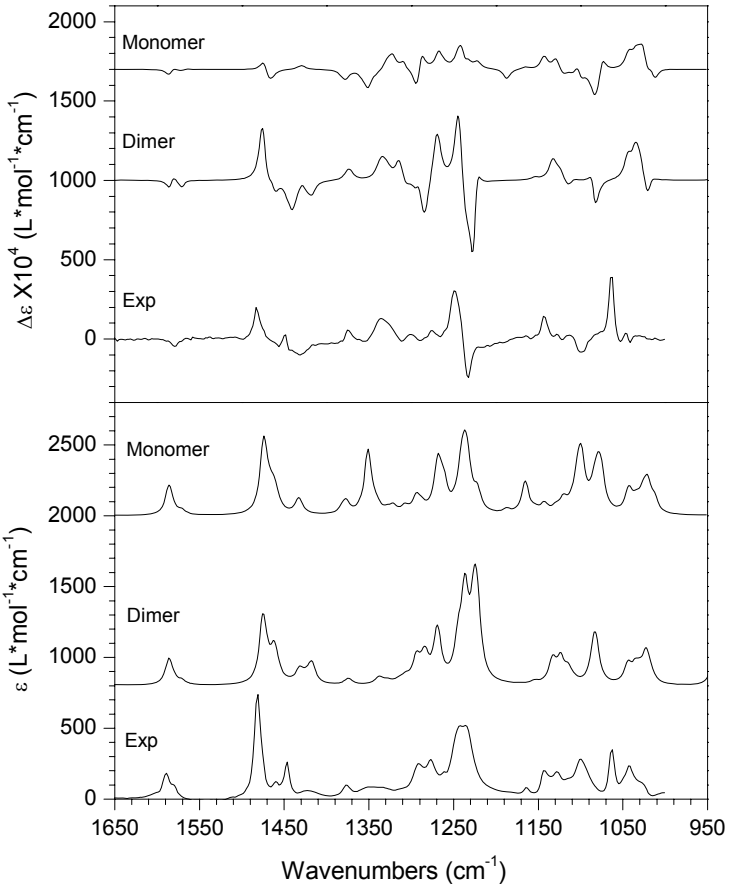

Figure 4-23. Comparison between experimental and predicted vibrational absorption (bottom panel) and VCD (top panel) spectra of 2-(2-chlorophenoxy) propanoic acid. The experimental measurements were made for (+)-enantiomer and calculations were done for (*R*)-configuration.

In the absorption spectra of Figure 4-23, the predicted dimer spectra can be seen to be in much better agreement with experimental spectrum, while predicted monomeric acid spectrum is not. The region from ~1650 cm^{-1} to 1000 cm^{-1} has a good agreement between experimental and predicted dimer spectra. The predicted monomer absorption spectrum on the other hand shows two extra peaks around 1340 and 1160 cm^{-1}. In the VCD spectra of Figure 4-23, the predicted dimer spectrum has a much better agreement, compared to the spectrum calculated for monomeric acid, with the experimental spectrum in the ~1600-1000 cm^{-1} region. One discrepancy is in the region near 1275 cm^{-1} where predicted spectrum shows an extra negative-positive couplet. Nevertheless, the predicted spectrum of dimer satisfactorily reproduces the positive-negative couplet seen around 1240 cm^{-1} in the experimental spectrum, while the predicted monomer spectrum failed to reproduce this feature. From the calculated vibrational displacements, the vibration that generated this positive-negative couplet is found to involve the hydrogen atoms in the carboxylic groups of dimer. This explains why the predicted spectrum for the monomer acid cannot reproduce this couplet.

Since a reasonable agreement, in both absorption and VCD spectra, is seen between the predicted dimer spectra and experimental spectra in solution, the dimer conformations used in calculation can be considered to represent the conformations in the solution. Furthermore, since experimental VCD spectra were obtained for (+)-enantiomer and calculations were done for the (*R*)-configuration, the absolute configuration can be assigned as (+)-(*R*), as was concluded from prior investigations on methyl ester of this acid.

2-(3-chlorophenoxy) propanoic acid: Location of chlorine atom at position 3 of phenyl group in (*R*)-**2** makes the energy barrier less when the dihedral angle $C^2C^1O^7C^8$ is varied. As a result there is one additional conformation here than in the case of (*R*)-**1**. Four stable conformers 1, 2, 3, 4 of monomeric acid are similar to conformers 1, 2, 4, and 3 of the corresponding methyl ester. These conformers (labeled as Con1, Con2, Con3 and Con4) are used to construct dimer conformers, which lead to ten starting dimer structures. All of these 10 conformers are submitted to geometry optimization. The seven most stable conformers are listed in Table 4-10. The remaining three conformers with higher energy are not listed because their populations are negligible for the present purposes. Again, the monomer components in dimer have the geometries similar to those optimized for monomeric acids. The structure of the lowest energy dimer conformer, Con2-Con2, is shown in Figure 4-22 B.

Table 4-10. The optimized geometries, Gibbs energies, and populations of conformers of (*R*)-2-(3-chlorophenoxy) propanoic acid dimer[a].

Conformer	Monomer 1				Monomer 2				ΔE (kJ/mol)	Pop.[b] (%)
	D_1	D_2	D_3	D_4	D_1	D_2	D_3	D_4		
Con2-Con2	0.1	73	-158	-176	0.1	72	-158	-176	0	18.98
Con3-Con3	178	72	-154	-176	179	72	-154	-176	0.181	17.64
Con2-Con3	0.1	72	-160	-177	179	71	-157	-177	0.328	16.62
Con3-Con4	178	72	-156	-176	-1	71	32	179	1.000	12.67
Con1-Con3	177	71	35	178	178	72	-156	-177	1.082	12.27
Con1-Con2	177	71	33	178	0.1	72	-157	-177	1.166	11.86
Con2-Con4	-0.4	72	-157	-177	-2	71	33	178	1.599	9.96

[a]The labels Con1, Con2, Con3, and Con4 are for the optimized conformations of monomeric acid. The dihedral angle definitions for D1, D2, D3, and D4 are, respectively, $C^2C^1O^7C^8$, $C^1O^7C^8C^9$, $O^7C^8C^9O^{10}$, $C^8C^9O^{10}H^{11}$.
[b]population based on Gibbs energies

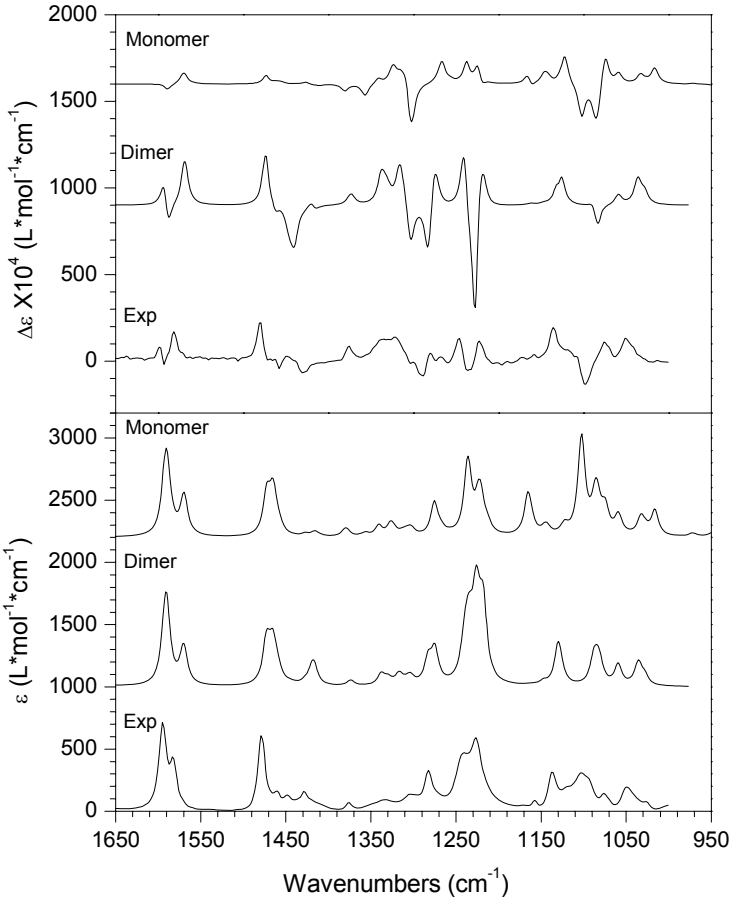

Figure 4-24. Comparison between experimental and predicted vibrational absorption (bottom panel) and VCD (top panel) spectra of 2-(3-chlorophenoxy) propanoic acid. The experimental measurements were made for (+)-enantiomer and calculations were done for (*R*)-configuration.

The vibrational spectra of (*R*)-**2** dimers are calculated at the optimized geometries. The populations of dimer conformers deduced from Gibbs energies are also listed in Table 4-10. The absorption and VCD spectra are compared to the experimental spectra in Figure 4-24. In the absorption spectra of Figure 4-24, we see an excellent agreement again between experimental and predicted dimer spectra, but not between experimental and predicted monomer spectra. The relative intensities of predicted dimer VCD bands in the 1360 cm^{-1} to 1200 cm^{-1} region are somewhat larger than the experimental values.

When positive and negative VCD bands appear next to each other, separation between their band positions will influence their relative intensities due to mutual cancellation. Thus unless band positions are predicted accurately, which is difficult at B3LYP/6-31G* level, the relative intensities of overlapping VCD bands cannot be reproduced well. The overall agreement between experimental and predicted dimer VCD spectra is much better than that between the experimental and predicted monomer VCD spectra. In particular, the signs of VCD bands in predicted dimer and experimental spectra agree very well in the region from ~1650 cm^{-1} to 1000 cm^{-1}. Thus the dimer conformations used can be considered to represent the conformations in solution. From the comparison between predicted dimer and experimental spectra, the absolute configuration of **2** can be assigned as (+)-(*R*), as concluded from investigations on corresponding methyl esters.

Table 4-11**.** The optimized geometries, Gibbs energies, and populations of conformers of (*R*)-2-(4-chloro-2-methylphenoxy) propanoic acid dimer[a].

Conformer	Monomer 1				Monomer 2				ΔE (kJ/mol)	Pop.[b] (%)
	D_1	D_2	D_3	D_4	D_1	D_2	D_3	D_4		
Con2-Con2	180	71	-155	-176	180	71	-155	-176	0	54.65
Con1-Con2	180	70	33	178	180	71	-156	-176	1.452	30.42
Con1-Con1	179	71	31	178	179	71	31	178	3.216	14.93

[a]The labels Con1 and Con2 are for the optimized conformations of monomeric acid. The dihedral angle definitions for D1, D2, D3, and D4 are, respectively, $C^2C^1O^7C^8$, $C^1O^7C^8C^9$, $O^7C^8C^9O^{10}$, $C^8C^9O^{10}H^{11}$.
[b]population based on Gibbs energies

2-(4-chloro-2-methylphenoxy) propanoic acid: For this acid, the conformers 1 and 2 (labeled as Con1 and Con2) in both acid and its methyl ester account for about 90% of the population. Therefore, only conformers 1 and 2 are chosen to construct dimer

structures. This will generate three starting dimer structures. All of these three conformers are submitted for geometry optimization. Their optimized structures are listed in Table 4-11. Here also the monomer components in dimer have the geometries similar to those optimized for monomeric acids. The structure of the lowest energy dimer conformer, Con2-Con2, is shown in Figure 4-22 C.

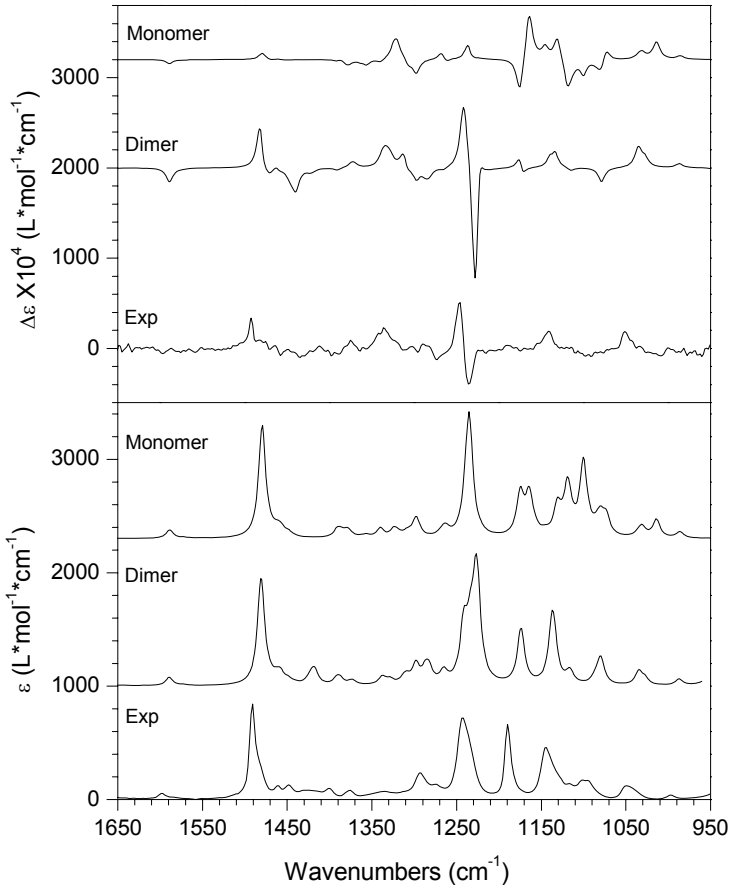

Figure 4-25. Comparison between experimental and predicted vibrational absorption (bottom panel) and VCD (top panel) spectra of 2-(4-chloro-2-methylphenoxy) propanoic acid. The experimental measurements were made for (+)-enantiomer and calculations were done for (*R*)-configuration.

The absorption and VCD spectra are calculated for these three conformers at their optimized geometries. The population weighted predicted spectra for dimeric acids are shown in Figure 4-25. In the absorption spectra of Figure 4-25, we notice an excellent agreement again between experimental and predicted dimer spectra. There are some minor differences in the relative absorption intensities among predicted dimer and experimental spectra, but the relative intensities cannot be expected to match well at B3LYP/6-31G* level used here. In the VCD spectra of Figure 4-25, the major positive and negative VCD bands agree well between experimental and predicted dimer spectra. The experimental positive-negative VCD couplet around 1240 cm^{-1}, which does not show up in the predicted spectrum of monomeric acid is reproduced very nicely in predicted dimer spectrum. Thus the dimer conformations used can be considered to represent the conformations in solution. Since the signs of VCD bands in predicted dimer and experimental spectra agree very well in Figure 4-25, the absolute configuration of **3** can be assigned as (+)-(*R*), as deduced from investigations on corresponding methyl ester.

2-(2,4-dichlorophenoxy) propanoic acid: For (*R*)-**4**, three conformers (labeled Con1, Con2, Con3) account for most of the population of monomer acid conformers. Thus these three conformers are used to construct the dimer structures, resulting in six starting dimer conformations. The optimized dimer structures are listed in Table 4-12. Here also the monomer components in dimer have the geometries similar to those optimized for monomeric acids. The structure of the most stable conformer, Con2-Con2, is shown in Figure 4-22 D.

Table 4-12. The optimized geometries, Gibbs energies, and populations of conformers of (*R*)-2-(2,4-dichlorophenoxy) propanoic acid dimer[a].

Conformer	Monomer 1				Monomer 2				ΔE (kJ/mol)	Pop.[b] (%)
	D_1	D_2	D_3	D_4	D_1	D_2	D_3	D_4		
Con2-Con2	178	72	-155	-176	178	72	-155	-176	0	23.40
Con1-Con2	177	71	31	178	178	72	-158	-176	0.415	19.79
Con2-Con3	178	73	-162	-176	79	81	-171	-178	0.848	16.62
Con3-Con3	80	81	-171	-178	80	81	-171	-178	0.898	16.28
Con1-Con3	177	71	34	178	80	80	-168	-178	1.286	13.92
Con1-Con1	177	71	32	178	177	71	32	178	2.108	9.99

[a]The labels Con1, Con2 and Con3 are for the optimized conformations of monomeric acid. The dihedral angle definitions for D1, D2, D3, and D4 are, respectively, $C^2C^1O^7C^8$, $C^1O^7C^8C^9$, $O^7C^8C^9O^{10}$, $C^8C^9O^{10}H^{11}$.

[b]population based on Gibbs energies

The predicted absorption and VCD spectra for dimeric acid are shown in Figure 4-26. The agreement between experimental and predicted dimer spectra is quite good, while that between experimental and predicted monomer spectra is rather poor. Some minor discrepancies however should be noted. In the 1250 cm^{-1} region, the experimental absorption spectrum shows a broad band while the predicted dimer absorption spectrum shows three resolved bands. In the region from 1060 cm^{-1} to 1150 cm^{-1}, the predicted dimer spectrum shows two well-separated peaks while experimental spectrum shows two partially separated peaks. These discrepancies are attributed to the errors in predicted band positions at the B3LYP/631G* level. Nevertheless, the fact the experimental spectra are reasonably well reproduced by the predicted dimer spectra and not by the predicted monomer spectra, suggests that the dimer conformations used here represent those in solution. Moreover, since the signs of all major VCD bands in predicted dimer and experimental spectra agree very well, the absolute configuration of **4** can be assigned as

(+)-(*R*), agreeing with the conclusion arrived at from the investigations on corresponding methyl ester.

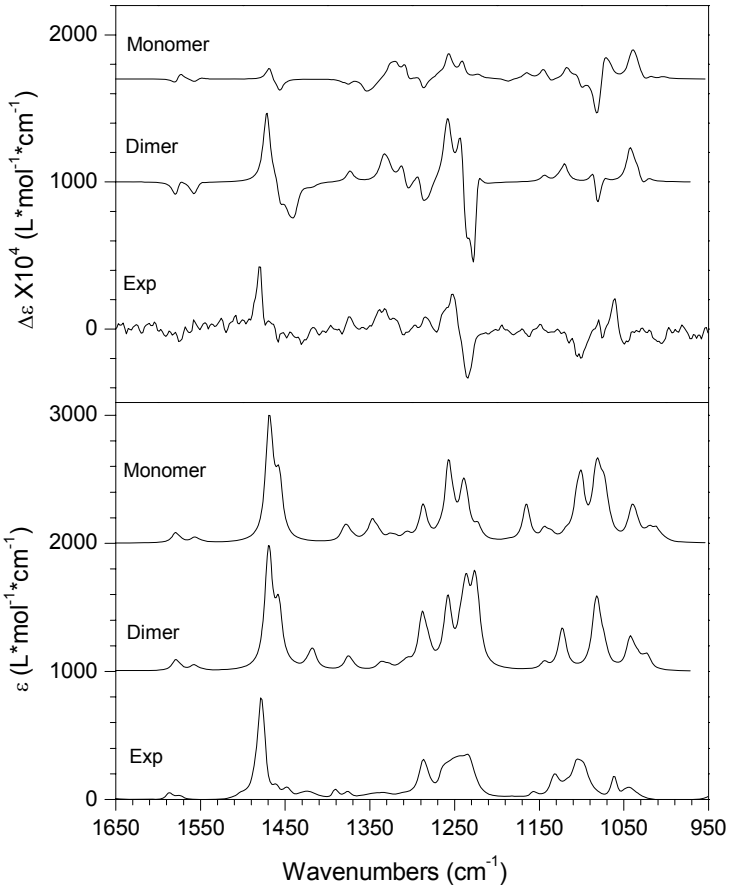

Figure 4-26. Comparison between experimental and predicted vibrational absorption (bottom panel) and VCD (top panel) spectra of 2-(2,4-dichlorophenoxy) propanoic acid. The experimental measurements were made for (+)-enantiomer and calculations were done for (*R*)-configuration.

The vibrational absorption spectra in the carbonyl region are shown in Figure 4-27 for all four acids considered. Concentrations used for the experimental absorption spectra in Figure 4-27 are same as those for the spectra in Figures 4-23 to 4-26. The experimental VCD spectra in this region are not shown because VCD bands in this region are very weak.

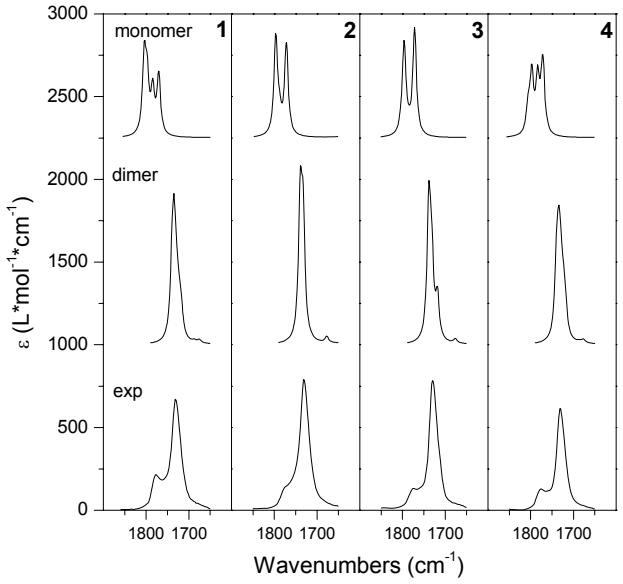

Figure 4-27. The experimental (bottom trace) and predicted (top two traces) vibrational absorption spectra for acids **1**-**4** in the carbonyl region.

The predicted dimer absorption spectra have better agreement with experimental absorption spectra compared to the predicted monomer spectra. The strong peak around 1730 cm^{-1} in the experimental spectra is reproduced well in the predicted dimer spectra. The high frequency shoulder at 1774 cm^{-1} in the experimental spectra is assigned to the carbonyl vibration of monomer. Although some amount of monomer conformers is present in solution, the absorption and VCD in the 1650-950 cm^{-1} region are mostly determined by the dimer conformations as can be inferred from Figures 4-23 to 4-26 and from concentration dependent studies (vide infra). If the goals were to compare the experimental and calculated spectra quantitatively, then one would have to simulate the predicted spectra with a certain amount of monomer conformers. Alternately, it would be possible to determine the percent populations of monomers and dimers using a regression analysis of the experimental and predicted intensities[22], if the predicted absorption and

VCD intensities are quantitatively accurate. But it was pointed out in early chapters that B3LYP predictions of absorption and VCD intensities are not sufficiently accurate for quantitative comparisons, even when large basis sets are used for small molecules. For this reason we did not attempt to obtain the simulated spectra with an admixture of monomer and dimer contributions.

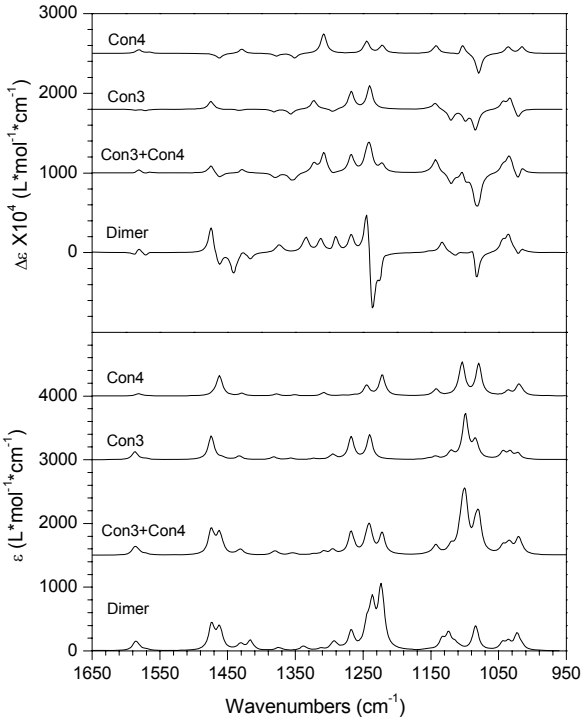

Figure 4-28. Evaluation of spectra additivity predicted spectra for 2-(2-chlorophenoxy) propanoic acid. (a) .Vibrational absorption (bottom panel); (b). VCD (top panel) Con3 and Con4 are the monomer spectra predicted for these two conformations. Con3+Con4 represents the numerical sum of the spectra predicted for monomer conformers 3 and 4, while dimer spectra represent those predicted for the dimer Con3-Con4.

Spectral Additivity: When dealing with large molecular systems, it would be tempting to undertake the calculations on different fragments of the molecule of interest

and add the results to represent the property of full molecule. Such an approach would be valid if the interactions between different fragments do not influence the property of interest. In the case of vibrational properties, however, the very nature of normal coordinates imposes cross talk between fragments of a molecule. So it is of interest to know if the vibrational spectra of fragments can be additive to represent the vibrational spectrum of full molecules. Since dimers are viewed as a combination of two monomers, it would be useful to verify the additivity of the spectra of monomers. In Figure 4-28, the predicted vibrational spectra for monomer conformers 3 and 4, their numerical sum and of dimer derived from these monomers are compared for 2-(2-chlorophenoxy) propanoic acid. In the 1150-950 cm^{-1} region, the numerically added VCD spectrum compares reasonably well with the predicted VCD spectrum of dimer. But the numerically added absorption spectrum in this region does not match with the predicted absorption spectrum of dimer. In the 1400-1150 cm^{-1} region, both absorption and VCD spectra predicted for dimer are significantly different from the corresponding numerically added spectra for monomers contained therein. The vibrational modes involving intermolecular hydrogen bonding appear in the 1400-1150 cm^{-1} region, as noted for other hydrogen-bonded systems[23] such as butanol. Thus the concept of additivity for vibrational absorption and VCD spectra of α-aryl propanoic acids does not work in the spectral regions where vibrational modes involving intermolecular hydrogen bonds occur.

Conclusion

The predicted absorption and VCD spectra for monomer conformations of α-aryloxypropanoic acids did not reproduce the corresponding experimental spectra. This

is believed to be due to dimer formation for acids in solution. The intermolecular hydrogen bonding effects were eliminated by converting the acids to corresponding methyl esters. The experimental spectra of esters in solution and predicted spectra for isolated methyl ester molecules matched very well and allowed unambiguous determination of absolute configuration of the esters as (+)-(*R*). This conclusion is safely extended to the parent acids since esterification with diazomethane does not invert the absolute configuration of the acid. Although this method helps to determine the absolute configuration of these four acids, it can not provide information about the predominant conformation.

Noting that the predicted structures of monomeric acids are very similar to those of corresponding methyl esters, we hypothesized that the lowest energy structures of monomeric acids can be used to construct the starting structures for dimeric acids. The starting geometries of dimer structures were optimized at B3LYP/6-31G* level. In the optimized dimer structures, the individual monomer components are found to have structures similar to the optimized conformers of monomeric acids. To verify the reliability of optimized dimer structures, absorption and VCD spectra have been calculated at the optimized geometries. The population weighted predicted absorption and VCD spectra for dimeric acids are found to be in good agreement with the corresponding spectra in $CDCl_3$ solution. This approach provides the information about both the absolute configuration and predominant conformations.

Based on the present work, we can suggest a general approach for interpreting the vibrational spectra of carboxylic acids in solution. This approach involves first finding the lowest energy conformers of a monomeric acid and its methyl ester. If the lowest

energy conformers of acid and its ester are similar, then one can use these lowest energy optimized structures for generating dimer conformers. Vibrational spectra calculated for the optimized dimer conformers can then be compared to the experimental spectra to evaluate the validity of these conformers in solution. In this manner, one can determine the predominant conformations of dimeric acids, as well as their absolute configuration, using density functional predictions of absorption and VCD spectra.

CHAPTER V

ASSIGNING THE ABSOLUTE CONFIGURATION OF GLUTAMIC ACID HOMOLOGUE COMPOUNDS BY VIBRATIONAL CIRCULAR DICHROISM AND OPTICAL ROTATION

Introduction

(*S*)-Glutamic acid (Glu), the main excitatory neurotransmitter in the mammalian central nervous system, is involved in the physiological regulation of processes such as learning and memory. On the other hand, glutamatergic hyperactivity leads to neurotoxicity typical of some acute and chronic neurodegenerative diseases, i.e., cerebral ischemia, epilepsy, amyotrophic lateral sclerosis, Parkinson's and Alzheimer's diseases. Glu acts at specific receptors belonging to two heterogeneous families: the ionotropic and the metabotropic glutamate receptors (iGluRs and mGluRs, respectively).[90-93]

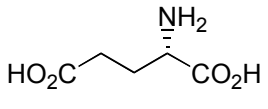

Glu

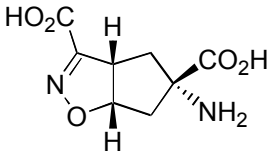

(±)-**1**

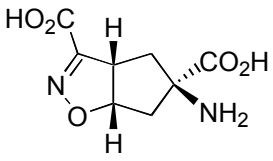

(±)-**2**

Figure 5-1. Structure of the reference and investigated ligands of the glutamate receptors.

In the search for new subtype selective ligands at the different glutamate receptors, a group of 3-carboxy-Δ^2-isoxazoline acidic amino acids, especially were designed as new conformationally constrained analogues (or homologues) of Glu.[94-96] In these compounds, two stereoisomeric homologues of Glu: 5-amino-4,5,6,6a-tetrahydro-3a*H*-cyclopenta[*d*]isoxazole-3,5-dicarboxylic acids (±)-**1** and (±)-**2**, characterized by an extended conformation embedded in a bicyclic ring system, exhibit interesting anticonvulsant activity.[97]

To further investigate the biological activity of (±)-**1** and (±)-**2,** they were separated to enantiopure compounds. Due to the assignment of the absolute configuration of (+)-**1**/(−)-**1** and (+)-**2**/(−)-**2** by X-ray crystallography was failed, (−)-**1** and (−)-**2** were methyl esterification to their methyl esters (−)-**3** and (−)-**4**. In this chapter, the absolute configuration of (−)-**3** and (−)-**4** were assigned by comparing the experimental and theoretical vibrational circular dichroism (VCD) spectra. These absolute configurations were further confirmed using experimental and theoretical specific rotations.

Experimental Section

The absorbance and VCD spectra were recorded on a commercial Fourier transform VCD spectrometer, Chiralir. The VCD spectra were recorded with three-hour data collection time at 4 cm^{-1} resolution. Spectra were measured in $CDCl_3$ solutions at a concentration of about 15 mg/mL. The sample was held in a variable path length cell with BaF_2 windows. In the absorption spectra presented, the solvent absorption was subtracted out. In the VCD spectra presented, the raw VCD spectrum of the solvent was subtracted. Optical rotation of (−)-**3** and (−)-**4** were measured at 589 nm in $CHCl_3$ solutions on an

Autopol IV polarimeter. Intrinsic rotation, $\{\alpha\}_D$ (specific rotation in the limit of zero concentration) was extracted from a plot of experimental specific rotation, $[\alpha]_D$, versus concentration.

The vibrational frequencies, absorption and VCD intensities were calculated for the two diastereomers using Gaussian program.[8] The calculations used the density functional theory with B3LYP functional and 6-31G* and aug-cc-pVDZ basis sets. The theoretical absorption and VCD spectra of the two diasteromers were simulated with Lorentzian band shapes and 5 cm^{-1} half-width. The B3LYP/6-31G* calculated frequencies were scaled with 0.96. The specific rotations were calculated using the Dalton program.[9]

Results and Discussion

Configuration and Conformation Analysis. 5-Amino-4,5,6,6a-tetrahydro-3a*H*-cyclopenta[*d*]isoxazole-3,5-dicarboxylic acid dimethyl ester contains three stereogenic centers (C-3a, C-5, and C-6a) (Figure 5-2A). This will generate 2^3=8 possible absolute configuration. Owing to the *cis* relationship existing between the two hydrogens at C-3a and C-6a, which have the same configuration, the number of diastereomers is reduced to four. Two diastereomers, (3a*S*,5*S*,6a*S*)-**3** and (3a*S*,5*R*,6a*S*)-**4** were chosen for theoretical analyses (Figure 5-2A). The remaining two diastereomers (3a*R*,5*R*,6a*R*)-**3** and (3a*R*,5*S*,6a*R*)-**4** are mirror images to the chosen isomers.

The 4,5-dihydroisoxazole moiety of the bicyclic ring is relatively rigid due to the C=N double bond. On the contrary, the cyclopentane ring is more flexible than the 4,5-dihydroisoxazole ring. The $-NH_2$ (or $-COOCH_3$) group at C-5 can adopt either an

equatorial or axial orientation (Figure 5-2B). There is conformational freedom around the two single bonds (C3-C7 and C5-C10) between the bicyclic ring and the carboxylate

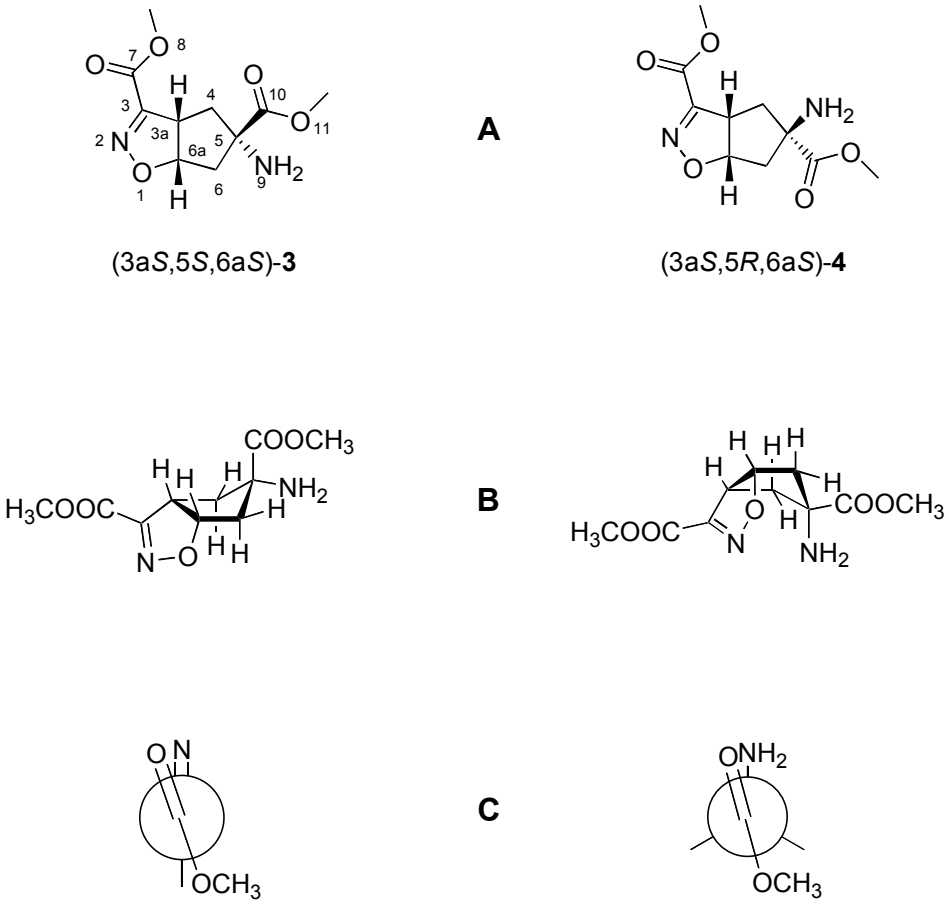

Figure 5-2. Structures of the investigated diastereomers. (**A**) (3a*S*,5*S*,6a*S*)-**3** and (3a*S*,5*R*,6a*S*)-**4**. (**B**) Equatorial and axial orientations at C-5. (**C**) Newman projections around C3-C7 and C5-C10.

groups. To investigate this conformational mobility, we performed a relaxed potential energy scan (PES) by varying the dihedral angles, N2-C3-C7-O8 and N9-C5-C10-O11,around these two single bonds. The Newman projections around these two single bonds are shown in Figure 5-2C. The scan step of the dihedral angle is 20^{o}. For the single bond C3-C7, between the 4,5-dihydroisoxazole ring and the carboxylate group, a 360^{o}

PES was performed. For the single bond C5-C10 between the cyclopentane ring and the carboxylate group, an 180° PES was carried out because the environment is almost symmetric for another 180° dihedral angle change. The results, reported in Figure 5-3, show the presence of two potential energy minima for each of the two dihedral angles. These minima are at 2° and 182° for the dihedral angle N2-C3-C7-O8 (connecting the 4,5-dihydroisoxazole ring to the carboxylate group), and at 128° and 308° for the dihedral angle N9-C5-C10-O11 (connecting the cyclopentane ring to the carboxylate group).

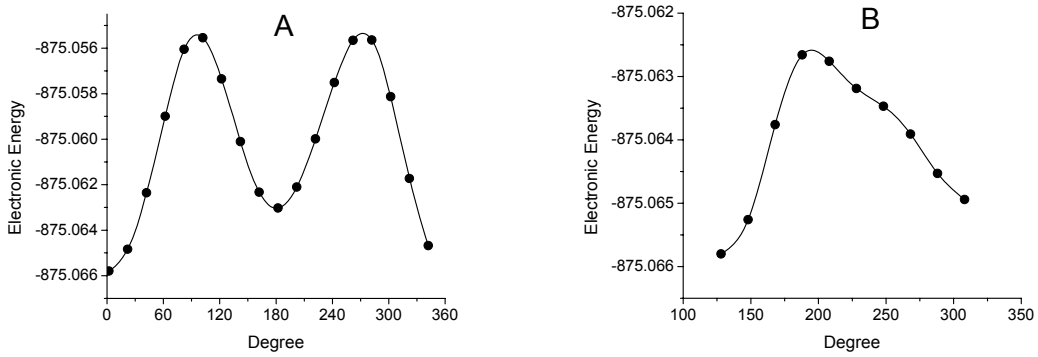

Figure 5-3. The potential energy scan results for (3a*S*,5*S*,6a*S*)-**3**. **A**: energy (in Hartrees) vs dihedral angle N2-C3-C7-O8. **B**: energy (in Hartrees) vs dihedral angle N9-C5-C10-O11.

These four conformations, in combination with the equatorial and axial orientations at C-5, result in eight possible conformations for each of the two diastereomers studied. Geometry optimization of these eight conformations was undertaken with density functional theory using B3LYP functional and 6-31G* basis set. The most stable five conformations were also investigated using a larger basis set aug-cc-pVDZ for improved accuracy in the calculations. The optimized geometrical parameters for the stable conformations are listed in Table 5-1. The structure of the lowest energy conformer is displayed in Figure 5-4 for both (3a*S*,5*S*,6a*S*)-**3** and (3a*S*,5*R*,6a*S*)-**4**.

Figure 5-4. B3LYP/6-31G* optimized structures for the lowest energy conformer of (3a*S*,5*S*,6a*S*)-**3** (left) and of (3a*S*,5*R*,6a*S*)-**4** (right).

Table 5-1. Optimized structural parameters[a] for investigated diastereomers (3a*S*,5*S*,6a*S*)-**3** and (3a*S*,5*R*,6a*S*)-**4**.

(3aS,5S,6aS)-**3**								
Conf-ormer	B3LYP/6-31G*				B3LYP/aug-cc-pVDZ			
	Energy[b]	D1	D2	D3	Energy[b]	D1	D2	D3
2	-874.862438	0.8	-176.7	150.9(e)	-874.989847	-1.8	-174.6	152.3(e)
1	-874.861389	1.6	4.9	150.3(e)	-874.989984	-1.1	12.5	149.0(e)
6	-874.860838	1.9	-167.4	85.2(a)	-874.988636	-0.4	-165.3	85.7(a)
5	-874.860387	2.8	34.3	78.4(a)	-874.988946	0.5	43.4	79.2(a)
4	-874.859747	178.1	-175.1	154.3(e)	-874.986741	175.6	-172.5	152.6(e)
3	-874.858740	177.7	4.6	150.9(e)	---	---	---	---
8	-874.858164	180.0	-165.3	84.8(a)	---	---	---	---
7	-874.857979	180.0	32.7	78.6(a)	---	---	---	---

(3aS,5R,6aS)-**4**								
Conf-ormer	B3LYP/6-31G*				B3LYP/aug-cc-pVDZ			
	Energy[b]	D1	D2	D3	Energy[b]	D1	D2	D3
6	-874.863450	2.6	180.0	-161.3(e)	-874.991578	0.6	180.0	-160.0(e)
5	-874.862036	2.3	-1.0	-157.8(e)	-874.987907	-0.2	-1.8	-156.7(e)
1	-874.861358	0.1	69.1	-84.1(a)	-874.988963	-3.5	74.6	-85.2(a)
8	-874.861087	180.0	178.3	-161.1(e)	-874.988928	177.9	178.5	-160.0(e)
7	-874.859665	180.0	3.0	-157.7(e)	-874.985415	177.3	34.2	-158.2(e)
2	Not Converged							
3								
4								

[a]Dihedral angles D_1, D_2 and D_3 represent, respectively, the angles of N2-C3-C7-O8, N9-C5-C10-O11 and C6a-C6-C5-C10 (a and e indicate axial and equatorial orientation of the carboxylic group on the cyclopentane ring). [b]Gibbs energy (in units of Hartree).

Vibrational Circular Dichroism: The absorption and vibrational circular dichroism spectra of the five most stable conformers were calculated by using Gaussian 98 program,[9] at both B3LYP/6-31G* and B3LYP/aug-cc-pVDZ levels. The absorption and vibrational circular dichroism spectra of (–)-**3** and (–)-**4** were measured in $CDCl_3$ solution

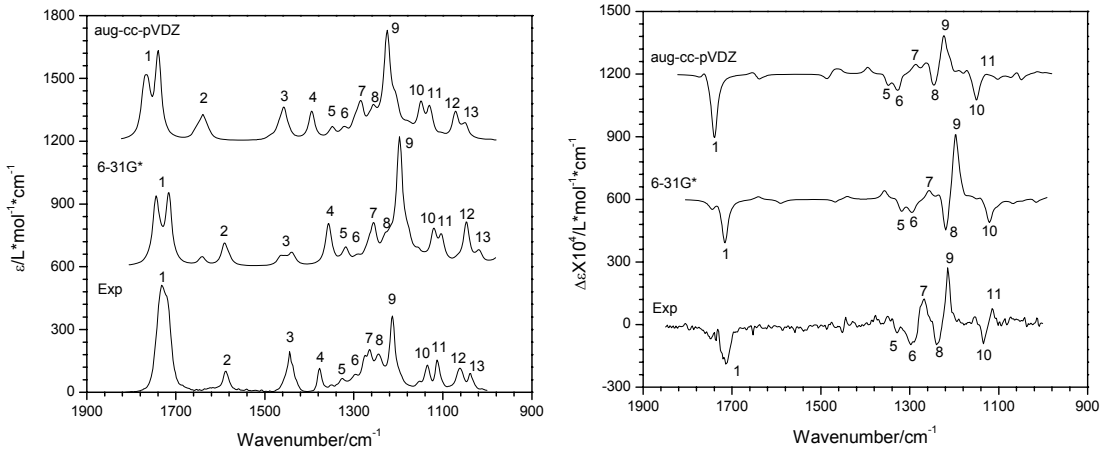

Figure 5-5**.** The comparison between the experimental spectra of (–)-**3** and the predicted spectra for (3a*S*,5*S*,6a*S*)-**3** isomer. Left: IR absorption spectra. Right: VCD spectra.

The comparison of the experimental spectra of the amino diester (–)-**3** and the calculated spectra for the (3a*S*,5*S*,6a*S*)-**3** is shown in Figure 5-5. The experimental absorption spectrum agrees quite well with the calculated absorption spectrum obtained in B3LYP/aug-cc-pVDZ calculation, except for one difference. The 1740 cm^{-1} band (labeled as 1) in the experimental spectrum contains two sub-bands, which are not well resolved. However, B3LYP/aug-cc-pVDZ calculation predicts two well separated corresponding bands. The agreement between experimental absorption and B3LYP/6-31G* predicted spectra is not as good as that found between experimental absorption and B3LYP/aug-cc-pVDZ predicted spectra. In the experimental absorption spectrum, the

region from 1700 cm^{-1} to 1400 cm^{-1} shows two bands (labeled as 2 and 3), while the B3LYP/-631G* predicted spectrum shows two separated bands, each for the corresponding experimental bands 2 and 3. The experimental VCD spectrum agrees quite well with the calculated VCD spectrum obtained in both B3LYP/6-31G* and B3LYP/aug-cc-pVDZ calculations, except for one significant difference; that is, the negative-positive couplet in the 1300-1250 cm^{-1} region (labeled as 6, 7) is clearly seen in the experimental spectrum, whereas the corresponding bands in the predicted VCD spectra are characterized by low relative intensities. The major negative-positive couplet in the 1250-1200 cm^{-1} region (labeled as 8, 9) observed in the experimental VCD spectrum, however is reproduced in the predicted spectra.

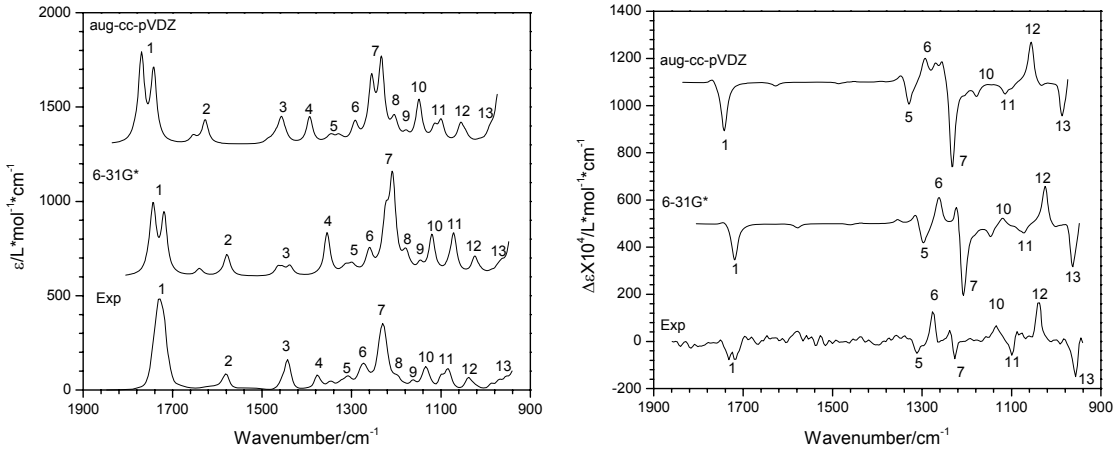

Figure 5-6. The comparison between the experimental spectra of (–)-**4** and the predicted spectra for (3a*S*,5*R*,6a*S*)-**4** isomer. Left: IR absorption spectra. Right: VCD spectra.

The experimental spectra for the amino diester (–)-**4** and the calculated spectra for the (3a*S*,5*R*,6a*S*)-**4** are shown in Figure 5-6. The experimental absorption spectrum agrees quite well with the calculated absorption spectrum obtained in both B3LYP/6-31G* and

B3LYP/aug-cc-pVDZ calculations, except for the following significant differences. The experimental bands at 1740 and 1230 cm^{-1} (labeled as 1 and 7, respectively) do not show any splittings, at variance with the predicted spectra, in which well-separated splittings for the corresponding bands are observed. In the VCD spectra, a good agreement is observed for the negative-positive couplet ~1300 cm^{-1} (labeled 5, 6) in both experimental and predicted spectra. Conversely, the experimental intensity of the positive-negative couplet (labeled 7) at ~1220 cm^{-1} is smaller than that in the predicted spectra. The reason for such a discrepancy is that this experimental band is accompanied by two not well-resolved sub-bands. These two bands have opposite signed VCD which tend to cancel each other when they are not well separated. In the predicted spectra, the corresponding two bands are well separated from each other, so the intensity is larger. Finally, the positive VCD band at 1050 cm^{-1} (labeled as 12) and negative band at 950 cm^{-1} (labeled as 13) are clearly evident in both experimental and predicted spectra.

Based on the comparison of experimental VCD spectra with those predicted for the two epimers, it can be concluded that the absolute configuration for compound (–)-**3** is (3a*S*,5*S*,6a*S*) and that for compound (–)-**4** is (3a*S*,5*R*,6a*S*). As a consequence, the absolute configuration can be assigned to the related epimeric amino acids [(–)-(3a*S*,5*S*,6a*S*)-**1** and (–)-(3a*S*,5*R*,6a*S*)-**2**] and to their enantiomers [(+)-(3a*R*,5*R*,6a*R*)-**1** and (+)-(3a*R*,5*S*,6a*R*)-**2**, respectively].

Optical Rotation: The optical rotations of the two epimeric bicyclic isoxazolines were measured at the sodium D line. To eliminate the influence of solute-solute interactions, intrinsic rotation (specific rotation in the limit of zero concentration) was obtained. The experimental specific rotation against concentration is shown for both

compounds in Figure 5-7 and was analyzed with weighted least squares method. The intrinsic rotation values are –120.0±1.3 for (–)-17 and –163.8±1.3 for (–)-18 (in units of degree×g^{-1}×mL×dm^{-1}).

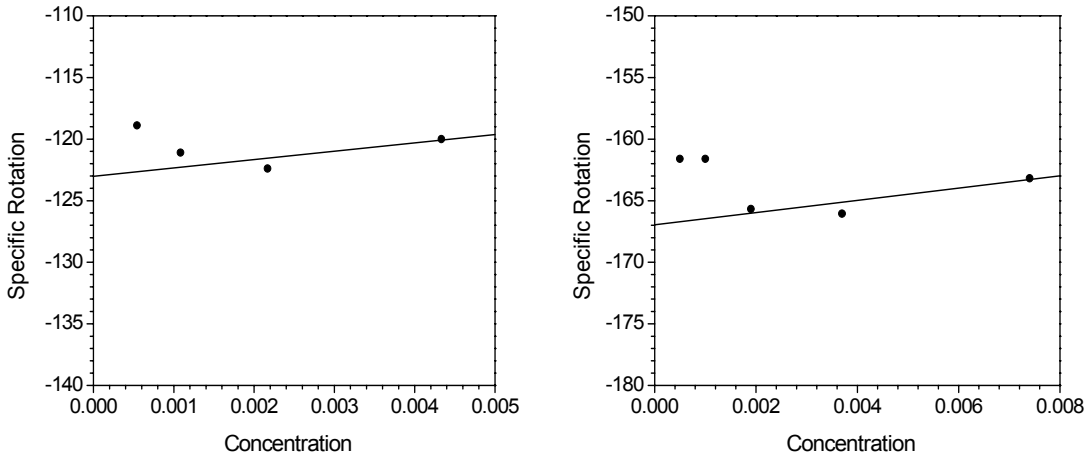

Figure 5-7. The experimental specific rotation vs. concentration (g/mL) for the two epimers. Left: compound (–)-**3**, the data were fit to $[\alpha]_D$=677.5*c–123.0. Right: compound (–)-**4**, the data were fit to $[\alpha]_D$=498.4*c–167.0.

The specific rotations of the stable conformers of the two diastereomers were calculated at both B3LYP/6-31G* and B3LYP/aug-cc-pVDZ level. The predicted specific rotations for the diastereomers are the population-weighted sum of the specific rotations of individual conformers. The calculated specific rotations are summarized in Tables 5-2 and 5-3.

Table 5-2. The calculated specific rotation, $[\alpha]_D$, of (3a*S*, 5*S*,6a*S*)-**3** diastereomer and the observed intrinsic rotation of derivative (–)-**3**.

B3LYP/6-31G*			B3LYP/aug-cc-pVDZ		
Conformer	Population	$[\alpha]_D$	Conformer	Population	$[\alpha]_D$
2	0.5935	–206.6	1	0.4049	–190.2
1	0.1955	–197.7	2	0.3502	–200.4
6	0.1090	–219.6	5	0.1348	–268.4
5	0.0676	–222.8	6	0.0971	–259.2
4	0.0344	–187.9	4	0.0130	–169.4
Population weighted		–206.7	Population weighted		–210.7
Observed intrinsic rotation		–123.0	Observed intrinsic rotation		–123.0

Table 5-3. The calculated specific rotation, $[\alpha]_D$, of (3a*S*, 5*R*,6a*S*)-**4** diastereomer and the observed intrinsic rotation of derivative (–)-**4**.

B3LYP/6-31G*			B3LYP/aug-cc-pVDZ		
Conformer	Population	$[\alpha]_D$	Conformer	Population	$[\alpha]_D$
6	0.6980	–277.5	6	0.8733	–297.5
5	0.1561	–262.6	1	0.0547	–351.8
1	0.0761	–312.9	8	0.0527	–267.7
8	0.0571	–267.1	5	0.0179	–276.7
7	0.0127	–275.5	7	0.0014	–388.6
Population weighted		–277.3	Population weighted		–295.2
Observed intrinsic rotation		–167.0	Observed intrinsic rotation		–167.0

The calculated specific rotations for (3a*S*,5*S*,6a*S*)-**3** are –206.7 in B3LYP/6-31G* calculation and –210.7 in B3LYP/aug-cc-pVDZ calculation (Table 5-2). The calculated specific rotations for (3a*S*,5*R*,6a*S*)-**4** are –277.3 in B3LYP/6-31G* calculation and –295.2 in B3LYP/aug-cc-pVDZ calculation (Table 5-3). Since the intrinsic rotations observed for (–)-**3** and (–)-**4** are –123 and –167, respectively, the magnitudes of calculated specific rotations are larger than the experimental intrinsic rotations by ~1.7. Nevertheless, based on the relative magnitude of intrinsic rotations, the configuration of the amino diester with the smaller absolute experimental intrinsic rotation is assigned as

that of the srereoisomer predicted to have a smaller specific rotation. Thus, the absolute configuration of (−)-**3** is assigned as (3a*S*,5*S*,6a*S*) and that of (−)-**4** as (3a*S*,5*R*,6a*S*). These assignments are consistent with those deduced from VCD spectra.

Conclusion

The absolute configuration of (−)-**3** is assigned as (3a*S*,5*S*,6a*S*) and that of (−)-**4** as (3a*S*,5*R*,6a*S*) by comparing the experimental VCD features with those obtained from theoretical calculations. A parallel experimental/theoretical protocol applied to the values of specific rotation led to the same configurational assignment obtained through VCD. Since the methyl esterification do not change the absolute configuration of the target molecules **1** and **2**, the absolute configuration of (-)-**1** should be the same as (−)-**3**, which is (3a*S*,5*S*,6a*S*); the absolute configuration of (-)-**2** should be the same as (−)-**4**, which is (3a*S*,5*R*,6a*S*).

CHAPTER VI

ASSIGNING THE HELICITY OF SUBSTITUTED POLYGUANIDINE BY VIBRATIONAL CIRCULAR DICHROISM

Introduction

Synthetic chiral polymers can be prepared by including chiral centers in the polymers chains or attaching chiral moieties to the polymer chain. The VCD spectra of this kind of chiral polymers were already reported.[98] The VCD spectra of this kind of polymers are close to their chiral monomer unit. A relatively new synthetic chiral polymer which does not have traditional chiral centers was prepared recently.[99, 100] Their chirality depends on the helical conformation of their polymer chain. The helicity of the polymer can be either *P* (plus) for clockwise helix or *M* (minus) for count-clockwise helix. Helical polymers continue to attract great interest because of potential applications in chiral separation medium, sensor data storage, optical devices, and liquid crystalline displays.[101]

The helical polyguanidine (see Figure 6-1) was synthesized by helix-sense-selective polymerization of an achiral carbodiimide monomer in the presence of chiral titanium catalyst.[102] Since most helical polymers are labile to helix inversion under mild condition, bulky side groups are incorporated in the polyguanidine to stabilize the helix structure. To further investigate the different properties of this kind of polymers, the absolute configuration of their helix must be assigned. In this chapter, we try to assign the helicity of polyguanidine by the combination of vibrational circular dichroism and density functional theory (DFT) calculations. The VCD spectra of the polymers were also

recorded at different temperatures and in different solvents to study the stability of the helix structure.

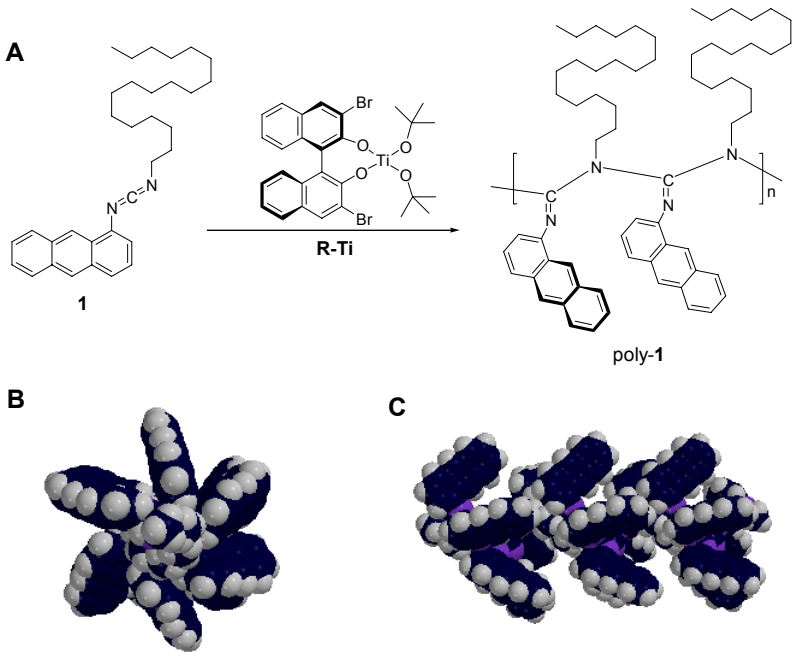

Figure 6-1. Synthesis of helical polyguanidine (A). Top view (B) and side view (C) of the 6_1 helical structure of polyguanidine (18-mer). To clarify the anthracene groups orientation, methyl groups replace *n*-octadecyl groups in polyguanidine.

Experimental Section

The synthesis of these polymers was already published in several papers.[99, 100, 102] Regioregular, stereoregular polyguanidine (Mw = 16,000, Mw/Mn = 2.7) was obtained by helix-sense-selective polymerization of achiral carbodiimide using chiral catalyst **R-Ti** at room temperature for one week. The solvent used for the polymerization is chloroform.

The typical concentration for the VCD measurement is around 20mg/mL in $CDCl_3$. The path length is around 200μm. The samples were held in a variable path length cell with BaF_2 windows for room temperature measurements and in a fixed path length cell with CaF_2 windows for high temperature measurements. The temperature of

the cell was controlled by a Monogram temperature controller (Omega Engineering, Stamford, CT). The solvent absorption and VCD were subtracted from the respective sample solution spectra.

Results and Discussion

Two series of polyguanidine helical polymers were studied in this chapter. One series polyguanidine helical polymers have anthracene and *n*-octadecyl (C-18) side chain (Series I). The other series polyguanidine helical polymers have benzene and *n*-hexyl (C-6) side chain (Series II).

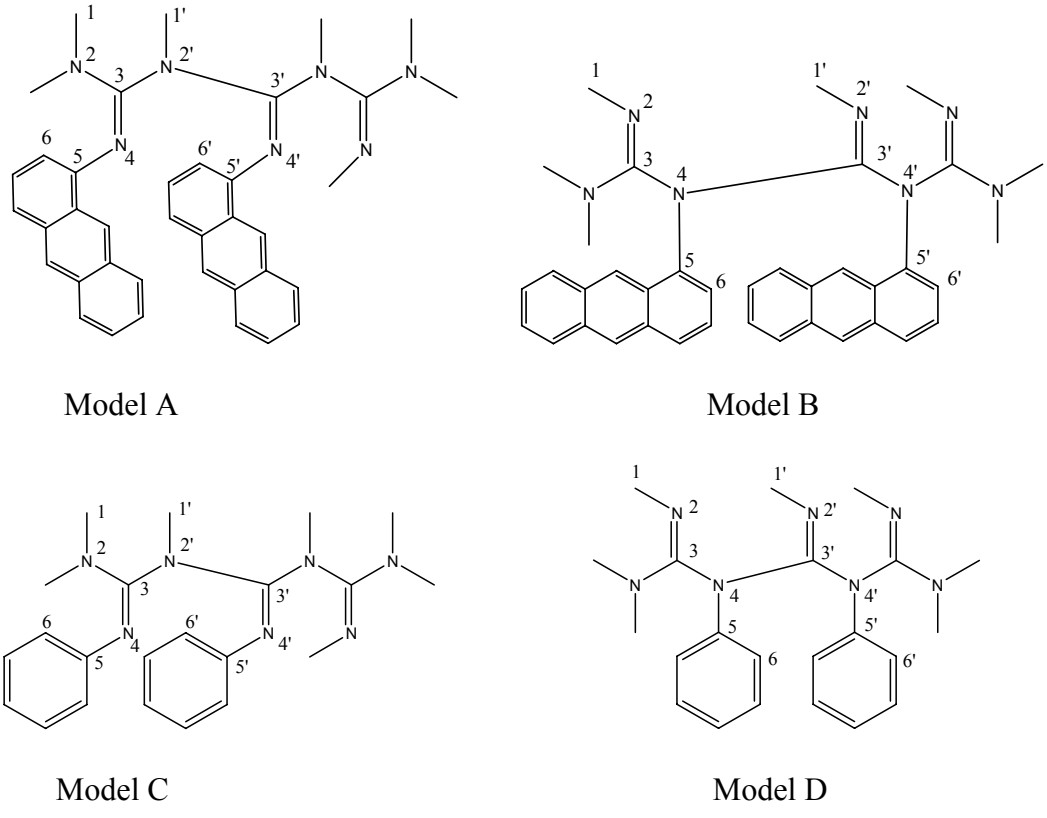

Figure 6-2. The structures of the four model compounds.

Model building: Another question we would like to address other than helicity is the position of anthracene/benzene group. Therefore four model molecules (see Figure 6-2) were built for the further investigation. As we can see in Figure 6-2, these four model compounds have only two repeating monomer units to reduce the calculation time. In addition, C-18 or C-6 side chains were substituted by methyl group for the same purpose. Model compound A represents the polymer structure in which anthracene group is attached to C=N or imine nitrogen. Model compound B represents the polymer structure in which anthracene group is attached to C-N or amine nitrogen. Model compound C represents the polymer structure in which benzene group is attached to C=N or imine nitrogen. Model compound D represents the polymer structure in which benzene group is attached to C-N or amine nitrogen. In order to directly compare the relative energies in each pair of model compounds (A vs. B and C vs. D), we adjusted the end groups of these four compounds to make A has identical chemical composition to B, and C has identical chemical composition to D.

The initial structure of the model compounds are constructed from molecular mechanics optimized polymer structures which have P helicity. The model compounds are further optimized by density functional theory using B3LYP functional and 6-31G* basis set. All structures are successfully optimized. Some important dihedral angles are shown in Table 6-1.The dihedral angles C1N2C3N4, N2C3N4C5, and C3N4C5C6 will determine the structure of monomer unit. The dihedral angles C1'N2'C3'N4', N2'C3'N4'C5', and C3'N4'C5'C6' are the same dihedral angles in the next monomer unit). From Table 6-1, one can see the similarity between the structures of the monomer unit. The dihedral angle N2C3N2'C3' (model compound A and C) and C3N4C3'N4'

(model compound B and D) will determine the relative position of the monomer units in the polymer. If we extended the structure of repeat monomer in these model compounds, the resulting polymers will have P helicity.

Table 6-1. The dihedral angles in the model compounds

Dihedral Angles	Model A	Model B	Model C	Model D
C1N2C3N4	-150	-165	-147	-164
C1'N2'C3'N4'	-153	-174	-154	-173
N2'C3N4C5	-166	-141	-169	-142
N2'C3'N4'C5'	-168	-142	-170	-150
C3N4C5C6	63	50	67	44
C3'N4'C5'C6'	66	38	70	35
N2C3N2'C3'	-103	---	-104	---
C3N4C3'N4'	---	-123	---	-123

The Gibbs energy difference between model compounds A and B is 75.6 kJ/mol with model compound A (-1854.132809 Hartree) lower in energy than model compound B(-1854.161586 Hartree). The Gibbs energy difference between model compounds C and D is 41.5 kJ/mol with model compound C (-1239.769845 Hartree) lower in energy than model compound D (-1239.754052 Hartree). Therefore, the structures with aromatic ring attached to C=N or imine nitrogen have lower energy than structures with aromatic ring attached to C-N or amine nitrogen.

Series I polymer

The vibrational spectra of these model compounds are calculated at the same B3LYP/6-31G* level and compared with experimental spectra. The absorption and VCD spectra of polymer series I are shown in Figure 6-3.

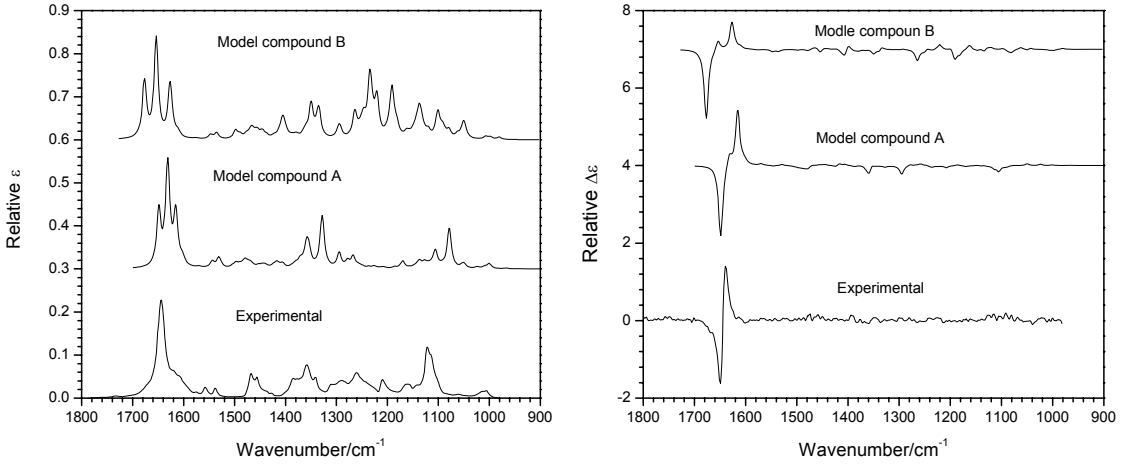

Figure 6-3. The experimental absorption (left) and VCD (right) spectra of series I polymer and predicted absorption and VCD spectra of model compounds A and B.

In the absorption spectra of Figure 6-3, we can see the absorption spectrum of model compound A has a better agreement with experiment spectrum compared to model compound B. Especially in the region from 1150 to 1250 cm^{-1}, the predicted spectrum of model compound B has several extra peaks which do not show up in the experimental spectrum. Thus model compound A should represent the real structure of the polymer. Also the energy of model compound A is much lower than that of model compound B, which also suggests the model A to be the preferred structure. In the VCD spectra of Figure 6-3, the negative positive couplet around 1640cm^{-1} in the experimental spectrum is nicely reproduced in the predicted VCD spectrum of model compound A. According to

the calculation, this couplet comes from the vibration of C=N double bond. Since the helicity of the model compound A is P and we get a good match between the experimental VCD spectrum and predicted spectrum of model compound A, the helicity of the polymer used in experimental studies is assigned as P-helix.

For series I polymer, we also measured the VCD spectra at room temperature and 70ºC. At different temperatures, the VCD spectra are essentially the same. This means that the helix structure in the polymer is very stable. Two different solvents ($CDCl_3$ and toluene) were used for the VCD measurements. The VCD spectra in these two solvents are also the same, which suggests that the helical structure remaining unchanged in different solvent environments.

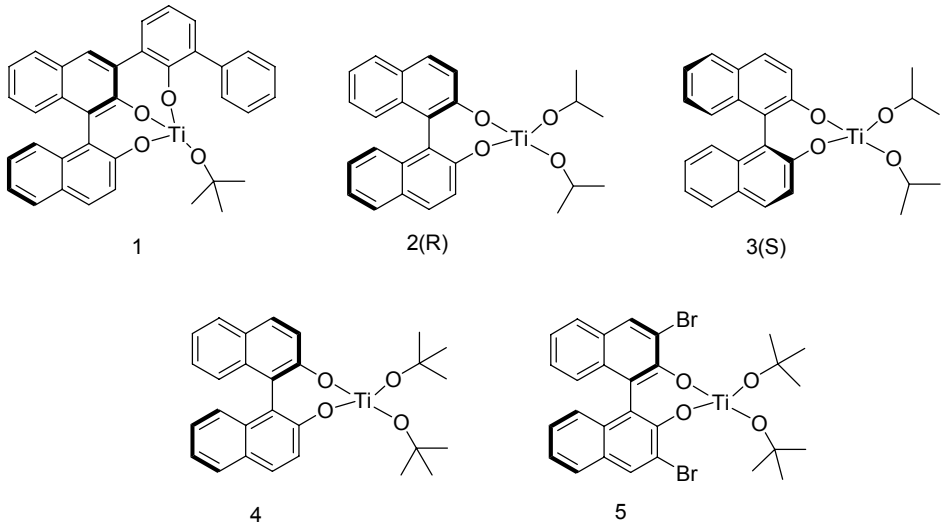

Figure 6-4. The catalysts used in preparing series II polymers.

Series II polymer

Two model molecules C and D with two repeat units were built to predict the spectra of series II helix polymers. Their structures are shown in Figure 6-2. Their

optimized structures are used for the prediction of IR and VCD spectra. For series II polymers, we have several polymers which were synthesized under different chiral catalysts (see Figure 6-4).

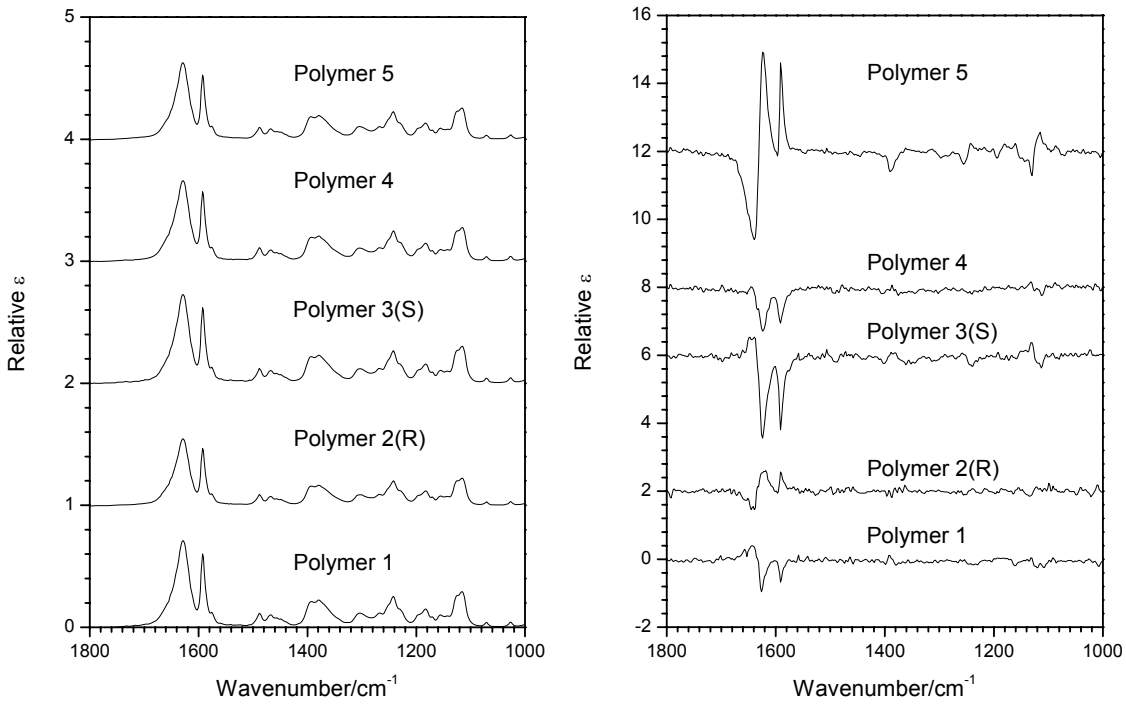

Figure 6-5. Experimental absorption (left) and VCD (right) spectra of series II polymers

The absorbance and VCD spectra of these five polymers are shown in Figure 6-5. The absorbance spectra of all five polymers are essential same. The VCD spectra of these five polymers show large difference between them. First we can classify these five polymers into two categories according to the signs of peaks of 1640cm^{-1}, 1623cm^{-1}, 1590cm^{-1}. Polymer 1, 3(S), and 4 have (+)-1640cm^{-1}, (-)-1623cm^{-1}, and (-)-1590cm^{-1} pattern. Polymer 2(R) and 5 have the reverse pattern. These two categories are consistent with their optical rotation signs. Polymer 1, 3(S), and 4 have minus optical rotation while polymer 2(R) and 5 have the plus optical rotation at the sodium D line. The peak

intensities of these three peaks: 1640cm^{-1}, 1623cm^{-1}, 1590cm^{-1} are also different. Polymer 5 has the strongest peak intensity, which may suggest that the catalyst used in preparing polymer 5 is more efficient in preparing a helical polymer.

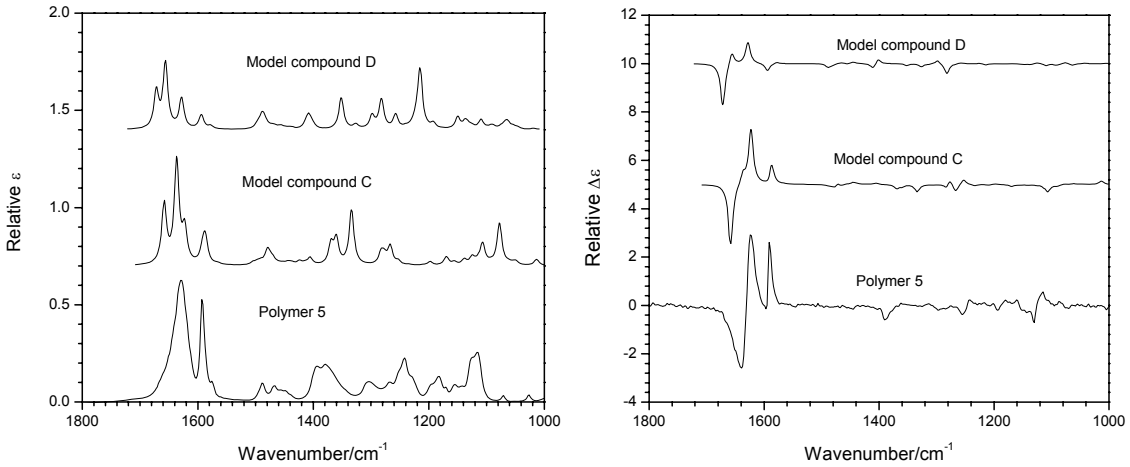

Figure 6-6. The experimental absorption (left) and VCD (right) spectra of series II polymer and predicted absorption and VCD spectra of model compounds C and D.

To determine the helical handedness of these polymers, their experimental VCD need to be compared with predicted VCD. We just show the comparison between polymer 5 and model molecules. The spectral comparisons are shown in Figure 6-6 for absorption and VCD spectra. From this comparison, we can see that the spectra of model compound C are more close to the experimental spectra. Model molecule C also has a lower energy than model molecule B. Therefore, we use model molecule C to predict the helical handedness of the polymers. From Figure 6-6, we can see the signs of three major VCD peaks around 1600cm^{-1} agree well between spectra of polymer 5 and predicted spectra. So the helical handedness of polymer 5 should be same as the model molecule C, which is P helix. Since the VCD spectra of polymer 2(R) and 5 have same sign, they have

same P helix. The VCD spectra of polymer 1, 3(S), and 4 are reverse to polymer 2(R) and 5. Therefore, they should have M helix.

Conclusion

The helicity of polyguanidines are successfully assigned by comparing experimental and predicted VCD spectra. In addition to this information, VCD spectra also show the backbone of the polyguanidines remains the same with the change of solvent or temperature. The theoretical calculation also provides the information about the position of aromatic groups. In summary, VCD can be successfully used in studying the structure of synthetic helical polymers.

CHAPTER VII

ABSOLUTE CONFIGURATION OF C76 FULLERENE FROM OPTICAL ROTATORY DISPERSION

Introduction

C_{76} is the simplest chiral fullerene and represents a challenging model fullerene molecule for deducing molecular stereochemistry.[103] The atomic numberings of C_{76} are

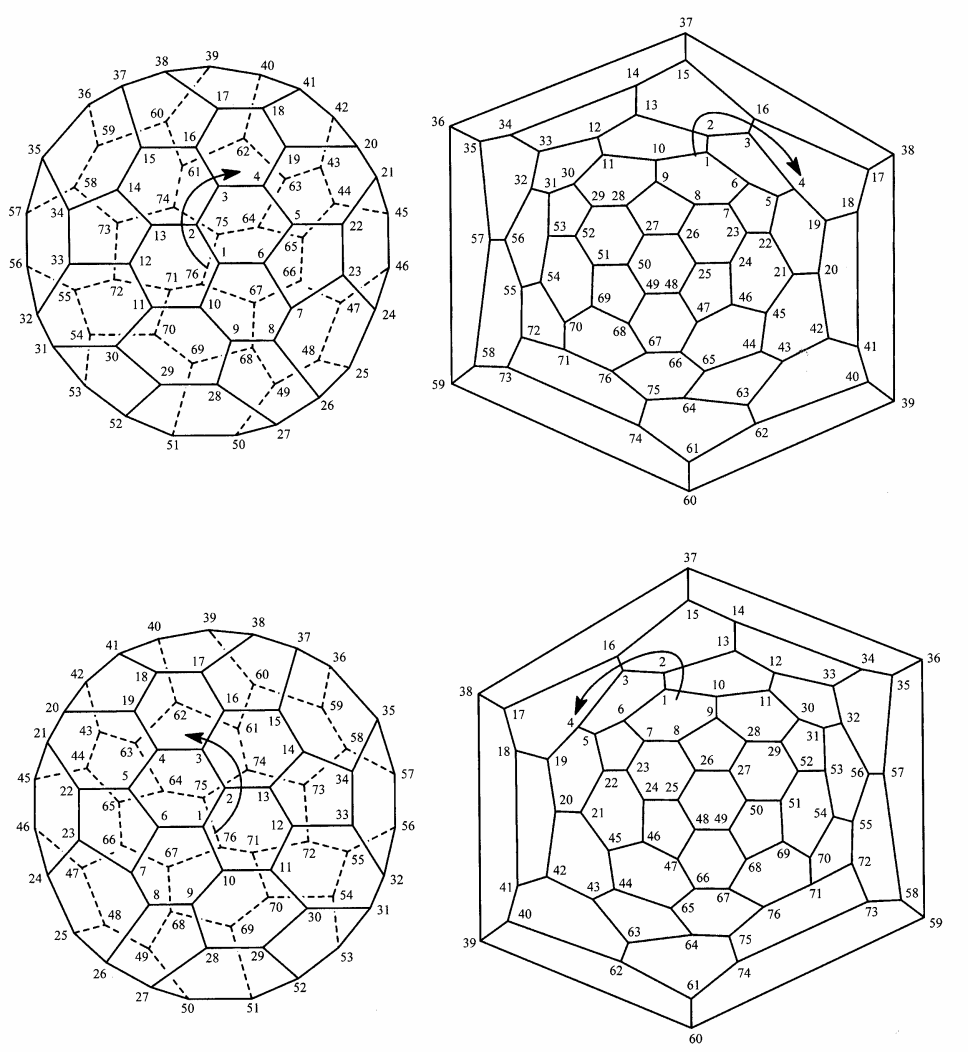

Figure 7-1. Three dimensional and Schlegel diagrams of the chiral fullerene C76 with atomic numbering.

shown in Figure 7-1. Because the fullerene C_{76} is inherently chiral, one scheme of numbering only applies to one enantiomer. If the helix which goes continuously from carbon number 1 to carbon number 76 is clockwise, the handedness of this enantiomer is assigned as (^{f}C)-C_{76}. If the helix from carbon number 1 to carbon number 76 is anticlockwise, the handedness of this fullerene is assigned as (^{f}A)-C_{76}. The 'f' superscript represents the fullerene.[104]

The synthesis of enantiomers of C_{76} was first reported by Hawkins and Meyer, together with the electronic circular dichroism (ECD) spectra in the 300-800 nm region.[105] The maximum specific rotation at 589 nm was also reported as 4000 ± 400, but the relation between the sign of the specific rotation and a particular enantiomer was not given. The experimental specific rotations of chiral fullerenes are not generally measured due to the excessive absorbance of these molecules in the visible spectral region. As a result, the correlation between absolute configuration and specific rotation of chiral fullerenes has not been made to date.

Diederich and coworkers[106] have synthesized enantiomerically pure C_{76} via retro-Bingel reaction and reported the ECD spectra. The ECD intensities reported by Diederich and coworkers (210 L/(mol·cm) at 407 nm) were 6.6 times larger than those (31.6 L/(mol·cm) at 405 nm) reported by Hawkins and Meyer.[105] This discrepancy may originate from low enantiomeric purity or from an error in the concentration used by Hawkins and Meyer. A similar conclusion was made by Okamato and coworkers,[107] who separated the enantiomers of C_{76} on a chiral column. As a result, the reported specific rotation of C_{76} remains uncertain. In the absence of a correlation between the specific rotation and the absolute configuration of C_{76}, an alternative approach for the

determination of the absolute configuration of C_{76} using ECD has been used.[108] ECD predictions using semi-empirical MO calculations have been reported for C_{76}.[109] Based on these semi-empirical MO calculations of the ECD of C_{76}, the absolute configuration has been assigned as [CD(+)281]-(^{f}C)-C_{76}.

From the above introduction it is clear that the magnitude of the specific rotation of C_{76} and the relation between absolute configuration and specific rotation of chiral fullerenes are not known. This void can be filled with the latest advances in quantum mechanical calculations of chiroptical properties. Since then numerous advances in the theoretical determination of the specific rotation, including the application of density functional theory (DFT), have taken place and standard software[8, 9] has become available. As a result, the theoretical predictions of specific rotations needed for establishing molecular stereochemistry is becoming increasingly important and attractive.[59-61, 63, 110-113] Similarly, with the adaptation of DFT methods for predicting ECD spectra,[114-116] and the availability of software to predict ECD, the use of theoretical calculations of ECD[117, 118] for establishing molecular stereochemistry is also becoming increasingly important. In contrast to the semi-empirical MO calculations mentioned above, the DFT calculations represent the state-of-the-art and need to be verified for accurate predictions. The absolute configuration of C_{84} was recently suggested using DFT predictions of ECD.[119] Similarly, the DFT prediction of the ORD was recently reported for C_{84},[120] but the lack of experimental ORD data precluded the analysis of the predicted data. One DFT calculation for C_{76} has been reported by Yabana and Bertsch[121], but neither a comparison with experimental ORD nor a correlation between ORD and absolute configuration have been reported.

The experimental optical rotatory dispersion (ORD) data, let alone specific rotations at a single wavelength, are not available for chiral fullerenes. Nevertheless, experimental ORD data can be derived from the experimental ECD spectra using the Kramers-Kronig (KK) transformation and compared to the theoretical predictions.[122, 123] In the present work, we report the first combined experimental and theoretical study of ORD for a chiral fullerene. We also specify the absolute configuration for C_{76} using the optical rotation for the first time.

Experimental Section

The experimental ECD spectrum of ent-C_{76} (which is characterized by a positive ECD band at 281 nm), reported by Diederich and coworkers[106], was fit to gaussian band profiles using the Peakfit program.[29] Bandwidths and peak intensities were adjusted until an R^2=0.998 was achieved. Band positions, intensities and bandwidths in the 200-300 nm region were estimated from the ECD spectrum reported in Ref. 107. Different methods for the KK transform were explored and the numerical method suggested by Ohta and Ishida[124] was found to be equivalent to the method suggested by Moscowitz[122]. The peak intensities and band widths listed in Table 7-2 were used to simulate the gaussian intensity profile at constant intervals and these data were used in the KK transform. *Computational Methods*: All calculations were done for (^{f}C)-C_{76}, where (^{f}C) and (^{f}A) are the configurational descriptors for fullerenes.[103] The BHLYP, B3LYP and BLYP functionals and the 6-31G* basis set, available in the appropriate program libraries, were used for all calculations. Geometry optimization at the B3LYP/631G* and HF/6-31G* levels was carried out on a desktop computer using the Gaussian program. The ECD

intensities for 60 electronic transitions were calculated at the optimized geometry using either Gaussian 03 program[8] on an IBM P690 computer at NCSA (University of Illinois) or Dalton program[9] on an HP-Itanium cluster located at the University of Tromsø. Since the excitation energies predicted by the B3LYP and BLYP functionals are lower, and those by HF method are higher, than the observed energies,[125] it is a common practice to shift the transition wavelengths, as suggested previously by Ahlrichs and coworkers. Therefore transition wavelengths were blue shifted by 4000 cm^{-1} for simulating the B3LYP and BLYP ECD spectra, and red shifted by 6000 cm^{-1} for simulating the HF ECD spectrum. No such shift was necessary for transition wavelengths predicted with BHLYP functional. In all cases, gaussian band profiles with 40 nm half-width at 1/e of peak height were used. The predicted and experimental ECD spectra are presented on the same intensity scale, in units of L/(mol·cm), and it was not necessary to scale the predicted intensities. Optical rotatory dispersion, using the resonant optical rotation code[120], was calculated at the B3LYP/6-31G* optimized geometry using the Dalton program on a HP-Itanium TFlops computer cluster at the University of Tromsø. Lifetimes of 500 cm^{-1} were used for all excited states. In presenting the predicted ORD spectrum the wavelengths used in the calculations were shifted (as mentioned earlier for ECD) except for the BHLYP results where wavelength shift was not necessary. Predicted and experimental ORD spectra are presented on the same intensity scale as molar rotation, in units of deg-cm^2/dmol. Molar rotation is given as $[M] = \frac{100\alpha}{cl} x \frac{M}{100} = [\alpha] x \frac{M}{100}$, where c is concentration in g/100cc, l is the optical path lengthand, and M is the molar mass. [M] can be converted to specific rotations, $[\alpha]$, in units of deg·cc/(g·dm), by multiplying with 100/M.

Results and Discussion

The geometry of (^{f}C)-C_{76} was first optimized at B3LYP/6-31G* and HF/6-31G* theoretical levels. The B3LYP/6-31G* optimized geometry was used for calculating ECD intensities using BHLYP/6-31G*, B3LYP/6-31G* and BLYP/6-31G*. The BHLYP functional[114] uses an increased admixture of HF exchange in TDDFT calculations, to overcome the problems in representing excited electronic states of delocalized pi-systems. The ECD intensities obtained with BHLYP/6-31G* are summarized in Table 7-1. The transition wavelengths calculated with BHLYP/6-31G* did not require any scaling but those calculated with B3LYP/6-31G* and BLYP/6-31G* were blue shifted[125] by 0.49 eV and those calculated with HF/6-31G* were red shifted by 0.74 eV. The predicted ECD spectra were simulated using gaussian band shapes and a 40 nm half width at 1/e of the peak height. The predicted ECD spectra for (^{f}C)-C_{76} are compared to the experimental ECD spectrum of [CD(+)281]-C_{76} in Figure 7-2. The experimental ECD spectrum is taken from the work of Diederich and coworkers.[106]

The agreement between experimental and BHLYP calculated ECD spectra in the 490-790 nm region is excellent. A weak and broad negative ECD band at 700 nm in the experimental spectrum corresponds to a negative band at 712 nm in the BHLYP predicted spectrum. Two positive ECD bands at ~570 and ~530 nm in the experimental spectrum are also nicely reproduced in the BHLYP predicted spectrum. The negative ECD bands at ~460 and 405 nm in the experimental spectrum collectively correspond to the negative ECD band at ~440 nm in the BHLYP predicted spectrum. The strong positive ECD band at 282 nm seen in the experimental spectrum corresponds to the strong positive band at 330 nm in the predicted spectrum. Thus transition wavelengths

Table 7-1. BHLYP/6-31G* predicted electronic transition wavelengths and rotational strengths for (^{f}C)-C_{76}

λ (nm)	Rotational Strength[i]	λ (nm)	Rotational Strength[a]
711.9	-82.7	323.5	46.0
609.1	-330.1	322.2	-90.8
592.7	471.8	320.2	64.8
582.7	52.4	309.7	186.7
534.2	97.5	309.0	326.8
455.5	-29.4	306.1	-92.6
448.7	-135.9	301.3	43.9
445.7	-342.8	299.8	-6.5
439.6	-35.5	296.5	10.4
423.2	111.7	293.5	-45.1
415.7	-219.3	292.3	113.4
411.0	-14.3	288.3	-49.6
399.5	46.1	285.0	-152.9
390.0	-0.7	285.0	-163.6
389.0	-136.6	284.3	-28.8
388.5	64.1	281.7	-0.4
387.2	68.9	280.1	-68.4
381.2	127.7	277.2	-161.9
378.5	-13.7	277.0	-21.4
375.3	73.6	276.8	-80.4
362.2	-71.7	273.4	-30.5
359.6	144.9	272.5	-54.6
359.3	-170.7	272.3	-26.5
359.2	0.6	268.7	42.0
356.4	-73.5	268.6	-10.8
346.3	-69.0	267.2	-265.3
335.5	244.4	266.2	-47.4
330.7	1.1	265.1	311.3
329.5	562.4	263.1	-106.6
328.4	113.0	259.2	141.7

[a]in units of 10^{-40} esu^2cm^2

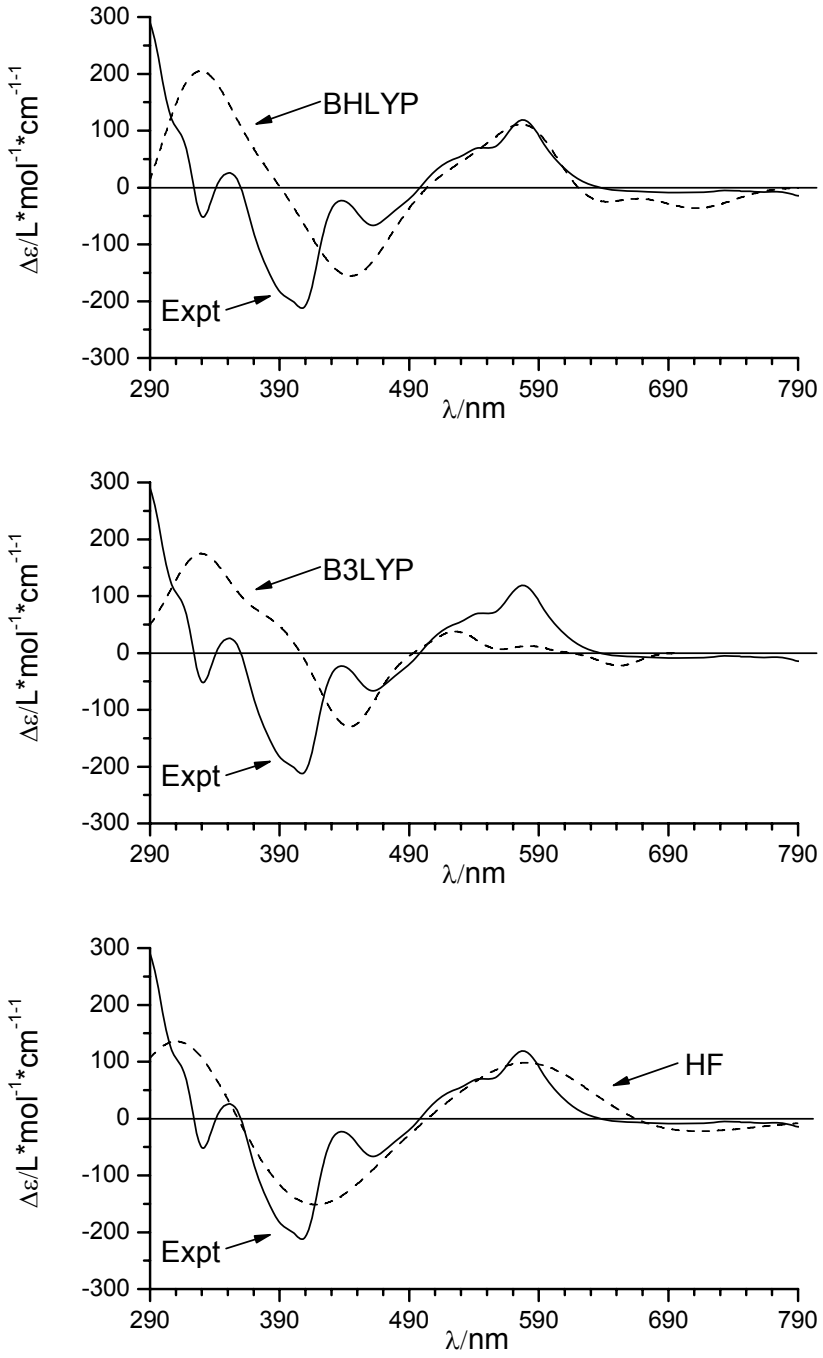

Figure 7-2. Comparison of predicted ECD spectrum (dashed line) with BHLYP/6-31G* (top panel), B3LYP/6-31G* (center panel) and HF/6-31G* (bottom panel) for (^{f}C)-C_{76} with the experimental ECD spectrum (thick solid line) of [CD(+)281]-C_{76}. The B3LYP calculated transition wavelengths were blue shifted by 4000 cm^{-1} and the HF calculated transition wavelengths were red shifted by 6000 cm^{-1}. The BHLYP calculated transition wavelengths were not shifted. The predicted ECD spectra were simulated with Gaussian band profiles and 40 nm half-width at 1/e of peak height. The structure displayed is that for (^{f}C)-C_{76} optimized with the B3LYP functional and 6-31G* basis set.

below 450 nm appear to be predicted at wavelengths longer than those seen in the experimental spectrum. The B3LYP predicted ECD spectrum, with transition wavelengths blue shifted by 0.49 eV, is similar in appearance, but the agreement with the experimental ECD spectrum is not as good as that seen for BHLYP predicted spectrum. The BLYP predicted ECD spectrum (not shown) is in poor agreement with the experimental ECD spectrum. However, the HF predicted ECD spectrum, with wavelengths red shifted by 0.74 eV, reproduced the experimental ECD spectrum surprisingly well. The predicted ECD spectra for (^{f}C)-C_{76} and the observed ECD spectrum for [CD(+)281]-C_{76} are in fairly good agreement (Figure 7-2), confirming the previous[108] assignment of [CD(+)281]-(^{f}C)-C_{76}. Our results seem to indicate that the BHLYP functional[114] is much better for representing the lowest excited states in delocalized pi-systems, although for higher excited states its performance is less than desired.

For deriving the experimental ORD, the experimental ECD spectrum[106] of [CD(+)-281]-C_{76} was fit (R^2=0.99) to gaussian band shapes using the Peakfit program.[18] For the ECD bands in the 200-320 nm region, the band positions, intensities and half-widths (Table 7-2) were estimated from the experimental spectrum reported in Ref. [5]. The peak positions, intensities and bandwidths at 1/e of peak height as summarized in Table 7-2 were used for deriving the ORD spectrum using the KK transformation. The numerical procedure of Ohta and Ishida[124] was used for this transformation, as described previously. The experimental ORD, derived from the KK transform of the experimental ECD spectrum, for [CD(+)281]-C_{76} is shown in Figure 7-3.

Table 7-2. Experimental ECD band parameters[a] for [CD(+)281]-C_{76}

Band center/ nm	Peak intensity/ L/(mol·cm)	Half-width[b]
700	-9.06	87.62
603.96	34.47	20.64
577.32	111.71	18.64
543.84	63.88	19.1
517.31	34.02	15.21
464.07	-64.82	22.92
409.57	-178.01	15.45
385.27	-151.24	18.94
353.53	34.39	10.52
331.64	-53.88	6.34
316[c]	80	15
282[c]	357	21
240[c]	-220.5	10.5

[a]From fitting the experimental spectrum of ref. 105 to gaussian band profiles
[b]at 1/e of peak intensity, in nm
[c]band positions, intensities and half-widths estimated from the ECD spectrum reported in ref. 107

The theoretical ORD for (^{f}C)-C_{76} has been obtained with two different methods. (A). using the linear response theory for the calculation of the optical rotation in the resonance region, developed by Norman, Ruud and Helgaker[120] , the ORD was calculated at discrete wavelengths assuming excite-state lifetimes of 500 cm^{-1}. The linear response results obtained with BHLYP/6-31G* are summarized in Table 7-3. The BHLYP predicted ORD is compared to experimental ORD in Figure 7-3, along with B3LYP predicted ORD. (B). The theoretical ECD spectra (Figure 7-2) obtained with BHLYP/6-31G*, B3LYP/6-31G* and HF/6-31G* were converted[20] to ORD using the KK transform (Figure 7-3). It may be noted that both methods A and B gave identical results (see Figure 7-3). However, linear response calculations performed at smaller wavelength intervals provided higher resolution than KK transform method.

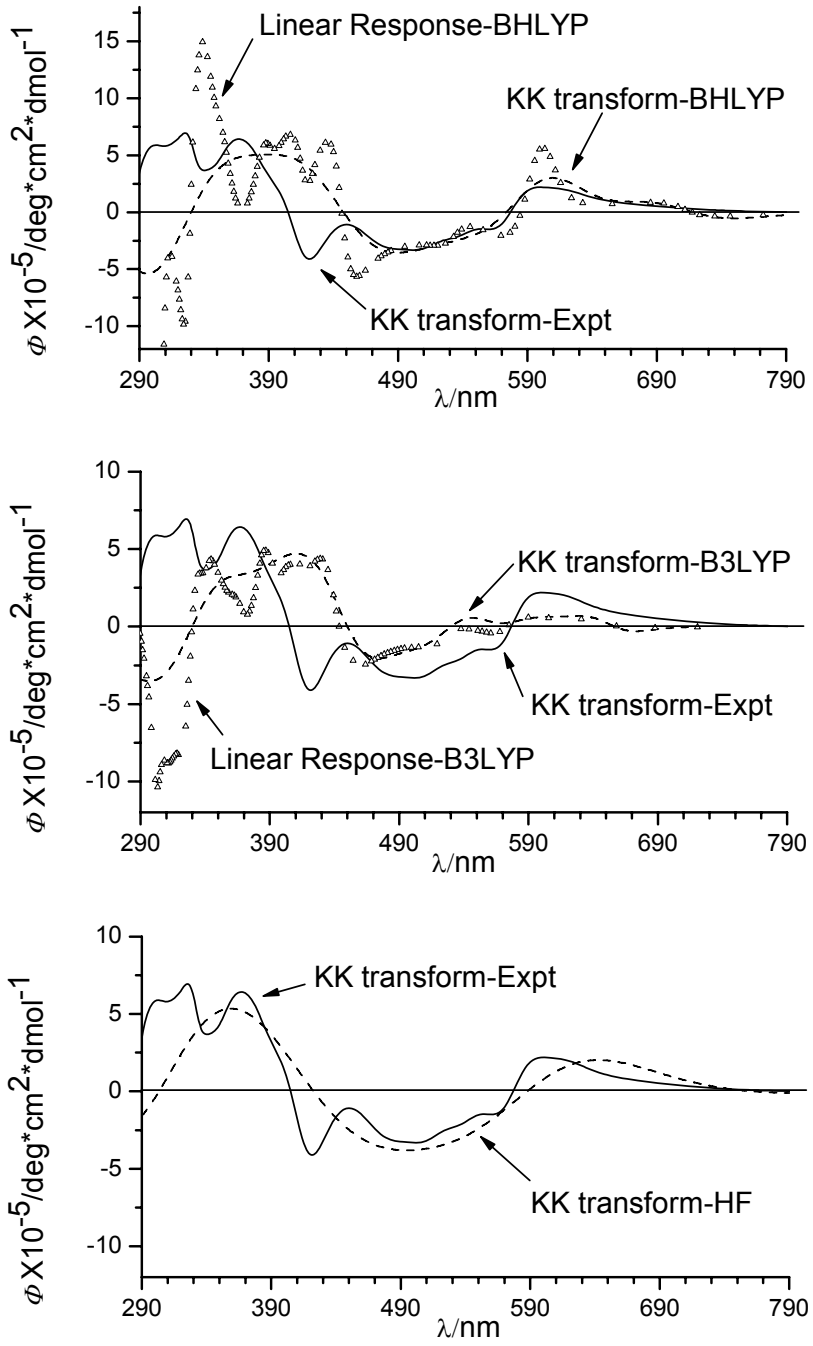

Figure 7-3. Comparison of predicted ORD with BHLYP/6-31G* (top panel), B3LYP/6-31G* (center panel) and HF/6-31G* (bottom panel) for (^{f}C)-C_{76} with the experimental ORD of [CD(+)281]-C_{76}. ORD predicted by the linear response method is displayed as triangles and that by the KK transform as dashed line. Experimental ORD is displayed as thick solid line. The B3LYP calculated transition wavelengths were blue shifted by 4000 cm^{-1} and HF calculated transition wavelengths were red shifted by 6000 cm^{-1}. The BHLYP calculated transition wavelengths were not shifted.

Table 7-3. BHLYP/6-31G* predicted ORD using Linear Response theory for (^{f}C)-C_{76}

Wave Length λ	Specific Rotation [α]	Wave Length λ	Specific Rotation [α]	Wave Length λ	Specific Rotation [α]	Wave Length λ	Specific Rotation [α]
1012.5	-233	545.7	-12829	425.8	41545	358.8	42904
949.2	-356	539.2	-14861	423.9	33946	357.4	52480
893.4	-559	536.0	-17818	421.9	27645	356.0	61819
843.8	-919	532.9	-21519	418.0	28429	354.6	70007
799.4	-1607	526.7	-27318	416.1	36717	351.8	82093
772.3	-2418	520.7	-29120	414.2	47270	349.1	93286
746.9	-3499	517.8	-29200	412.3	56714	347.8	100724
734.9	-3630	514.8	-29098	410.5	63252	346.5	109665
723.2	-2137	512.0	-28963	406.8	68184	345.2	119286
717.5	-277	506.3	-28880	403.2	66485	342.6	136560
711.9	2207	495.3	-30130	401.4	64087	338.8	149554
706.4	4734	484.7	-33768	399.7	61123	336.3	137872
695.6	7895	482.2	-35130	397.9	58319	335.0	124597
685.2	8581	479.6	-36704	394.5	55919	333.8	108386
655.6	7386	477.1	-38508	391.1	58498	331.4	61249
632.8	8097	474.6	-40557	389.4	60265	330.2	24151
624.2	12436	464.9	-50975	387.8	60675	329.0	-18573
615.7	25886	460.2	-55697	386.1	58794	327.8	-57010
611.6	37064	457.9	-56465	382.9	48017	325.5	-95982
607.5	48570	455.6	-54957	381.3	39971	324.3	-98256
603.5	55906	453.4	-49829	379.7	31654	323.1	-93737
599.5	55143	451.1	-39455	378.1	24190	322.0	-85587
595.6	45238	448.9	-22803	376.6	17741	320.9	-76585
591.7	28917	446.7	-1114	375.0	12175	319.7	-68325
587.9	11416	444.5	21517	373.5	7825	318.6	-60759
584.2	-2894	442.4	40338	366.0	8032	315.3	-39105
580.4	-12496	440.2	52944	364.5	12124	312.1	-40339
576.8	-17875	438.1	59655	363.1	17983	311.0	-57006
569.5	-20547	433.9	61150	361.6	25373	310.0	-84046
555.7	-15669	429.8	54144	360.2	33783	308.9	-115957

wavelength λ in nm; specific rotation [α] in deg.cc/(g.dm).

The experimental ORD in the 490-790 nm region is reproduced quite well by the theoretical predictions at all levels. Below 490 nm, a negative ORD at 456 nm and broad positive ORD in the 434-339 nm region predicted with BHLYP functional correspond respectively to negative ORD at 425 nm and broad positive ORD in the 370-300 nm region of experimental spectrum. Thus a blue shift of ~30 nm appears necessary for BHLYP predicted ORD below 490 nm. A similar shift appears necessary for B3LYP result also (in addition to a constant 0.49 eV blue shift already applied). For the HF predicted ORD, a constant red shift of 0.74 eV already applied appears adequate in the entire region. The overall agreement between experimental and predicted ORD at the B3LYP/6-31G* level is not as good as that seen at the BHLYP/6-31G* level. The shape of the experimental ORD in the entire region is nicely reproduced by the KK transform of the HF/6-31G* ECD spectrum.

Although the present calculations were carried out using a moderate 6-31G* basis set, the number of basis functions involved in this calculation is 1064, which already required tremendous computational resources (B3LYP linear response calculations of the ORD with the Dalton program on a HP-Itanium TFlops computer cluster at University of Tromsø using 40 processors required 13 days CPU time and thus about 10 hours wall-time). Thus calculations with any larger basis set may not be completed in reasonable amount of time. Nevertheless, in the interest of improving the predicted ECD and ORD, calculations with a larger aug-cc-pVDZ basis set have been attempted, but 1700 basis functions involved with this basis set resulted in linear dependencies and convergence problems which made it difficult to pursue these calculations. We also expect that although diffuse functions have been demonstrated to be important for OR

calculations,[113] the diffuse functions would be less important for a compact molecule such as C_{76}, since the basis functions on the neighboring atoms will act as diffuse polarizing functions.

The differences between experimental and predicted ORD magnitudes may be attributed to the approximate life times assumed for excited states in the linear response method. In addition, there is a very high density of states in the short wavelength region, which may give inaccuracies in the approach of Ref. 119 since relaxation in this approach is only allowed to the ground state and only from one excited state at a time. Still, apart from the blue-shift needed at shorter wavelengths than 490 nm, the agreement with the experimental KK-transformed ORD data is remarkably good at the BHLYP/6-31G* level of theory.

The molar rotation at 589 nm, derived from the KK transform of the experimental ECD, is 181220 deg·cm^2/dmol [equivalent to a specific rotation of 19852 deg·cc/(g.dm)]. Assuming that the C_{76} sample prepared by Diederich and coworkers had 100% ee, the maximum specific rotation of C_{76} at 589 nm can then be stated as 19852 deg·cc/(g·dm), which appears to be the largest ever reported. The BHLYP predicted molar rotation at ~588 nm is 104213 deg cm^2/dmol (equivalent to a specific rotation of 11416 deg·cc/(g·dm)), which compares favorably with the experimental rotation. The difference between predicted and observed magnitudes of the specific rotation can be attributed to the difficulty in correctly representing the higher excited states at the BHLYP/6-31G* level, as well as the choice of the lifetime of the excited states. Nevertheless, the excellent agreement between the calculated and observed ORD (Figure 7-3) pattern suggests that

the absolute configuration is $(+)_{589}$-(^{f}C)-C_{76}. The same conclusion is obtained from the ORD data obtained in B3LYP/6-31G* and HF/6-31G* calculations.

Conclusion

The absolute configuration of C_{76} has been determined as $(+)_{589}$-(^{f}C)-C_{76} for the first time by comparing the experimental and predicted optical rotatory dispersion (ORD). The experimental ORD was derived from the experimental ECD spectrum using Kramers-Kronig (KK) transform. The theoretical ORD spectra were calculated in the resonant region using the linear response theory and also using the KK transform of the theoretical ECD spectrum, at different theoretical levels, namely BHLYP/6-31G*, B3LYP/6-31G*, BLYP/6-31G* and HF/6-31G*. Good agreement noted between experimental and predicted spectra allow for an unambiguous determination of the absolute configuration.

REFERENCES

(1) Holzwarth, G.; Hsu, E. C.; Mosher, H. S.; Faulkner, T. R.; Moscowitz, A. *Journal of the American Chemical Society* **1974**, *96*, 251.

(2) Nafie, L. A.; Keiderling, T. A.; Stephens, P. J. *Journal of the American Chemical Society* **1976**, *98*, 2715.

(3) Nafie, L. A.; Diem, M.; Vidrine, D. W. *Journal of the American Chemical Society* **1979**, *101*, 496.

(4) Nafie, L. A. *Applied Spectroscopy* **2000**, *54*, 1634.

(5) Becke, A. D. *Journal of Chemical Physics* **1993**, *98*, 1372.

(6) Becke, A. D. *Journal of Chemical Physics* **1993**, *98*, 5648.

(7) Cheeseman, J. R.; Frisch, M. J.; Devlin, F. J.; Stephens, P. J. *Chemical Physics Letters* **1996**, *252*, 211.

(8) Frisch, M. J. T., G. W.; Schlegel, H. B.; Scuseria, G. E.; Robb, M. A.; Cheeseman, J. R.; Montgomery, Jr., J. A.; Vreven, T.; Kudin, K. N.; Burant, J. C.; Millam, J. M.; Iyengar, S. S.; Tomasi, J.; Barone, V.; Mennucci, B.; Cossi, M.; Scalmani, G.; Rega, N.; Petersson, G. A.; Nakatsuji, H.; Hada, M.; Ehara, M.; Toyota, K.; Fukuda, R.; Hasegawa, J.; Ishida, M.; Nakajima, T.; Honda, Y.; Kitao, O.; Nakai, H.; Klene, M.; Li, X.; Knox, J. E.; Hratchian, H. P.; Cross, J. B.; Bakken, V.; Adamo, C.; Jaramillo, J.; Gomperts, R.; Stratmann, R. E.; Yazyev, O.; Austin, A. J.; Cammi, R.; Pomelli, C.; Ochterski, J. W.; Ayala, P. Y.; Morokuma, K.; Voth, G. A.; Salvador, P.; Dannenberg, J. J.; Zakrzewski, V. G.; Dapprich, S.; Daniels, A. D.; Strain, M. C.; Farkas, O.; Malick, D. K.; Rabuck, A. D.; Raghavachari, K.; Foresman, J. B.; Ortiz, J. V.; Cui, Q.; Baboul, A. G.; Clifford, S.; Cioslowski, J.; Stefanov, B. B.; Liu, G.; Liashenko, A.; Piskorz, P.; Komaromi, I.; Martin, R. L.; Fox, D. J.; Keith, T.; Al-Laham, M. A.; Peng, C. Y.; Nanayakkara, A.; Challacombe, M.; Gill, P. M. W.; Johnson, B.; Chen, W.; Wong, M. W.; Gonzalez, C.; and Pople, J. A.; Gaussian, Inc.: Wallingford CT, 2004.

(9) Helgaker, T.; Jensen, H. J. A.; Joergensen, P.; Olsen, J.; Ruud, K.; Aagren, H.; Auer, A. A.; Bak, K. L.; Bakken, V.; Christiansen, O.; Coriani, S.; Dahle, P.; Dalskov, E. K.; Enevoldsen, T.; Fernandez, B.; Haettig, C.; Hald, K.; Halkier, A.; Heiberg, H.; Hettema, H.; Jonsson, D.; Kirpekar, S.; Kobayashi, R.; Koch, H.; Mikkelsen, K. V.; Norman, P.; Packer, M. J.; Pedersen, T. B.; Ruden, T. A.; Sanchez, A.; Saue, T.; Sauer, S. P. A.; Schimmelpfennig, B.; Sylvester-Hvid, K. O.; Taylor, P. R.; Vahtras, O., 1.1 ed.; University of Oslo: Oslo, 2001.

(10) Faulkner, T. R., University of Minnesota, Minneapolis, MN, 1976.

(11) Eliel, E. L.; Wilen, S. H.; Doyle, M. P. *Basic organic stereochemistry*; Wiley-Interscience: New York, 2001.

(12) Polavarapu, P. L. *Molecular Physics* **1997**, *91*, 551.

(13) Stephens, P. J.; Devlin, F. J.; Cheeseman, J. R.; Frisch, M. J.; Rosini, C. *Organic Letters* **2002**, *4*, 4595.

(14) Polavarapu, P. L.; Chakraborty, D. K. *Chemical Physics* **1999**, *240*, 1.

(15) Parr, R. G.; Yang, W. *Density-functional theory of atoms and molecules*; Oxford University Press: Oxford [England], 1989.

(16) Wang, F.; Wang, Y.; Polavarapu, P. L.; Li, T. Y.; Drabowicz, J.; Pietrusiewicz, K. M.; Zygo, K. *Journal of Organic Chemistry* **2002**, *67*, 6539.

(17) Freedman, T. B.; Dukor, R. K.; van Hoof, P.; Kellenbach, E. R.; Nafie, L. A. *Helvetica Chimica Acta* **2002**, *85*, 1160.

(18) Devlin, F. J.; Stephens, P. J.; Osterle, C.; Wiberg, K. B.; Cheeseman, J. R.; Frisch, M. J. *Journal of Organic Chemistry* **2002**, *67*, 8090.

(19) Ashvar, C. S.; Stephens, P. J.; Eggimann, T.; Wieser, H. *Tetrahedron-Asymmetry* **1998**, *9*, 1107.

(20) Devlin, F. J.; Stephens, P. J. *Journal of the American Chemical Society* **1999**, *121*, 7413.

(21) Wang, P.; Polavarapu, P. L. *Journal of Physical Chemistry A* **2000**, *104*, 6189.

(22) Wiberg, K. B.; Vaccaro, P. H.; Cheeseman, J. R. *Journal of the American Chemical Society* **2003**, *125*, 1888.

(23) Polavarapu, P. L.; Petrovic, A.; Wang, F. *Chirality* **2003**, *15*, S143.

(24) Muller, T.; Wiberg, K. B.; Vaccaro, P. H. *Journal of Physical Chemistry A* **2000**, *104*, 5959.

(25) Muller, T.; Wiberg, K. B.; Vaccaro, P. H.; Cheeseman, J. R.; Frisch, M. J. *Journal of the Optical Society of America B-Optical Physics* **2002**, *19*, 125.

(26) Munyemana, F.; Frisquehesbain, A. M.; Devos, A.; Ghosez, L. *Tetrahedron Letters* **1989**, *30*, 3077.

(27) Brandsma, L.; Verkruijsse, H. D. *Synthesis of acetylenes, allenes, and cumulenes : a laboratory manual*; Elsevier Scientific Pub: New York, 1981.

(28) Curme, H. G.; Heller, W. In *Techniques of chemistry*; Weissberger, A., Rossiter, B. W., Eds.; Wiley: New York, 1972; Vol. 1, pp 51.

(29) PeakFit*,* 4.1.1 ed.; SPSS Inc.: Chicago, IL.

(30) DataFit*,* 7.1 ed.; Oakdale Engineering: Oakdale, PA.

(31) www.emsl.pnl.gov:2080/forms.

(32) Helgaker, T.; Ruud, K.; Bak, K. L.; Jorgensen, P.; Olsen, J. *Faraday Discussions* **1994**, 165.

(33) Wang, F.; Polavarapu, P. L. *Journal of Physical Chemistry A* **2000**, *104*, 1822.

(34) Cappelli, C.; Corni, S.; Mennucci, B.; Cammi, R.; Tomasi, J. *Journal of Physical Chemistry A* **2002**, *106*, 12331.

(35) Altona, C.; Geise, H. J.; Romers, C. *Tetrahedron* **1968**, *24*, 13.

(36) Duax, W. L.; Weeks, C. M.; Rohrer, D. C. In *Topics in Stereochemistry*, 1976; Vol. 9, pp 271.

(37) Pitner, T. P.; Edwards, W. B.; Bassfield, R. L.; Whidby, J. F. *Journal of the American Chemical Society* **1978**, *100*, 246.

(38) Boese, R.; Oberhammer, H.; Pulay, P.; Waterfeld, A. *Journal of Physical Chemistry* **1993**, *97*, 9625.

(39) Brutcher, F. V.; Roberts, t.; Barr, S. J.; Pearson, N. *Journal of the American Chemical Society* **1959**, *81*, 4915.

(40) Dzakula, Z.; DeRider, M. L.; Markley, J. L. *Journal of the American Chemical Society* **1996**, *118*, 12796.

(41) Holland, K. D.; Naritoku, D. K.; McKeon, A. C.; Ferrendelli, J. A.; Covey, D. F. *Molecular Pharmacology* **1990**, *37*, 98.

(42) Wellman, K. M.; Bunnenberg, E.; Djerassi, C. *Journal of the American Chemical Society* **1963**, *85*, 1870.

(43) Richardson, F. S.; Shillady, D. D.; Bloor, J. E. *Journal of Physical Chemistry* **1971**, *75*, 2466.

(44) Li, Y. S. *Journal of Molecular Spectroscopy* **1984**, *104*, 302

.

(45) Charro, M. E.; Alonso, J. L. *Journal of Molecular Spectroscopy* **1996**, *176*, 251.

(46) Polavarapu, P. L.; Bose, P. K.; Hecht, L.; Barron, L. D. *Journal of Physical Chemistry* **1993**, *97*, 11211.

(47) Potts, A. R.; Nesselrodt, D. R.; Baer, T.; Driscoll, J. W.; Bays, J. P. *Journal of Physical Chemistry* **1995**, *99*, 12090.

(48) Polavarapu, P. L.; Zhao, C. X. *Chemical Physics Letters* **1998**, *296*, 105.

(49) Polavarapu, P. L. *Chirality* **2002**, *14*, 768.

(50) Polavarapu, P. L. *Chirality* **2003**, *15*, 284.

(51) Kim, D.; Baer, T. *Chemical Physics* **2000**, *256*, 251.

(52) Hammer, N. I.; Gao, F.; Pagni, R. M.; Compton, R. N. *Journal of Chemical Physics* **2002**, *117*, 4299.

(53) Castiglioni, E.; Lebon, F.; Longhi, G.; Abbate, S. *Enantiomer* **2002**, *7*, 161.

(54) Longhi, G.; Gangemi, R.; Lebon, F.; Castiglioni, E.; Abbate, S.; Pultz, V. M.; Lightner, D. A. *Journal of Physical Chemistry A* **2004**, *108*, 5338.

(55) Langley, C. H.; Lii, J. H.; Allinger, N. L. *Journal of Computational Chemistry* **2001**, *22*, 1451.

(56) Nasipuri, D. *Stereochemistry of organic compounds : principles and applications*; John Wiley & Sons: New York, 1991.

(57) Polavarapu, P. L.; He, J. T. *Analytical Chemistry* **2004**, *76*, 61A.

(58) Freedman, T. B.; Cao, X. L.; Dukor, R. K.; Nafie, L. A. *Chirality* **2003**, *15*, 743.

(59) Goldsmith, M. R.; Jayasuriya, N.; Beratan, D. N.; Wipf, P. *Journal of the American Chemical Society* **2003**, *125*, 15696.

(60) Giorgio, E.; Minichino, C.; Viglione, R. G.; Zanasi, R.; Rosini, C. *Journal of Organic Chemistry* **2003**, *68*, 5186.

(61) Grimme, S.; Bahlmann, A.; Haufe, G. *Chirality* **2002**, *14*, 793.

(62) Stephens, P. J.; Devlin, F. J.; Cheeseman, J. R.; Frisch, M. J.; Bortolini, O.; Besse, P. *Chirality* **2003**, *15*, S57.

(63) Mennucci, B.; Tomasi, J.; Cammi, R.; Cheeseman, J. R.; Frisch, M. J.; Devlin, F. J.; Gabriel, S.; Stephens, P. J. *Journal of Physical Chemistry A* **2002**, *106*, 6102.

(64) Stephens, P. J.; Devlin, F. J.; Cheeseman, J. R.; Frisch, M. J.; Mennucci, B.; Tomasi, J. *Tetrahedron-Asymmetry* **2000**, *11*, 2443.

(65) Buser, H. R.; Muller, M. D. *Environmental Science & Technology* **1997**, *31*, 1960.

(66) Sheldon, R. A. *Chirotechnology: Industrial Synthesis of Optically Active Compounds*; Marcel Dekker: New York, 1993.

(67) Loos, M. A. *Phenoxyalkanoic acids In Herbicides: Chemistry, Degradation and Mode of Action*; Marcel Dekker: New York, 1975.

(68) Testa, B.; Trager, W. F. *Chirality* **1990**, *2*, 129.

(69) Buser, H. R.; Muller, M. D.; Theobald, N. *Environmental Science & Technology* **1998**, *32*, 188.

(70) Zipper, C.; Suter, M. J. F.; Haderlein, S. B.; Gruhl, M.; Kohler, H. P. E. *Environmental Science & Technology* **1998**, *32*, 2070.

(71) Zipper, C.; Bunk, M.; Zehnder, A. J. B.; Kohler, H. P. E. *Journal of Bacteriology* **1998**, *180*, 3368.

(72) Matell, M. *Kgl. Lantbruks-Hogskolans Ann.* **1953**, *20*, 205.

(73) Jourdain, F.; Hirokawa, T.; Kogane, T. *Tetrahedron Letters* **1999**, *40*, 2509.

(74) Booth, T. D.; Wainer, I. W. *Journal of Chromatography A* **1996**, *737*, 157.

(75) Miyazawa, T.; Kurita, S.; Shimaoka, M.; Ueji, S.; Yamada, T. *Chirality* **1999**, *11*, 554.

(76) Gabard, J.; Collet, A. *Nouveau Journal De Chimie-New Journal of Chemistry* **1986**, *10*, 685.

(77) Polavarapu, P. L. *Vibrational spectra : principles and applications with emphasis on optical activity*; Elsevier: New York, 1998.

(78) Barron, L. D. *Molecular light scattering and optical activity*; Cambridge University Press: New York, 1982.

(79) Jeffrey, G. A. *An introduction to hydrogen bond*; Oxford University Press: New York, 1997.

(80) Watson, J. D.; Crick, F. H. C. *Nature* **1953**, *171*, 737.

(81) Pauling, L.; Corey, R. B.; Branson, H. R. *Proc. Natl. Acad. Sci. USA* **1951**, *37*, 205.

(82) Scheiner, S. *Hydrogen bond, a theoretical perspective*; Oxford University Press: New York, 1997.

(83) Hadzi, D. *Theoretical treatments of hydrogen bonding*; John Wiley: Chichester, England ; New York, 1997.

(84) Wang, F.; Polavarapu, P. L.; Drabowicz, J.; Kielbasinski, P.; Potrzebowski, M. J.; Mikolajczyk, M.; Wieczorek, M. W.; Majzner, W. W.; Lazewska, I. *Journal of Physical Chemistry A* **2004**, *108*, 2072.

(85) Ngan, F.; Toofan, M. *Journal of Chromatographic Science* **1991**, *29*, 8.

(86) Wong, M. W. *Chemical Physics Letters* **1996**, *256*, 391.

(87) Smith, G.; Kennard, C. H. L.; White, A. H. *Acta Crystallographica Section B-Structural Science* **1981**, *37*, 275.

(88) Mak, T. C. W.; Smith, G.; Kennard, C. H. L. *Acta Crystallographica Section C-Crystal Structure Communications* **1986**, *42*, 310.

(89) Almenningen, A.; Bastiansen, O.; Motzfeldt, T. *Acta Chemica Scandinavica* **1969**, *23*, 2848.

(90) Roda, G.; Conti, P.; De Amici, M.; He, J. T.; Polavarapu, P. L.; De Micheli, C. *Tetrahedron-Asymmetry* **2004**, *15*, 3079.

(91) Wheal, H. V.; Thomson, A. M. *Excitatory amino acids and synaptic transmission*; Academic Press: London ; San Diego, 1991.

(92) Brauner-Osborne, H.; Egebjerg, J.; Nielsen, E. O.; Madsen, U.; Krogsgaard-Larsen, P. *Journal of Medicinal Chemistry* **2000**, *43*, 2609.

(93) Ozawa, S.; Kamiya, H.; Tsuzuki, K. *Progress in Neurobiology* **1998**, *54*, 581.

(94) Conti, P.; De Amici, M.; De Sarro, G.; Stensbol, T. B.; Brauner-Osborne, H.; Madsen, U.; De Micheli, C. *Journal of Medicinal Chemistry* **1998**, *41*, 3759.

(95) Conti, P.; De Amici, M.; Roda, G.; Vistoli, G.; Stensbol, T. B.; Brauner-Osborne, H.; Madsen, U.; Toma, L.; De Micheli, C. *Tetrahedron* **2003**, *59*, 1443.

(96) Conti, P.; De Amici, M.; Grazioso, G.; Roda, G.; Stensbol, T. B.; Brauner-Osborne, H.; Madsen, U.; Toma, L.; De Micheli, C. *European Journal of Organic Chemistry* **2003**, 4455.

(97) Conti, P.; De Amici, M.; di Ventimiglia, S. J.; Stensbol, T. B.; Madsen, U.; Brauner-Osborne, H.; Russo, E.; De Sarro, G.; Bruno, G.; De Micheli, C. *Journal of Medicinal Chemistry* **2003**, *46*, 3102.

(98) Andrushchenko, V.; McCann, J. L.; van de Sande, J. H.; Wieser, H. *Vibrational Spectroscopy* **2000**, *22*, 101.

(99) Tian, G. L.; Lu, Y. J.; Novak, B. M. *Journal of the American Chemical Society* **2004**, *126*, 4082.

(100) Tang, H. Z.; Lu, Y. J.; Tian, G. L.; Capracotta, M. D.; Novak, B. M. *Journal of the American Chemical Society* **2004**, *126*, 3722.

(101) Cornelissen, J. J. L. M.; Rowan, A. E.; Nolte, R. J. M.; Sommerdijk, N. A. J. M. *Chemical Reviews* **2001**, *101*, 4039.

(102) Tang, H. Z.; Boyle, P. D.; Novak, B. M. *Journal of the American Chemical Society* **2005**, *127*, 2136.

(103) Thilgen, C.; Goose, I.; Diederich, F. *Topics in stereochemistry*; John Wiley & Sons: New York, 2003.

(104) Powell, W. H.; Cozzi, F.; Moss, G. P.; Thilgen, C.; Hwu, R. J. R.; Yerin, A. *Pure and Applied Chemistry* **2002**, *74*, 629.

(105) Hawkins, J. M.; Meyer, A. *Science* **1993**, *260*, 1918.

(106) Kessinger, R.; Crassous, J.; Herrmann, A.; Ruttimann, M.; Echegoyen, L.; Diederich, F. *Angewandte Chemie-International Edition* **1998**, *37*, 1919.

(107) Yamamoto, C.; Hayashi, T.; Okamoto, Y.; Ohkubo, S.; Kato, T. *Chemical Communications* **2001**, 925.

(108) Goto, H.; Harada, N.; Crassous, J.; Diederich, F. *Journal of the Chemical Society-Perkin Transactions 2* **1998**, 1719.

(109) Orlandi, G.; Poggi, G.; Zerbetto, F. *Chemical Physics Letters* **1994**, *224*, 113.

(110) Pecul, M.; Ruud, K.; Rizzo, A.; Helgaker, T. *Journal of Physical Chemistry A* **2004**, *108*, 4269.

(111) Tam, M. C.; Russ, N. J.; Crawford, T. D. *Journal of Chemical Physics* **2004**, *121*, 3550.

(112) Pedersen, T. B.; Koch, H.; Boman, L.; de Meras, A. M. J. S. *Chemical Physics Letters* **2004**, *393*, 319.

(113) Wiberg, K. B.; Wang, Y. G.; Vaccaro, P. H.; Cheeseman, J. R.; Trucks, G.; Frisch, M. J. *Journal of Physical Chemistry A* **2004**, *108*, 32.

(114) Diedrich, C.; Grimme, S. *Journal of Physical Chemistry A* **2003**, *107*, 2524.

(115) Pecul, M.; Ruud, K.; Helgaker, T. *Chemical Physics Letters* **2004**, *388*, 110.

(116) Pedersen, T. B.; Koch, H.; Ruud, K. *Journal of Chemical Physics* **1999**, *110*, 2883.

(117) Furche, F.; Ahlrichs, R.; Wachsmann, C.; Weber, E.; Sobanski, A.; Vogtle, F.; Grimme, S. *Journal of the American Chemical Society* **2000**, *122*, 1717.

(118) Stephens, P. J.; McCann, D. M.; Butkus, E.; Stoncius, S.; Cheeseman, J. R.; Frisch, M. J. *Journal of Organic Chemistry* **2004**, *69*, 1948.

(119) Furche, F.; Ahlrichs, R. *Journal of the American Chemical Society* **2002**, *124*, 3804.

(120) Norman, P.; Ruud, K.; Helgaker, T. *Journal of Chemical Physics* **2004**, *120*, 5027.

(121) Yabana, K.; Bertsch, G. F. *Physical Review A* **1999**, *60*, 1271.

(122) Djerassi, C. *Optical rotatory dispersion; applications to organic chemistry*; McGraw-Hill: New York,, 1960.

(123) Barron, L. D. *Molecular light scattering and optical activity*, 2nd , rev. and enl. ed.; Cambridge University Press: Cambridge, UK ; New York, 2004.

(124) Ohta, K.; Ishida, H. *Applied Spectroscopy* **1988**, *42*, 952.

(125) Bauernschmitt, R.; Ahlrichs, R. *Chemical Physics Letters* **1996**, *256*, 454.